Quantifying new water fractions and transit time distributions using ensemble hydrograph separation: theory and benchmark tests

James W. Kirchner[1,2,3]

[1]Dept. of Environmental Systems Science, ETH Zurich, CH-8092 Zürich, Switzerland
5 [2]Swiss Federal Research Institute WSL, CH-8903 Birmensdorf, Switzerland
[3]Dept. of Earth and Planetary Science, University of California, Berkeley, CA, 94720, U.S.A.

Correspondence to: James W. Kirchner (kirchner@ethz.ch)

Abstract. Decades of hydrograph separation studies have estimated the proportions of recent precipitation in streamflow
10 using end-member mixing of chemical or isotopic tracers. Here I propose an ensemble approach to hydrograph separation
that uses regressions between tracer fluctuations in precipitation and discharge to estimate the average fraction of new water
(e.g., same-day or same-week precipitation) in streamflow across an ensemble of time steps. The points comprising this
ensemble can be selected to isolate conditions of particular interest, making it possible to study how the new water fraction
varies as a function of catchment and storm characteristics. Even when new water fractions are highly variable over time,
15 one can show mathematically (and confirm with benchmark tests) that ensemble hydrograph separation will accurately
estimate their average. Because ensemble hydrograph separation is based on correlations between tracer fluctuations rather
than on tracer mass balances, it does not require that the end-member signatures are constant over time, or that all the end-
members are sampled or even known, and it is relatively unaffected by evaporative isotopic fractionation.

20 Ensemble hydrograph separation can also be extended to a multiple regression that estimates the average (or "marginal")
transit time distribution directly from observational data. This approach can estimate both "backward" transit time
distributions (the fraction of streamflow that originated as rainfall at different lag times) and "forward" transit time
distributions (the fraction of rainfall that will become future streamflow at different lag times), with and without volume-
weighting, up to a user-determined maximum time lag. The approach makes no assumption about the shapes of the transit
25 time distributions, nor does it assume that they are time-invariant, and it does not require continuous time series of tracer
measurements. Benchmark tests with a nonlinear, nonstationary catchment model confirm that ensemble hydrograph
separation reliably quantifies both new water fractions and transit time distributions across widely varying catchment
behaviors, using either daily or weekly tracer concentrations as input. Numerical experiments with the benchmark model
also illustrate how ensemble hydrograph separation can be used to quantify the effects of rainfall intensity, flow regime, and
30 antecedent wetness on new water fractions and transit time distributions.

1 Introduction

For nearly 50 years, chemical and isotopic tracers have been used to quantify the relative contributions of different water sources to streamflow following precipitation events (Pinder and Jones, 1969; Hubert et al., 1969); see also reviews by Buttle (1994) and Klaus and McDonnell (2013), and references therein. As reviewed by Klaus and McDonnell (2013),

5 chemical and isotopic hydrograph separation studies have led to many important insights into runoff generation. Foremost among these has been the realization that even at stormflow peaks, stream discharge is often composed primarily of "old" catchment storage rather than "new" recent precipitation (Sklash et al., 1976; Sklash, 1990; Neal and Rosier, 1990; Buttle, 1994). The previous dominant paradigm, based on little more than intuition, had held that because streamflow responds promptly to rainfall, the storm hydrograph must consist primarily of precipitation that reaches the channel quickly. Isotope

10 hydrograph separations showed that this intuition is often wrong, because the isotopic signatures of stormflow often resemble baseflow or groundwater rather than recent precipitation. These observations have not only overthrown the previous dominant paradigm, but also launched decades of research aimed at unraveling the paradox of how catchments store water for weeks or months, but release it within minutes following the onset of rainfall (Kirchner, 2003).

15 The foundations of conventional two-component hydrograph separation are straightforward. If one assumes that streamflow is a mixture of two end-members of fixed composition, which I will call for simplicity "new" and "old" water, then at any time j the mass balance for the water itself is

$$Q_j = Q_{\mathrm{new}_j} + Q_{\mathrm{old}_j} \qquad , \tag{1}$$

and the mass balance for a conservative tracer is

$$Q_j C_{\mathrm{Q}_j} = Q_{\mathrm{new}_j} C_{\mathrm{new}} + Q_{\mathrm{old}_j} C_{\mathrm{old}} \qquad , \tag{2}$$

where Q denotes water flux and C denotes the concentration of a passive chemical tracer or the δ value of ^{18}O or ^{2}H. One can straightforwardly solve Eqs. (1) and (2) to express the fraction of new water in streamflow at any time j as:

$$F_{\mathrm{new}_j} = \frac{Q_{\mathrm{new}_j}}{Q_j} = \frac{C_{\mathrm{Q}_j} - C_{\mathrm{old}}}{C_{\mathrm{new}} - C_{\mathrm{old}}} \qquad . \tag{3}$$

In typical applications, the "new" water is recent precipitation and the tracer signature of the "old" water is obtained from

25 pre-event baseflow, which is generally assumed to originate from long-term groundwater storage.

The assumptions underlying conventional hydrograph separation can be summarized as follows:
1. Streamflow is a mixture formed entirely from the sampled end-members; contributions from other possible streamflow sources (such as vadose zone water or surface storage) are negligible.

2. The samples of the end-members are representative (e.g., the sampled precipitation accurately reflects all precipitation, and the sampled baseflow reflects all pre-event water).

3. The tracer signatures of the end-members are constant through time, or their variations can be taken into account.

4. The tracer signatures of the end-members are significantly different from one another.

5 As reviewed by Rodhe (1987), Sklash (1990), Buttle (1994) and Klaus and McDonnell (2013), each of these assumptions can be problematic in practice:

1. Hydrograph separation studies often lead to implausible (including negative) inferred contributions of new water, and such anomalous results are sometimes attributed to contributions from un-sampled end-members (e.g., von Freyberg et al., 2017). In such cases, assumption #1 is clearly not met.

10 2. The isotopic composition of precipitation can vary considerably within an event, both spatially and temporally, even in small catchments (e.g., McDonnell et al., 1990; McGuire et al., 2005; Fischer et al., 2017; von Freyberg et al., 2017). Likewise, the isotopic signature of the baseflow or groundwater end-member has been shown to vary in space and time during snowmelt and rainfall events (e.g., Hooper and Shoemaker, 1986; Rodhe, 1987; Bishop, 1991; McDonnell et al., 1991). In these cases, assumptions #2 and #3 are not met. Various schemes have been

15 proposed to address this spatial and temporal variability by weighting the isotopic compositions of individual samples, but the validity of these schemes typically rests on strong assumptions about the nature of the runoff generation process and the heterogeneity to be averaged over.

3. When the difference between C_{new} and C_{old} is not large compared to their uncertainties, Eq. (3) becomes unstable and the resulting hydrograph separations become unreliable. This problem can be detected using Gaussian error

20 propagation (Genereux, 1998), but Bansah and Ali (2017) report that less than 20% of the hydrograph separation studies they reviewed have used it.

One can agree with Buttle (1994) that "despite frequent violations of some of its underlying assumptions, the isotopic hydrograph separation approach has proven to be sufficiently robust to be applied to the study of runoff generation in an

25 increasing number of basins," at least as a characterization of the community's widespread acceptance of the technique. Nonetheless, there is clearly room for new and different ways to quantify stormflow generation. In addition, weekly or even daily isotope measurements are now becoming available for many catchments, sometimes spanning periods of many years, and despite their many uses (particularly for calibrating hydrological models), there is an obvious need for new ways to extract hydrological insights from such time series.

Here I propose a new method for using isotopes and other conservative tracers to quantify the origins of streamflow. This method is based on statistical correlations among tracer fluctuations in streamflow and one or more candidate water sources, rather than mass balances. As such, it exploits the temporal variability in candidate end-members, rather than requiring them to be constant. It also does not require strict mass balance, and thus is relatively insensitive to the presence of unmeasured

end-members. Because this method quantifies the average proportions of source waters in streamflow across an ensemble of events or time steps, it does not answer the same question that traditional hydrograph separation does (namely, how fractions of new and old water change over time during individual storm events). Instead, it can answer new and different questions, such as how the average fractions of new and old water vary with stream discharge or precipitation intensity, antecedent

5 moisture, etc. The proposed method is designed to provide insights into stormflow generation from regularly sampled time series, even if those time series have gaps and even if they are sampled at frequencies much lower than the storm response timescale of the catchment.

The purpose of this paper is to describe the method, document its mathematical foundations, and test it against a benchmark

10 model, in which the method's results can be verified by age tracking. Applications to real-world catchments will follow in future papers. Because the proposed method is new and thus must be fully documented, several parts of the presentation (most notably Sects. 4.2-4.4 and Appendix B) necessarily contain strong doses of math. The math can be skipped, or lightly skimmed, by those who only need a general sense of the analysis. A table of symbols is provided at the end of the text.

2 Estimating new water fractions by ensemble hydrograph separation

15 Here I propose a new type of hydrograph separation based on correlations between tracer fluctuations in streamflow and in one or more end-members. This new approach to hydrograph separation does not have the same goal as conventional hydrograph separation. It does not estimate the contributions of end-members to streamflow for each time step (as in Eq. 3). Instead, it estimates the *average* end-member contributions to streamflow over an ensemble of time steps; hence its name, *ensemble* hydrograph separation. The ensemble of time steps may be chosen to reflect different catchment conditions, and

20 thus used to map out how those catchment conditions influence end-member contributions to streamflow.

2.1 Basic equations

I will first illustrate this approach with a simple example of a time-varying mixing model. Let's assume that we have measured tracer concentrations in streamflow, and in at least one contributing end-member, over an ensemble of time intervals j. The simplest possible mass balance for the water that makes up streamflow would be

$$Q_j = Q_{\mathrm{new}_j} + Q_{\mathrm{old}_j} \quad , \tag{4}$$

where Q_{new} represents the water flux in streamflow Q that originates from recent precipitation (or, potentially, any other end-member in which tracers can be measured) during time interval j. All other contributions to streamflow are lumped together as Q_{old}. Conservative mixing implies that

$$Q_j \, C_{\mathrm{Q}_j} = Q_{\mathrm{new}_j} \, C_{\mathrm{new}_j} + Q_{\mathrm{old}_j} \, C_{\mathrm{old}_j} \quad , \tag{5}$$

where C_Q and C_{new} are the tracer concentrations in the stream and the new water, and C_{old} is the tracer signature of all other sources that contribute to streamflow. Combining (4) and (5), we directly obtain

$$C_{Q_j} = F_{new_j} C_{new_j} + \left(1 - F_{new_j}\right) C_{old_j} \quad , \tag{6}$$

where $F_{new_j} = Q_{new_j}/Q_j$ is the fractional contribution of Q_{new} to streamflow Q. Equation (6) can be rewritten as

$$C_{Q_j} - C_{old_j} = F_{new_j} \left(C_{new_j} - C_{old_j}\right) \quad , \tag{7}$$

which in turn could be rearranged as a conventional mixing model (Eq. 3), with the important difference that the new and old water concentrations are time-varying rather than constant. If we represent the "old" water composition using the streamwater concentration during the previous time step, equation (7) becomes

$$C_{Q_j} - C_{Q_{j-1}} = F_{new_j} \left(C_{new_j} - C_{Q_{j-1}}\right) \quad , \tag{8}$$

10 The lagged concentration $C_{Q_{j-1}}$ serves as a reference level for measuring fluctuations in precipitation and streamflow tracer concentrations and the correlations between them. Thus, it is not necessary that $C_{Q_{j-1}}$ consists entirely of "old water" as defined in conventional hydrograph separations (i.e., groundwater or baseflow water). It is only necessary that $C_{Q_{j-1}}$ contains no "new" water (that is, no precipitation that fell during time step j), and this condition is automatically met because $C_{Q_{j-1}}$ is measured during the previous time step. The net effect of $C_{Q_{j-1}}$ is to factor out the legacy effects of previous tracer

15 inputs, and to filter out long-term variations in C_Q that could otherwise lead to spurious correlations with C_{new}.

The ensemble hydrograph separation approach is based on the observation that (8) is almost equivalent to the conventional linear regression equation,

$$y_j = \beta \, x_j + \alpha + \varepsilon_j \quad , \quad y_j = C_{Q_j} - C_{Q_{j-1}} \quad , \quad x_j = C_{new_j} - C_{Q_{j-1}} \quad , \tag{9}$$

20 where the intercept α and the error term ε_j can be viewed as subsuming any bias or random error introduced by measurement noise, evapoconcentration effects, and so forth. The analogy between (9) and (8) suggests that it may be possible to estimate the average value of F_{new_j} from the regression slope of a scatterplot of the streamflow concentration C_{Q_j} against the new water concentration C_{new_j}, both expressed relative to the lagged streamflow concentration $C_{Q_{j-1}}$.

25 However, astute readers will notice an important difference between (8) and (9): in (9), the regression slope β is a constant, whereas in (8), F_{new_j} varies from one time step to the next. It is not obvious how an estimate of the (constant) slope β will be related to the (non-constant) F_{new_j} or whether this relationship could be affected by the other variables in Eq. (8). The answer to this question can be derived analytically and tested using numerical experiments (see Appendix A). As explained

in Appendix A, the regression slope in a scatterplot of $C_{Q_j} - C_{Q_{j-1}}$ versus $C_{\text{new}_j} - C_{Q_{j-1}}$ (Fig. A1d) will closely approximate the average value of F_{new_j} (averaged over the ensemble of time steps j), under rather general conditions:

1. The slope of the relationship between F_{new_j} and $C_{\text{new}_j} - C_{Q_{j-1}}$, times the mean of $C_{\text{new}_j} - C_{Q_{j-1}}$, should be small compared to the average F_{new}. This will usually be true for conservative tracers, for two reasons. First, because all streamflow is ultimately derived from new water, mass conservation implies that the mean of $C_{\text{new}_j} - C_{Q_{j-1}}$ should usually be small. Second, unless there is a correlation between storm size and tracer concentration (not just between storm size and tracer variance), the slope of the relationship between F_{new_j} and $C_{\text{new}_j} - C_{Q_{j-1}}$ should also be small. Thus the product of these two small terms should be small.

2. Points with large leverage in the scatterplot (i.e., with $C_{\text{new}_j} - C_{Q_{j-1}}$ values far above and below the mean) should not be systematically associated with either high or low values of F_{new_j}. Such a systematic association is unlikely unless large storms (which are likely to generate large new water fractions) are also associated with both very high and very low tracer concentrations.

3. As expected for typical sampling and measurement errors, the error term ε_j should not be strongly correlated with $C_{\text{new}_j} - C_{Q_{j-1}}$.

Thus the analysis in Appendix A shows that a reasonable estimate of the ensemble average of F_{new} should, under typical conditions, be obtainable from the regression slope $\hat{\beta}$ of a plot of $x_j = C_{Q_j} - C_{Q_{j-1}}$ versus $y_j = C_{\text{new}_j} - C_{Q_{j-1}}$ (i.e., Eq. 9; Fig. A1d).

The least-squares solution of Eq. (9) can be expressed in several equivalent ways. For consistency with the analysis that will be developed in Sect. 4 below, I will use the following formulation, which is mathematically equivalent to those more commonly seen:

$$F_{new} = \hat{\beta} = \frac{\text{cov}(y_j, x_j)}{\text{var}(x_j)} \quad , \tag{10}$$

where $\hat{\beta}$ is the least-squares estimate of β, and F_{new} is the average of the F_{new_j} over the ensemble of points j. Values of y_j that lack a corresponding x_j, or vice versa (due to sampling gaps, for example, or lack of precipitation), are omitted.

2.2 Uncertainties

The uncertainty in F_{new}, expressed as a standard error, can be written as

$$\text{s.e.}(F_{new}) = \text{s.e.}(\hat{\beta}) = \frac{s_y}{s_x} \frac{\sqrt{1 - r_{xy}^2}}{\sqrt{n_{\text{eff}} - 2}} = \frac{\hat{\beta}}{\sqrt{n_{\text{eff}} - 2}} \sqrt{\frac{1}{r_{xy}^2} - 1} \quad , \tag{11}$$

where s_x and s_y are the standard deviations of x and y, r_{xy} is the correlation between them, and n_{eff} is the effective sample size, which can be adjusted to account for serial correlation in the residuals (Bayley and Hammersley, 1946; Brooks and Carruthers, 1953; Matalas and Langbein, 1962):

$$n_{eff} \approx n_{xy} \left[\frac{1 + r_{sc}}{1 - r_{sc}} - \frac{2}{n_{xy}} \frac{r_{sc}(1 - r_{sc}^n)}{(1 - r_{sc})^2} \right]^{-1} , \qquad (12)$$

where n_{xy} is the number of pairs of x_j and y_j, and r_{sc} is the lag-1 serial correlation in the regression residuals $y_j - \hat{\beta} x_j - \alpha$. For large n_{xy}, Eq. (12) can be approximated as (Mitchell et al., 1966)

$$n_{eff} \approx n_{xy} \left[\frac{1 - r_{sc}}{1 + r_{sc}} \right] , \qquad (13)$$

where for all positive r_{sc}, Eq. (13) is conservative (it underestimates n_{eff} from Eq. 12), and for $r_{sc} = 0.5$, and $n_{xy} > 50$, for example, Eqs. (12) and (13) differ by less than 3%. If the scatterplot of $y_j = C_{Qj} - C_{Qj-1}$ versus $x_j = C_{newj} - C_{Qj-1}$ contains outliers, a robust fitting technique such as Iteratively Reweighted Least Squares (IRLS) may yield more reliable estimates of F_{new} than ordinary least squares regression. However, the analyses presented here are based on outlier-free synthetic data generated from a benchmark model (see Sect. 3), so in this paper I have used conventional least squares (Eqs. 10-11) instead.

2.3 New water fraction for time steps with precipitation

The meaning of the new water fraction F_{new} depends on how the new water and streamwater are sampled. For example, if the new water concentrations C_{new} are measured in daily bulk precipitation samples and the stream water concentrations C_Q are measured in instantaneous grab samples taken at the end of each 24-hour precipitation sampling period, then F_{new} will estimate the average fraction of streamflow that is composed of precipitation from the preceding 24 hours. If the sampling interval is weekly instead of daily, then F_{new} will estimate the average fraction of streamflow that consists of precipitation from the preceding week. This will generally be larger than the F_{new} calculated from daily sampling, for the obvious reason that on average more precipitation will have fallen during the previous week than during the previous 24 hours, so this precipitation will comprise a larger fraction of streamflow. Also, if the weekly streamflow concentrations are measured in integrated composite samples rather than instantaneous grab samples, then F_{new} will estimate the fraction of same-week precipitation in average weekly streamflow rather than in the instantaneous end-of-week streamflow. The general rule is: F_{new} should generally estimate whatever new water has been sampled as C_{new}, expressed as a fraction of whatever streamflow has been sampled as C_Q.

In all of these cases, $\hat{\beta}$ from Eq. (10) estimates the average fraction of new water in streamflow during time steps with precipitation, because time steps without precipitation lack a "new water" tracer concentration C_{new_j} and thus must be left out from the regression in Eq. (9). Using Qp to denote discharge during periods with precipitation, we can represent this "event new water fraction" as $^{Qp}F_{new}$.

5   ## 2.4 New water fraction for all time steps

Periods without precipitation will inherently lack same-day (or same-week) precipitation in streamflow. Thus we can calculate the average fraction of new water in streamflow during all time steps, including those without precipitation, as

$$^{Q}F_{new} = \ ^{Qp}F_{new}\frac{n_p}{n} = \hat{\beta}\ \frac{n_p}{n} \quad , \tag{14}$$

where $^{Q}F_{new}$ is the new water fraction of all discharge, $^{Qp}F_{new}$ is the new water fraction of discharge during time steps with
10   precipitation (as estimated by the regression slope $\hat{\beta}$, from Eq. 10), and n_p/n is the fraction of time steps that have precipitation. The ratio n_p/n in Equation (14) accounts for the fact that during time steps without rain, the new-water contribution to streamflow is inherently zero. The same ratio is also used to estimate the uncertainty in $^{Q}F_{new}$:

$$\text{s.e.}\left(^{Q}F_{new}\right) = \frac{n_p}{n}\ \text{s.e.}\left(\hat{\beta}\right) = \frac{^{Q}F_{new}}{\sqrt{n_{eff}-2}}\sqrt{\frac{1}{r_{xy}^2}-1} \quad . \tag{15}$$

2.5 Volume-weighted new water fractions

15   The regression derived through Eqs. (4)-(9) gives each time interval j equal weight. As a result, $\hat{\beta}$ from Eq. (10) can be interpreted as estimating the time-weighted average new water fraction. Alternatively, one can estimate the volume-weighted new water fraction,

$$\hat{\beta}^* = \frac{\sum_{j\in(xy)} Q_j \left(y_j - \bar{y}^*_{(xy)}\right)\left(x_j - \bar{x}^*_{(xy)}\right)}{\sum_{j\in(xy)} Q_j \left(x_j - \bar{x}^*_{(xy)}\right)^2} \quad , \tag{16}$$

where $\bar{x}^*_{(xy)}$ and $\bar{y}^*_{(xy)}$ are the volume-weighted means of x and y (averaged over all j for which x_j and y_j are not missing),

$$\bar{x}^*_{(xy)} = \frac{\sum_{j\in(xy)} Q_j x_j}{\sum_{j\in(xy)} Q_j} \quad , \quad \bar{y}^*_{(xy)} = \frac{\sum_{j\in(xy)} Q_j y_j}{\sum_{j\in(xy)} Q_j} \tag{17}$$

and the notation $j \in (xy)$ indicates sums taken over all j for which x_j and y_j are not missing. Equations (16)-(17) yield the slope coefficient for linear regressions like Eq. (9), but with each point weighted by the discharge Q_j. We can denote the weighted regression slope $\hat{\beta}^*$ as $^{Qp}F_{new}^*$, the volume-weighted new water fraction of time intervals with precipitation, where the asterisk indicates volume-weighting.

If, instead, one wants to estimate the new water fraction in all discharge (during periods with and without precipitation), following the approach in Sect. 2.4 one simply rescales this regression slope by the sum of discharge during time steps with precipitation, divided by total discharge:

$$^{Q}F^*_{new} = \ ^{Qp}F^*_{new} \frac{\bar{Q}_p}{\bar{Q}} \frac{n_p}{n} = \ \hat{\beta}^* \frac{\bar{Q}_p}{\bar{Q}} \frac{n_p}{n} \quad , \tag{18}$$

where $^{Q}F^*_{new}$ is the volume-weighted new water fraction of all discharge, $^{Qp}F^*_{new}$ is the fitted regression slope $\hat{\beta}$ from Eq. (16), $\bar{Q}_p$ is the average discharge for time steps with precipitation, $\bar{Q}$ is the average discharge for all time steps (including during rainless periods), and n_p/n is the fraction of time steps with rain.

10   Because the volume-weighting will typically be uneven, the effective sample size will typically be smaller than n; for example, in the extreme case that one sample had nearly all the weight and the other samples had nearly none, the effective sample size would be roughly 1 instead of n_{xy}. Thus, uncertainty estimates for these volume-weighted new water fractions should take account of the unevenness of the weighting. One can account for uneven weighting by calculating the effective sample size, following Kish (1995), as:

$$n_{eff} = \frac{\left(\sum Q_{j(xy)}\right)^2}{\sum\left(Q^2_{j(xy)}\right)} \quad , \tag{19}$$

where the notation $Q_{j(xy)}$ indicates discharge at time steps j for which pairs of x_j and y_j exist. Equation (19) evaluates to n_{xy} (as it should) in the case of evenly weighted samples, and declines toward 1 (as it should) if a single sample has much greater weight than the others. To obtain an estimate of the effective sample size that accounts for both serial correlation and uneven weighting, one can multiply the expressions in Eqs. (19) and (12) or (13). Combining these approaches, one can

20   estimate the standard error of $^{Q}F^*_{new}$ as

$$\text{s.e.}\left(^{Q}F^*_{new}\right) = \frac{\sum Q_p}{\sum Q} \text{s.e.}\left(\hat{\beta}^*\right) = \frac{^{Q}F^*_{new}}{\sqrt{n_{eff}-2}} \sqrt{\frac{1}{r^2_{xy}} - 1} \quad = \quad , \qquad n_{eff} = \frac{\left(\sum Q_{j(xy)}\right)^2}{\sum\left(Q^2_{j(xy)}\right)} \left[\frac{1-r_{sc}}{1+r_{sc}}\right] \quad , \tag{20}$$

where $\hat{\beta}^*$ is the fitted regression slope from Eq. (16).

2.6 New water fraction of precipitation

One can also express the flux of new water as a fraction of precipitation rather than discharge. Recently, von Freyberg et al.

25   (2018) have noted, in the context of conventional hydrograph separation, that expressing event water as a proportion of

precipitation rather than discharge may lead to different insights into catchment storm response. Analogously, within the ensemble hydrograph separation framework we can estimate the "new water fraction of precipitation", denoted $^{\mathrm{P}}F_{\mathrm{new}}$, as

$$^{\mathrm{P}}F_{\mathrm{new}} = {}^{\mathrm{Qp}}F_{\mathrm{new}} \frac{\bar{Q}_{\mathrm{p}}}{\bar{P}_{\mathrm{p}}} \quad , \tag{21}$$

where $^{\mathrm{Qp}}F_{\mathrm{new}}$ is the new water fraction of discharge during time steps with precipitation (as estimated by the regression slope $\hat{\beta}$, from Eq. 10), and $\bar{Q}_{\mathrm{p}}$ and $\bar{P}_{\mathrm{p}}$ are the average discharge and precipitation during these time steps. An alternative strategy is to re-cast Eq. (8) by multiplying both sides by Q_j/P_j, such that the F_{new} on the right-hand-side now expresses new water as a fraction of precipitation,

$$\frac{Q_j}{P_j}\left(C_{\mathrm{Q}j} - C_{\mathrm{Q}j-1}\right) = \left(\frac{Q_j}{P_j} F_{\mathrm{new}j}\right)\left(C_{\mathrm{new}j} - C_{\mathrm{Q}j-1}\right) = {}^{\mathrm{P}}F_{\mathrm{new}j} \left(C_{\mathrm{new}j} - C_{\mathrm{Q}j-1}\right) \quad . \tag{22}$$

This yields a linear regression similar to Eq. (9), but with y_j re-scaled,

$$y_j = \beta\, x_j + \alpha + \varepsilon_j \quad , \quad y_j = \frac{Q_j}{P_j}\left(C_{\mathrm{Q}j} - C_{\mathrm{Q}j-1}\right) \quad , \quad x_j = \left(C_{\mathrm{new}j} - C_{\mathrm{Q}j-1}\right) \quad , \tag{23}$$

where the regression slope $\hat{\beta}$, which can be calculated from Eq. (10) with the new values y_j, should approximate the average new water fraction of precipitation $^{\mathrm{P}}F_{\mathrm{new}}$.

The approaches represented by Eqs. (21) and (22)-(23) are not equivalent. Equation (21) is based on the *ad hoc* assumption – which is verified by the benchmark tests in Sects. 3.3-3.5 – that the average of $^{\mathrm{P}}F_{\mathrm{new}j}$ (new water in streamflow, as a fraction of precipitation) should approximate the average $F_{\mathrm{new}j}$ (new water in streamflow, as a fraction of discharge), rescaled by the ratio of average discharge $Q_{\mathrm{p}j}$ to average precipitation $P_{\mathrm{p}j}$. This is only an approximation, of course; it relies on the approximation that appears in the middle of the following chain of expressions,

$$^{\mathrm{P}}F_{\mathrm{new}} = \langle\, ^{\mathrm{P}}F_{\mathrm{new}j}\rangle_{\mathrm{p}} = \langle F_{\mathrm{new}j} \frac{Q_j}{P_j}\rangle_{\mathrm{p}} \approx \langle F_{\mathrm{new}j}\rangle_{\mathrm{p}} \frac{\langle Q_j\rangle_{\mathrm{p}}}{\langle P_j\rangle_{\mathrm{p}}} = {}^{\mathrm{Qp}}F_{\mathrm{new}} \frac{\bar{Q}_{\mathrm{p}}}{\bar{P}_{\mathrm{p}}} \quad , \tag{24}$$

where the "p" subscripts on the angled brackets indicate averages taken only over time intervals with precipitation. Whether this is a good approximation will depend on how P_j, Q_j, and $F_{\mathrm{new}j}$ are distributed, and how they are correlated with one another. By contrast, the approach outlined in Eqs. (22)-(23) is based on the exact substitution of $F_{\mathrm{new}j} Q_j/P_j$ for $^{\mathrm{P}}F_{\mathrm{new}j}$, which requires no approximations. The same substitution also leads to two other algebraically equivalent formulations of Eq. (22),

$$\left(C_{Q_j} - C_{Q_{j-1}}\right) = {}^P F_{\text{new}_j} \frac{P_j}{Q_j} \left(C_{\text{new}_j} - C_{Q_{j-1}}\right) \tag{25}$$

and

$$Q_j \left(C_{Q_j} - C_{Q_{j-1}}\right) = {}^P F_{\text{new}_j} P_j \left(C_{\text{new}_j} - C_{Q_{j-1}}\right) \quad . \tag{26}$$

But although Eqs. (22), (25), and (26) are algebraically equivalent, their statistical behavior is different when they are used
5   as regression equations to estimate the average value of ${}^P F_{\text{new}}$. The regression estimate of ${}^P F_{\text{new}}$ depends on the distributions of P_j, Q_j, and F_{new_j} and their correlations with each other, and benchmark testing shows that Eq. (22) yields reasonably accurate estimates of ${}^P F_{\text{new}}$, but Eqs. (25) and (26) do not. One can also note that the approach outlined in Eq. (21) – the other approach that is successful in benchmark tests – represents an ad-hoc time averaging of P_j and Q_j in Eq. (22), because it is formally equivalent to

$$\frac{\bar{Q}_{\text{p}}}{\bar{P}_{\text{p}}} \left(C_{Q_j} - C_{Q_{j-1}}\right) = {}^P F_{\text{new}_j} \left(C_{\text{new}_j} - C_{Q_{j-1}}\right) \quad . \tag{27}$$

The precise interpretation of ${}^P F_{\text{new}}$ depends on how streamflow is sampled. If the streamflow tracer concentrations come from integrated composite samples over each day or week, then ${}^P F_{\text{new}}$ can be interpreted as the fraction of precipitation that becomes same-day or same-week streamflow. If the streamflow tracer concentrations instead come from instantaneous grab
15   samples (as is more typical), then ${}^P F_{\text{new}}$ can be interpreted as the rate of new water discharge at that time (typically the end of the precipitation sampling interval), as a fraction of the average rate of precipitation. Adapting terminology from the literature of transit time distributions, we can call ${}^P F_{\text{new}}$ the "forward" new water fraction because it represents the fraction of precipitation that will exit as streamflow soon (during the same time step), and call ${}^{Qp} F_{\text{new}}$ and ${}^Q F_{\text{new}}$ "backward" new water fractions because they represent the fraction of streamflow that entered the catchment a short time ago. Although the
20   "backward" new water fraction of discharge comes in two forms (${}^{Qp} F_{\text{new}}$ or ${}^Q F_{\text{new}}$), depending on whether one includes or excludes rainless periods, the "forward" new water fraction ${}^P F_{\text{new}}$ can only be defined for time steps with precipitation (otherwise ${}^P F_{\text{new}}$ represents the ratio between zero new water and zero precipitation, and thus is undefined).

Readers should keep in mind that although ${}^P F_{\text{new}}$ represents the fraction of precipitation that becomes same-day (or same-
25   week) streamflow, different fractions of precipitation may leave the catchment the same day (or week) by other pathways, most notably by evapotranspiration. One could also estimate ${}^P F_{\text{new}}$ for water that leaves the catchment by evapotranspiration if one had tracer time series for evapotranspiration fluxes, but at present such time series are not

available. Thus, to echo the principle outlined in Sect. 2.3 above, the "new water fraction of precipitation" does not represent the "forward" new water fraction for all possible pathways, but only whatever pathway has been sampled.

2.7 Volume-weighted new water fraction of precipitation

The new water fraction of precipitation as estimated by Eq. (21) is a time-weighted average, in which each day with precipitation counts equally. One may also want to estimate the volume-weighted new water fraction of precipitation, which we can denote as $^{P}F_{new}^{*}$, in keeping with the naming conventions used above. We can estimate $^{P}F_{new}^{*}$ at least two different ways. The first method involves recognizing that we are seeking the ratio between the total volume of "new water" – that is, same-day precipitation reaching streamflow – and the total volume of precipitation. This will equal the volume-weighted new water fraction of *discharge* (total new water divided by total discharge, which has already been derived in Sect. 2.5 above), rescaled by the ratio of total discharge to total precipitation:

$$^{P}F_{new}^{*} \;=\; ^{Q}F_{new}^{*}\,\frac{\bar{Q}}{\bar{P}} \;=\; ^{Qp}F_{new}^{*}\,\frac{\bar{Q}_{p}}{\bar{P}}\,\frac{n_{p}}{n} \quad . \tag{28}$$

where $\bar{Q}$ and $\bar{P}$ are the average rates of discharge and precipitation (averaged over all time steps), $\bar{Q}_{p}$ is the average discharge on days with rain, and n_{p}/n is the fraction of time steps with rain. An alternative strategy, which yields nearly equivalent results in benchmark tests, precipitation-weights the regression for $^{P}F_{new}$ (Eq. 22), yielding

$$\hat{\beta}^{*} = \frac{\sum_{j\in(xy)} P_{j}\left(y_{j} - \bar{y}^{*}{}_{(xy)}\right)\left(x_{j} - \bar{x}^{*}{}_{(xy)}\right)}{\sum_{j\in(xy)} P_{j}\left(x_{j} - \bar{x}^{*}{}_{(xy)}\right)^{2}} \quad , \qquad y_{j} = \frac{Q_{j}}{P_{j}}\left(C_{Q_{j}} - C_{Q_{j-1}}\right) \quad , \qquad x_{j} = \left(C_{new_{j}} - C_{Q_{j-1}}\right) \quad , \tag{29}$$

where $\bar{x}^{*}{}_{(xy)}$ and $\bar{y}^{*}{}_{(xy)}$ are the precipitation-weighted means of x and y (averaged over all j for which x_{j} and y_{j} are not missing),

$$\bar{x}^{*}{}_{(xy)} = \frac{\sum_{j\in(xy)} P_{j}x_{j}}{\sum_{j\in(xy)} P_{j}} \quad , \qquad \bar{y}^{*}{}_{(xy)} = \frac{\sum_{j\in(xy)} P_{j}y_{j}}{\sum_{j\in(xy)} P_{j}} \quad , \tag{30}$$

and where the regression slope $\hat{\beta}^{*}$ approximates the precipitation-weighted average "forward" new water fraction $^{P}F_{new}^{*}$.

3 Testing ensemble hydrograph separation with a simple non-stationary benchmark model

3.1 Benchmark model

To test the methods outlined in Sect. 2 above, I use synthetic data generated by a simple two-box lumped-parameter catchment model. This model is documented in greater detail in Kirchner (2016a), and will be described only briefly here. As shown in Fig. 1a, drainage L from the upper box is a power function of the storage S_{u} within the box; a fraction η of this

drainage flows directly to streamflow, and the complementary fraction 1-η recharges the lower box, which drains to streamflow at a rate Q_l that is a power function of its storage S_l. The model's behavior is determined by five parameters: the equilibrium storage levels $S_{u,ref}$ and $S_{l,ref}$ in the upper and lower boxes, their drainage exponents b_u and b_l, and the drainage partitioning coefficient η. For simplicity, evapotranspiration is not explicitly simulated; instead, the precipitation inputs can be considered to be effective precipitation, net of evapotranspiration losses. Discharge from both boxes is assumed to be non-age-selective, meaning that discharge is taken proportionally from each part of the age distribution. Tracer concentrations and mean ages are tracked under the assumption that the boxes are each well-mixed but also distinct from one another, so their tracer concentrations and water ages will differ. Water ages and tracer concentrations are also tracked in daily age bins up to an age of 70 days, and mean water ages are tracked in both the upper and lower boxes.

The model operates at a daily time step, with the storage evolution of the lower box calculated by a weighted combination of the partly implicit trapezoidal method (for greater accuracy) and the fully implicit backward Euler method (for guaranteed stability). Unlike in Kirchner (2016a), here the storage evolution of the upper box is calculated by forward Euler integration at 50 sub-daily time steps of 0.02 days (roughly 30 minutes) each. At this time step, forward Euler integration is stable across the entire parameter ranges used in this paper, and is more accurate than daily time steps of trapezoidal or backward Euler integration (which are still adequate for the lower box, where storage volumes change more slowly). Following Kirchner (2016a), the model is driven with three different real-world daily rainfall time series, representing a range of climatic regimes: a humid maritime climate with frequent rainfall and moderate seasonality (Plynlimon, Wales; Köppen climate zone Cfb), a Mediterranean climate marked by wet winters and very dry summers (Smith River, California, USA; Köppen climate zone Csb), and a humid temperate climate with very little seasonal variation in average rainfall (Broad River, Georgia, USA; Köppen climate zone Cfa). Synthetic daily precipitation tracer (deuterium) concentrations are generated randomly from a normal distribution with a standard deviation of 20 per mil and a lag-one serial correlation of 0.5, superimposed on a seasonal cycle with an amplitude of 10 per mil. The model is initialized at the equilibrium storage levels $S_{u,ref}$ and $S_{l,ref}$, with age distributions and tracer concentrations corresponding to steady-state equilibrium values at the mean input fluxes of water and tracer. The model is then run for a one-year spin-up period; the results reported here are from five-year simulations following this spin-up period.

For the simulations shown here, the drainage exponents b_u and b_l are randomly chosen from uniform distributions of logarithms spanning the range of 1-20, and the partitioning coefficient η is randomly chosen from a uniform distribution ranging from 0.1 to 0.9. The reference storage levels $S_{u,ref}$ and $S_{l,ref}$ are randomly chosen from a uniform distribution of logarithms spanning the ranges of 50-200 mm and 200-2000 mm, respectively. These parameter distributions encompass a wide range of possible behaviors, including both strong and damped response to rainfall inputs.

I illustrate the behavior of the model using two particular parameter sets, one that gives damped response to precipitation ($S_{u,ref}$ =100 mm, $S_{l,ref}$ =1000 mm, b_u=10, b_l=3, and η=0.3), and one that gives a more rapid response (the same parameters, except η=0.8). These parameter values are not preferable to others in any particular way; they simply generate strongly contrasting streamflow and tracer responses that look plausible as examples of small catchment behavior. They can be

5   interpreted as the behavior of two contrasting model catchments, which for simplicity (but with some linguistic imprecision) I will call the "damped catchment" and the "flashy catchment", as shorthand for "model catchment with parameters giving more damped response" and "model catchment with parameters giving more flashy response".

The model also simulates the sampling process and its associated errors. I assume that tracer concentrations cannot be

10   measured when precipitation rates are below a threshold of $P_{threshold}$=1 mm/day, such that tracer samples below this threshold will be missing. I further assume that 5% of all other precipitation tracer measurements, and 5% of all streamflow tracer measurements, will be lost at random times due to sampling or analysis failures. I have also added Gaussian random errors (with a standard deviation of 1 per mil) to all tracer measurements.
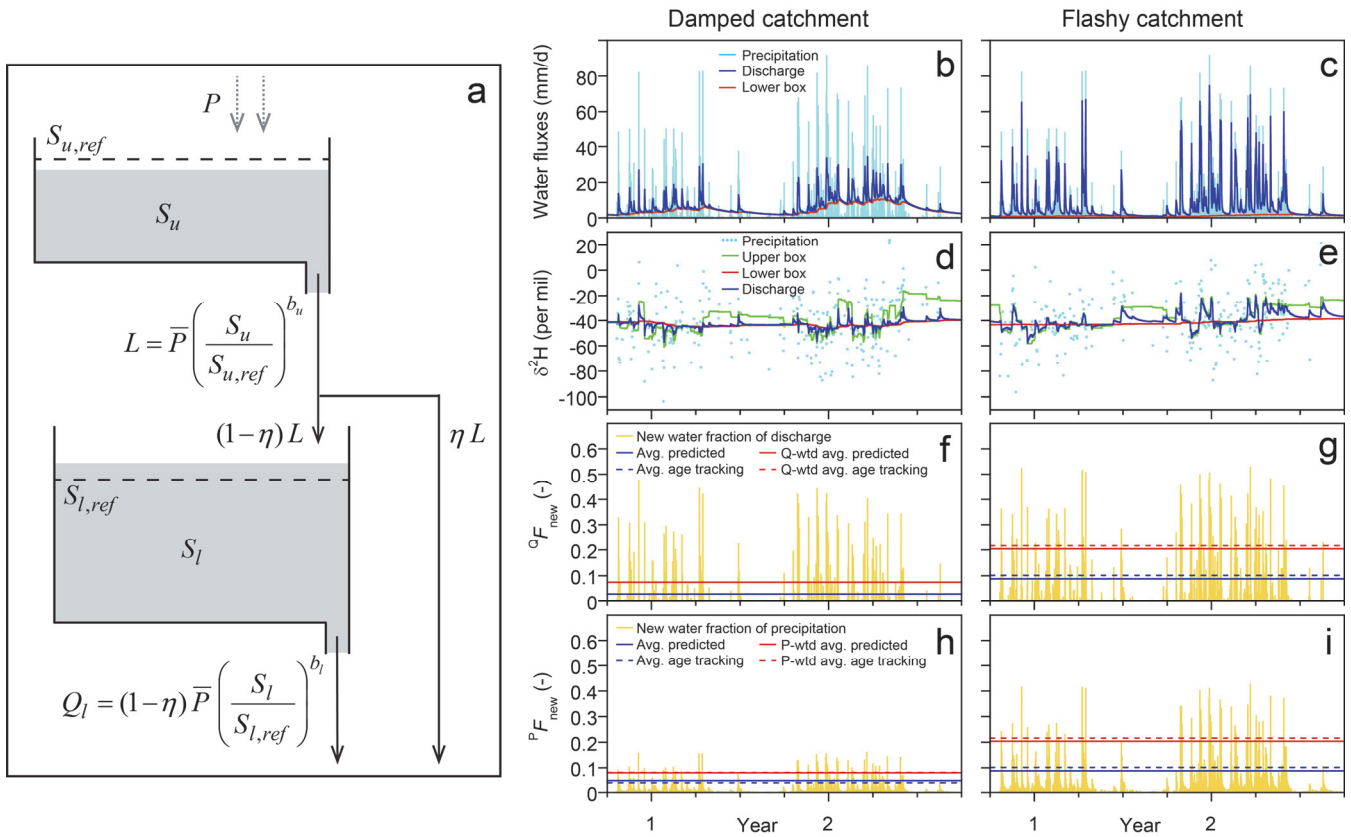
Figure 1. Schematic diagram of the benchmark model (a), with two-year excerpts from illustrative simulations of its behavior (b-i). Model parameters for simulations of damped catchment response (left panels) are $S_{u,ref}$ = 100 mm, $S_{l,ref}$ = 1000 mm, b_u = 10, and b_l = 3, and η = 0.3. For simulations of flashy catchment response (right panels), all but one of the parameters are the same; only η is changed to 0.8 and a different random realization of precipitation isotopes is used. The same daily precipitation time series (Smith River, Mediterranean climate) is used in both cases. The isotopic composition of streamflow exhibits complex dynamics over multiple time scales (blue line in panels d and e), as dominance shifts between the upper and lower boxes (green and orange lines, respectively, in panels d and e). Like the discharge and its isotopic composition, the fraction of discharge comprised of same-day precipitation (the new water fraction of discharge, $^{Q}F_{new}$, panels f and g) exhibits complex nonstationary dynamics. Nonetheless, its long-term average (dashed blue line) is well predicted by ensemble hydrograph separation (solid blue line); the same is true of the discharge-weighted average (dashed/solid red lines). The fraction of precipitation appearing in same-day discharge (the forward new water fraction, $^{P}F_{new}$, panels h and i) is somewhat less variable, but both its average and precipitation-weighted average are also well predicted by ensemble hydrograph separation (solid/dashed blue and red lines). In several cases the dashed and solid lines cannot be distinguished because they overlap.

3.2 Benchmark model behavior

Figure 1b-i shows two years of simulated daily behavior driven by the Smith River daily precipitation record applied to the damped and flashy catchment parameter sets. The simulated stream discharge responds promptly to rainfall inputs, and unsurprisingly the discharge response is larger in the flashy catchment (Fig. 1b-c). The streamflow isotopic response is strongly damped in both catchments, with isotope ratios between events returning to a relatively stable baseline value

composed mostly of discharge from the lower box (Fig. 1d-e). Like the stream discharge and the isotope tracer time series, the instantaneous new water fractions (determined by age tracking within the model) also exhibit complex nonstationary dynamics (Fig. 1f-i). Despite the complexity of the modeled time-series behavior, ensemble hydrograph separation (Eqs. 14, 18, 21, and 28) accurately predicts the averages of these new water fractions, both unweighted and time-weighted, as can be seen by comparing the dashed and solid lines (which sometimes overlap) in Fig. 1f-i.

It should be emphasized that the ensemble hydrograph separation and the benchmark model are completely independent of one another. The ensemble hydrograph separation does not know (or assume) anything about the internal workings of the benchmark model; it knows only the input and output water fluxes and their isotope signatures. This is crucial for it to work in the real world, where any particular assumptions about the processes driving runoff could potentially be violated. Likewise, the benchmark model is not designed to conform to the assumptions underlying the ensemble hydrograph separation method. It would be relatively trivial to model a tracer time series assuming that "new water" constituted a fixed fraction of discharge, and then demonstrate that this fraction can be retrieved from the tracer behavior. What Fig. 1 demonstrates is much less obvious, and more important: that even when the new water fraction is highly dynamic and nonstationary, an appropriate analysis of tracer behavior can accurately estimate its mean.

3.3 Benchmark tests: random parameter sets

This result holds not just for the two parameter sets shown in Fig. 1, but throughout the parameter ranges that are tested in the benchmark model. The scatterplots shown in Fig. 2 show new water fractions estimated by ensemble hydrograph separation, compared to the true average new water fractions determined by age tracking in the benchmark model, for 1000 random parameter sets spanning the parameter ranges described in Sect. 3.1. Figure 2 shows that ensemble hydrograph separation yields reasonably accurate estimates of average event new water fractions (Fig. 2a, b), new water fractions of discharge (Fig. 2c) and precipitation (Fig. 2d), and volume-weighted new water fractions (Fig. 2e, f). Estimates derived from single years of data (Fig. 2b) understandably exhibit greater scatter than those derived from five years of data (Fig. 2a), but in all of the plots shown in Fig. 2 there is no evidence of significant bias (the data clouds cluster around the 1:1 lines). The scatter of the points around the 1:1 line generally agrees with the standard errors estimated from Eqs. 11, 15 and 20, suggesting that these uncertainty estimates are also reliable.
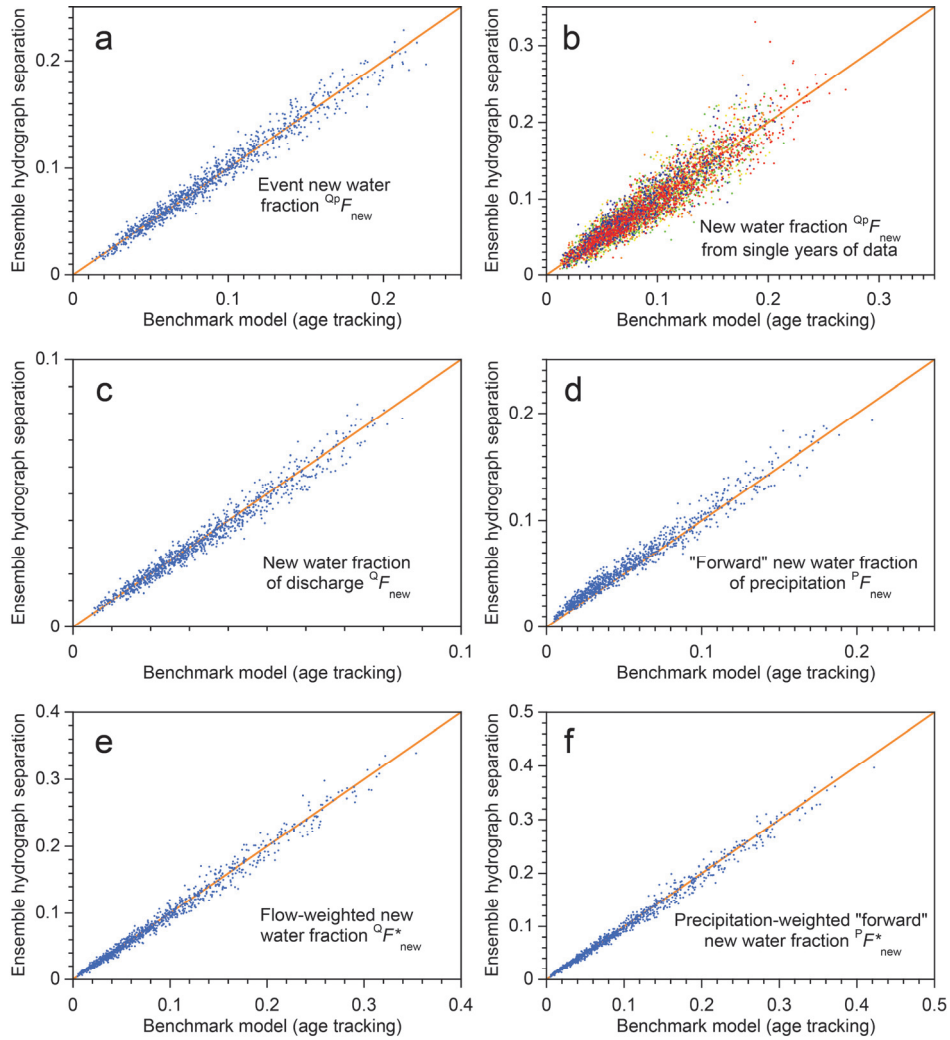
Figure 2. New water fractions predicted from tracer dynamics using ensemble hydrograph separation, compared to averages of time-varying new water fractions determined from age tracking in the benchmark model. Diagonal lines show perfect agreement. Each scatterplot shows 1000 points, each of which represents an individual catchment, with its own individual random set of model parameters (i.e., catchment characteristics), randomly generated precipitation tracer time series, and random set of measurement errors and missing values (see Sect. 3.1). The daily precipitation amounts are the same (Smith River time series; Mediterranean climate) in each case. The "event new water fraction" (panels a and b) is the average fraction of new (same-day) water in streamflow during time steps with precipitation, as described in Sect. 2.3. Panel (a) shows event new water fractions estimated from five years of simulated tracer data; panel (b) shows the same quantity estimated from single years (each year is denoted by a different color). Averaging over the five years reduces both the range and the scatter, compared to the single-year estimates. The new water fraction of discharge (panel c) is the fraction of same-day precipitation in streamflow, averaged over all time steps including rainless periods (Eq. 14, Sect. 2.4); its flow-weighted counterpart (panel e) is calculated using Eqs. (16)-(18) of Sect. 2.5. The "forward" new water fraction (the fraction of precipitation that becomes same-day streamflow; panel d) is calculated using Eq. (21), and its precipitation-weighted counterpart (panel f) is calculated using Eq. (28). In all cases there is little evidence of bias, and the scatter around the 1:1 line is relatively small.

Mean transit times have often been estimated in the catchment hydrology literature, often under the assumption that they should also be correlated with other time scales of catchment transport and mixing as well. This naturally leads to the question, in the context of the present study, of whether there is a systematic relationship between mean transit times and new water fractions, such that they could potentially be predicted from one another. The benchmark model allows a direct

5   test of this conjecture, because it tracks mean water ages as well as new water fractions. Figure 3a shows that, across the 1000 random parameter sets from Fig. 2, the relationship between new water fractions and mean transit times is a nearly perfect shotgun blast: mean transit times vary from about 40 to 400 days and new water fractions vary from nearly zero to nearly 0.1, with almost no correlation between them. Both of these quantities are estimated from age tracking in the benchmark model, so their lack of any systematic relationship does not arise from difficulties in estimating either of them

10   from tracer data. It instead arises because the upper tails of transit time distributions (reflecting the amounts of streamflow with very old ages) exert strong influence on mean transit times, but have no effect on new water fractions (reflecting same-day streamflow).

I have recently proposed the "young water fraction", the fraction of streamflow younger than about 2.3 months, as a more

15   robust metric of water age than the mean transit time (Kirchner, 2016b). Fig. 3b shows that, like the mean transit time, the young water fraction is also a poor predictor of the new water fraction, beyond the obvious constraint that new water ($\leq$1 day old) must be a small fraction of "young" water ($\leq$69 days old). The new water fraction will only be correlated with the young water fraction or mean transit time if the shape of the underlying transit time distribution is held constant, which is not the case for the 1000 random parameter sets considered here, and is unlikely to be true in real-world catchments either.
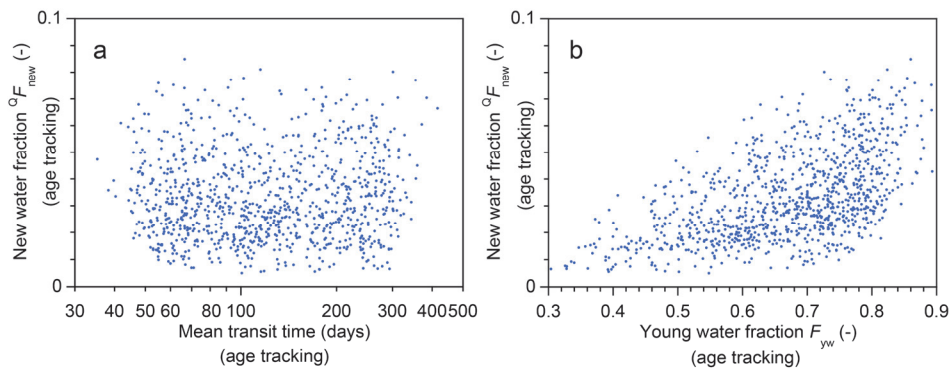
Figure 3. Average new water fractions (same-day precipitation in streamflow) for the 1000 simulated catchments (i.e., 1000 model parameter sets) shown in Fig. 2, compared to the catchment mean transit time and the young water fraction F_{yw} (the fraction of streamflow younger than 2.3 months). All values plotted here are determined from age tracking within the benchmark model, and

25   **thus are true values, without any errors associated with estimating these quantities from tracer data. Neither mean transit time nor the young water fraction can reliably predict the fraction of new water in streamflow.**

3.4 Benchmark tests: weekly tracer sampling

Many long-term water isotope time series have been sampled at weekly intervals. Can new water fractions be estimated reliably from such sparsely sampled records? To find out, I aggregated the benchmark model's daily time series to weekly intervals, volume-weighting the isotopic composition of precipitation to simulate the effects of weekly bulk precipitation sampling, and sub-sampling streamflow isotopes every seventh day to simulate weekly grab sampling. I then performed ensemble hydrograph separation on the aggregated weekly data, using the methods presented in Sect. 2.
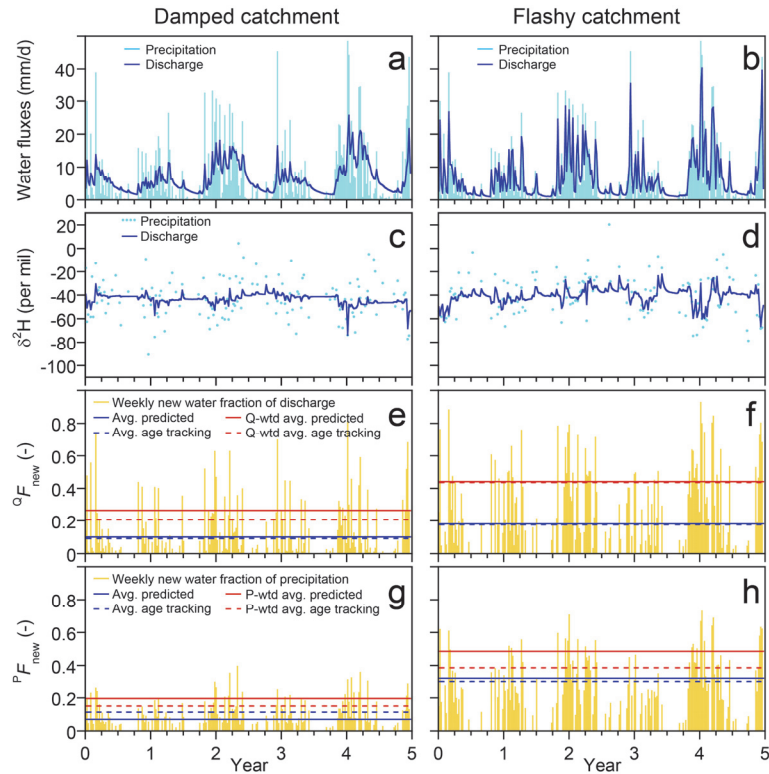
Figure 4. Illustrative simulations of weekly water fluxes, deuterium concentrations, and new water fractions. The benchmark model, precipitation forcing, and parameter values are identical to those in Fig. 1. Although the isotope tracer concentrations and new water fractions exhibit complex nonstationary dynamics, ensemble hydrograph separation yields reasonable estimates of the average "backward" and "forward" weekly new water fractions, as shown in panels (e-f) and (g-h), respectively. Panels (a-b) show weekly average rates of precipitation and discharge. Panels (c-d) show the weekly volume-weighted isotopic composition of precipitation (mimicking what would be collected in a weekly rain sample), and the instantaneous composition of discharge at the end of each week (mimicking what would be collected in a weekly grab sample). Panels (e-f) show the fraction of discharge that is composed of same-week precipitation (the weekly new water fraction; yellow lines), as determined from model age tracking, and its long-term average (dashed blue line), compared to the new water fraction predicted by ensemble hydrograph separation (solid blue line) from the weekly samples shown in panel (b). Panels (g-h) show the fraction of precipitation that becomes same-week discharge (the weekly new water fraction of precipitation, or "forward" new water fraction, yellow lines) as determined from model age tracking, and its long-term average (dashed blue line), compared to the new water fraction predicted by ensemble hydrograph separation (solid blue line). Discharge-weighted and precipitation-weighted average new water fractions, and their predicted values, are shown by red solid and dashed lines.
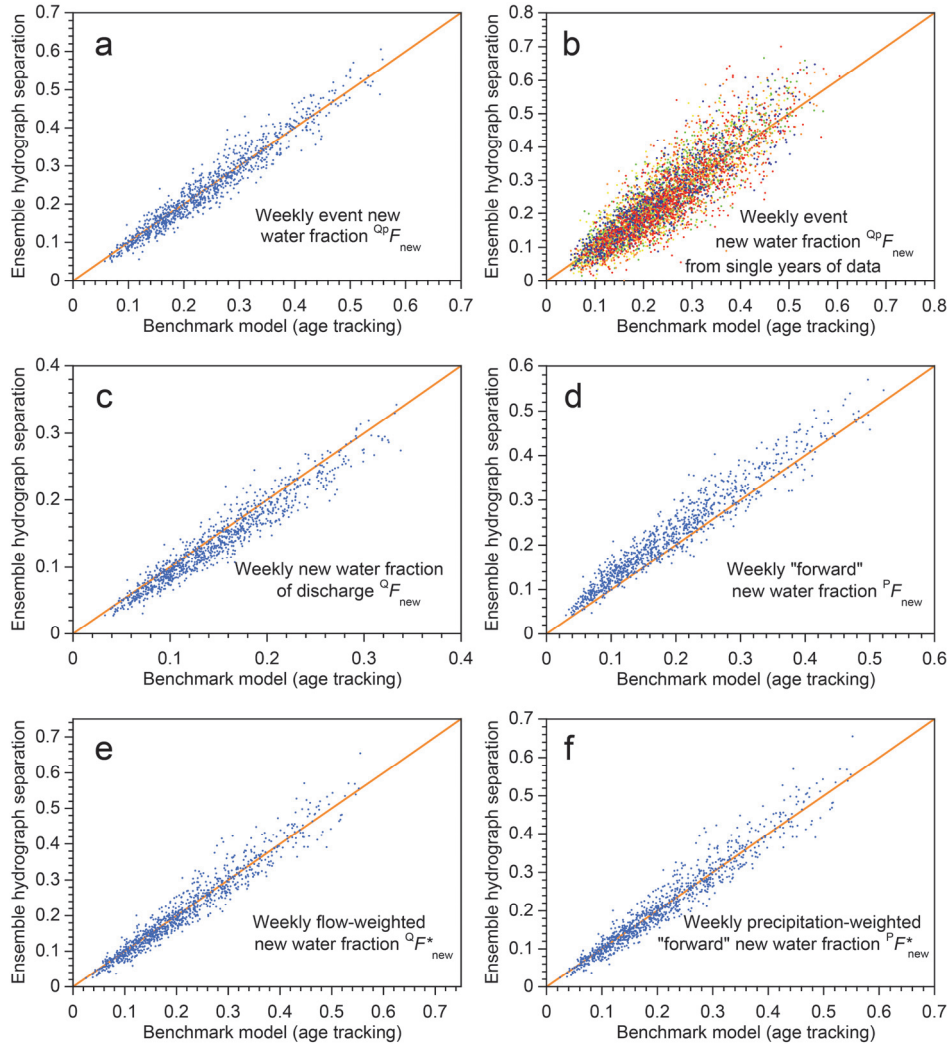
Figure 5. New water fractions estimated from weekly tracer dynamics using ensemble hydrograph separation, compared to averages of time-varying new water fractions determined from age tracking in the benchmark model. Plots are similar to those in Fig. 2, except here they are derived from simulated weekly sampling of tracer concentrations in precipitation and streamflow. Diagonal lines show perfect agreement. Each scatterplot shows 1000 points, each representing an individual random set of parameters, a randomly generated precipitation tracer time series, and a random set of measurement errors and missing values (see Sect. 3.1). The daily precipitation amounts are the same (Smith River time series) in each case. The "event new water fraction" (panels a and b) is the average fraction of new (same-day) water in streamflow during time steps with precipitation, as described in Sect. 2.3. Panel (a) shows event new water fractions estimated from five years of simulated weekly tracer data; panel (b) shows the same quantity estimated from single years of simulated weekly tracer data (each year is denoted by a different color). Averaging over the five years reduces scatter compared to the individual-year estimates. The new water fraction of discharge (panel c) is the fraction of same-day precipitation in streamflow, averaged over all time steps including rainless periods (Eq. 14, Sect. 2.4); its flow-weighted counterpart (panel e) is calculated using Eqs. (16)-(18) of Sect. 2.5. The "forward" new water fraction (the fraction of precipitation that becomes same-day streamflow; panel d) is calculated using Eq. (21), and its precipitation-weighted counterpart (panel f) is calculated using Eq. (28). There is only slight visual evidence of bias, and the scatter around the 1:1 line is small compared to the range spanned by the new water fractions.

Figure 4 shows the behavior of the benchmark model at weekly resolution for both the damped and flashy catchments. At the weekly time scale, the benchmark model exhibits complex nonstationary dynamics in discharge (panels a-b), water isotopes (panels c-d), and new water fractions (panels e-h). Nonetheless – and even though the weekly sampling timescale is much longer than the timescales of hydrologic response in the system – ensemble hydrograph separation yields reasonable
5 estimates for the mean new water fractions of both precipitation and discharge (both unweighted and flow-weighted), as one can see by comparing the dashed and solid lines in Fig. 4e-h.

A comparison of Figs. 1 and 4 shows that the isotopic signature of precipitation is less variable among the weekly samples than among the daily samples, reflecting the fact that the weekly bulk samples of precipitation will inherently average over
10 the sub-weekly variability in daily rainfall. By contrast, the weekly grab samples of streamflow lose all information about what is happening on shorter time scales. The new water fractions calculated from the weekly data are distinctly higher than those calculated from the daily data, owing to the fact that the definition of "new" water depends on the sampling frequency: the proportion of water ≤7 days old ("new" under weekly sampling) can never be less than the proportion ≤1 day old ("new" under daily sampling).

Figure 5 shows scatterplots comparing new water fractions estimated by ensemble hydrograph separation and those determined by age tracking in the benchmark model, analogous to Fig. 2 but for weekly instead of daily sampling. The weekly new water fractions are larger than the daily ones, for the reasons described above, and exhibit more scatter because they are based on fewer data points than their daily counterparts are. A small overestimation bias is visually evident in Fig.
20 2d, and an even smaller underestimation bias in Fig. 2c. These reservations notwithstanding, Fig. 5 shows that ensemble hydrograph separation can reliably predict new water fractions of both discharge and precipitation, with and without volume-weighting, based on weekly tracer samples.

3.5 Variations in new water fractions with discharge, precipitation, and seasonality

Ensemble hydrograph separation does not require continuous data as input, so it can be used to estimate F_{new} values for
25 (potentially discontinuous) subsets of a time series that reflect conditions of particular interest. For example, if we split the time series shown in Fig. 1 into several discharge ranges, we can see that at higher flows, tracer fluctuations in the stream are more strongly correlated with tracer fluctuations in precipitation (Fig. 6a-b). Each of the regression slopes in Fig. 6a-b defines the event new water fraction $^{Qp}F_{new}$ for the corresponding discharge range. Repeating this analysis for each 10-percent interval of the discharge distribution (0-10th percentile, 10th-20th percentile, etc.), plus the 95th-100th percentile, yields
30 the profiles of $^{Qp}F_{new}$ as functions of discharge, as shown by the blue dots in Fig. 6c-h. The green squares show the corresponding "forward" new water fractions $^{P}F_{new}$ for comparison. The light blue and light green lines show the corresponding true new water fractions determined by age tracking in the benchmark model.
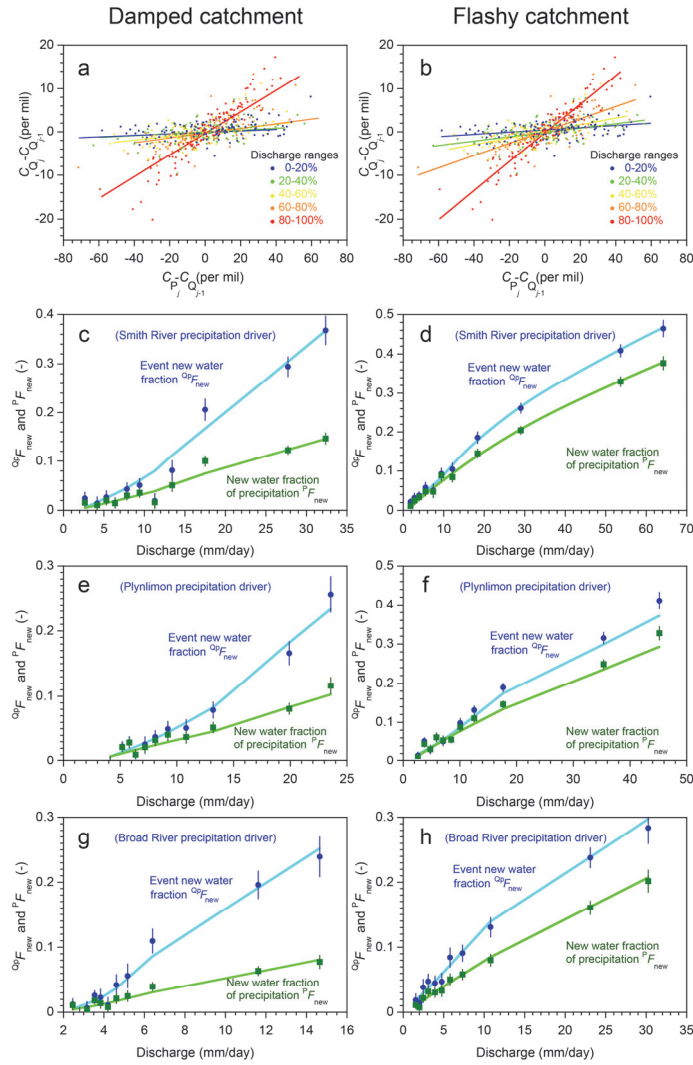
Figure 6. Variations in new water fractions across ranges of discharge. (a,b) Relationship between tracer concentrations in precipitation and streamflow in the benchmark model run shown in Fig. 1, stratified by percentiles of the frequency distribution of discharge, for damped and rapid response parameter sets. In these coordinates, the slopes of the regression lines through the ensembles of points estimate their average event new water fractions $^{Qp}F_{new}$ (Eq. 10; Sect. 2.3). **(c-h)** Variation in new water fractions across discharge bins in the benchmark model. Dark blue and green symbols show estimates of the event new water fraction of discharge ($^{Qp}F_{new}$) and the "forward" new water fraction (fraction of precipitation appearing in same-day streamflow, $^{P}F_{new}$, Eq. 21) for each decile of the daily discharge distribution (the left-most 10 points) and the uppermost 5 percent (the right-most point). Error bars show standard errors, where these are larger than the plotting symbols. Light blue and light green lines show the corresponding "true" new water fractions measured by age tracking in the benchmark model. The three rows (c-d, e-f, and g-h) show catchment response to three different precipitation climatologies (Smith River, Plynlimon, and Broad River), for both the damped response parameter set (left-hand plots c, e, and g) and the flashy response parameter set (right-hand plots d, f, and h). The new water fractions $^{Qp}F_{new}$ and $^{P}F_{new}$ vary strongly with discharge. Ensemble hydrograph separation accurately estimates both $^{Qp}F_{new}$ and $^{P}F_{new}$ across the full range of discharge for all three forcings and both parameter sets.
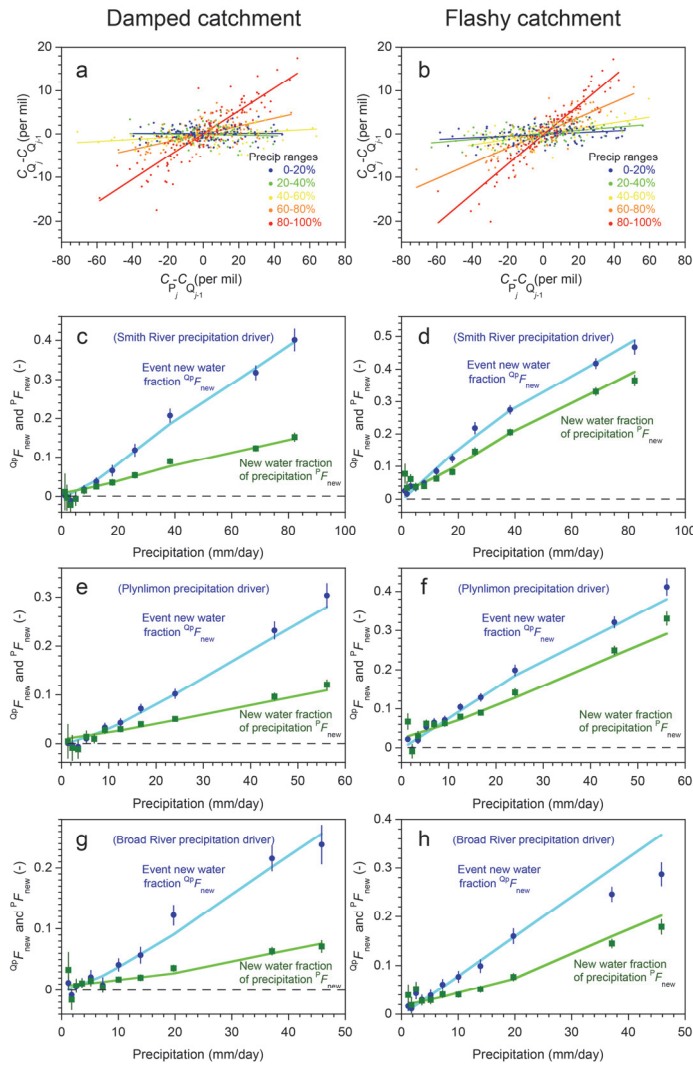
Figure 7. Variations in new water fractions across ranges of precipitation. (a,b) Relationship between tracer concentrations in precipitation and streamflow in the benchmark model run shown in Fig. 1, stratified by percentiles of the frequency distribution of precipitation, for damped and rapid response parameter sets. In these coordinates, the slope of the regression line through each ensemble of points estimates its average event new water fraction $^{Qp}F_{new}$ (Eq. 10; Sect. 2.3). (c-h) Variation in new water fractions across precipitation bins in the benchmark model. Dark blue and green symbols show estimates of the event new water fraction of discharge ($^{Qp}F_{new}$) and the "forward" new water fraction ($^{P}F_{new}$, the fraction of precipitation appearing in same-day streamflow; Eq. 21). Average $^{Qp}F_{new}$ and $^{P}F_{new}$ values are plotted for each decile of the daily precipitation distribution (the left-most 10 points) and the uppermost 5 percent (the right-most point), excluding precipitation amounts less than 1 mm/day (see text). Error bars show standard errors, where these are larger than the plotting symbols. Light blue and light green lines show the corresponding "true" new water fractions measured by age tracking in the benchmark model. The three rows (c-d, e-f, and g-h) show catchment response to three different precipitation climatologies (Smith River, Plynlimon, and Broad River), for both the damped response parameter set (left-hand plots c, e, and g) and the flashy response parameter set (right-hand plots d, f, and h). The new water fractions $^{Qp}F_{new}$ and $^{P}F_{new}$ vary strongly with daily precipitation. Ensemble hydrograph separation accurately estimates both $^{Qp}F_{new}$ and $^{P}F_{new}$ across the full range of precipitation for all three forcings and both parameter sets.

If, instead, we split the time series shown in Fig. 1 into subsets reflecting ranges of precipitation rates rather than discharge, we obtain Fig. 7. Figure 7 is a counterpart to Fig. 6, but with $^{Qp}F_{new}$ and $^{P}F_{new}$ plotted as functions of rainfall rates rather than discharge. The two figures exhibit broadly similar behavior. Unsurprisingly, new water fractions are higher at higher discharges and rainfall rates, because under these conditions a higher fraction of discharge comes from the upper box, which

5   has younger water. "Forward" new water fractions are typically smaller than event new water fractions, because during storms the rainfall rate is higher than the streamflow rate, so the ratio between same-day streamflow and the total rainfall rate ($^{P}F_{new}$) will necessarily be smaller than the ratio between same-day streamflow and the total streamflow rate ($^{Qp}F_{new}$). Exceptions to this rule arise when rainfall rates are lower than discharge rates, such as during periods of light rainfall while streamflow is still undergoing recession from previous heavy rain. Thus the green and blue curves cross over one another at

10   the left-hand edges of Figs. 7c-h, whereas in Figs. 6c-h they do not.

Three conclusions can be drawn from Figs. 6 and 7. First, in these model catchments, new water fractions vary dramatically between low flows and high flows, and between low and high precipitation rates, with the event new water fraction $^{Qp}F_{new}$ and the forward new water fraction $^{P}F_{new}$ diverging from one another more at higher flows and higher rainfall forcing.

15   Second, different catchment parameters (different columns in Fig. 6) and different precipitation forcings (different rows in Fig. 6) yield different patterns in the relationships between the new water fractions $^{Qp}F_{new}$ and $^{P}F_{new}$ on the one hand, and precipitation and discharge on the other. And third, these patterns are accurately quantified by ensemble hydrograph separation, which matches the age tracking results (shown by the solid lines) within the estimated standard errors in most cases.

Thus the patterns describing how new water fractions change with precipitation and discharge may be useful as signatures of catchment transport behavior, and can be estimated directly from tracer time series using ensemble hydrograph separation. These observations raise the question of whether any of these signatures of behavior, as inferred from the patterns in these plots (if not the individual numerical values) might imply something useful about the characteristics of the catchments

25   themselves, ideally in a way that is not substantially confounded by precipitation climatology. A comprehensive answer is not possible within the scope of this paper, since it focuses mostly on just two parameter sets and three precipitation records. But as a first approach, one can try superimposing the results in Figs. 6 and 7 on consistent axes (note that the axes in these figures' various panels differ from one another in order to show the full range of behavior). Doing so yields Fig. 8, which overlays the age tracking results from Figs. 6c-h and 7c-h in its left- and right-hand panels, respectively. In Fig. 8,

30   catchments with the damped and flashy parameter sets are denoted by green and blue curves, respectively, with different levels of brightness corresponding to the three different precipitation climatologies. The key question is: are there patterns in $^{Qp}F_{new}$ or $^{P}F_{new}$ that clearly distinguish the flashy catchment from the damped catchment, regardless of the precipitation forcing? Figure 8a shows an example where this is not the case; instead, the two catchments' behaviors largely overlap in a

tangle of blue and green lines. In the other three panels, however (and particularly for the trends in ^PF_new as a function of precipitation rates, as shown in Fig. 8d), the blue and green curves are relatively distinct from one another, but the different climatologies largely overlap for each catchment. This result suggests that these traces may be useful as diagnostic signatures of catchment characteristics, which are relatively insensitive to precipitation climatology. However, Fig. 8 can

5   only be considered a preliminary indication of what might be possible, rather than a definitive demonstration.
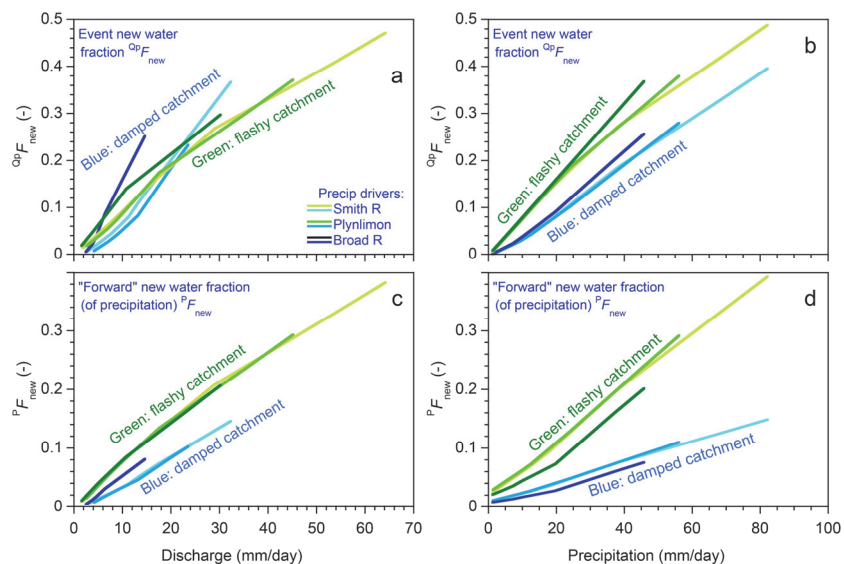
Figure 8. Effects of precipitation climatology and catchment properties on discharge- and precipitation-dependence of new water fractions. The lines plotted here superimpose the model age tracking results (solid lines) from Figs. 6 and 7. Left and right panels
10   **show how event new water fractions ($^{Qp}F_\text{new}$, Sect. 2.3) and "forward" new water fractions (^PF_new, Sect. 2.6) vary as functions of discharge and precipitation, respectively. Green and blue lines show benchmark model behavior under the flashy and damped parameter sets, with three levels of brightness corresponding to the three different precipitation climatologies: Mediterranean climate (Smith River, lightest colors), humid maritime climate (Plynlimon, intermediate colors), and humid temperate climate (Broad River, darkest colors). When event new water fractions are plotted as functions of discharge (panel a), different**
15   **catchments and precipitation climatologies overlap. By contrast, in the other three panels (and particularly in panel d, which shows "forward" new water fractions as functions of precipitation), the lines for the flashy catchment and the damped catchment are clearly distinct from one another, regardless of precipitation climatology. This suggests that these patterns may be diagnostic of the internal workings of the catchment, but relatively insensitive to the particular rainfall forcing.**

20   The behavior summarized in Figs. 6-8 shows that in general, new water fractions are functions of both catchment characteristics and precipitation climatology. Moreover, new water fractions will depend on the sequence of precipitation events, not just on their frequency distribution, because they will depend on antecedent wetness. Thus although the ensemble hydrograph separation approach does not require continuous data, and thus can be applied to time series with data gaps, any inferred new water fractions will obviously represent only the particular time intervals that are included in the
25   analysis.
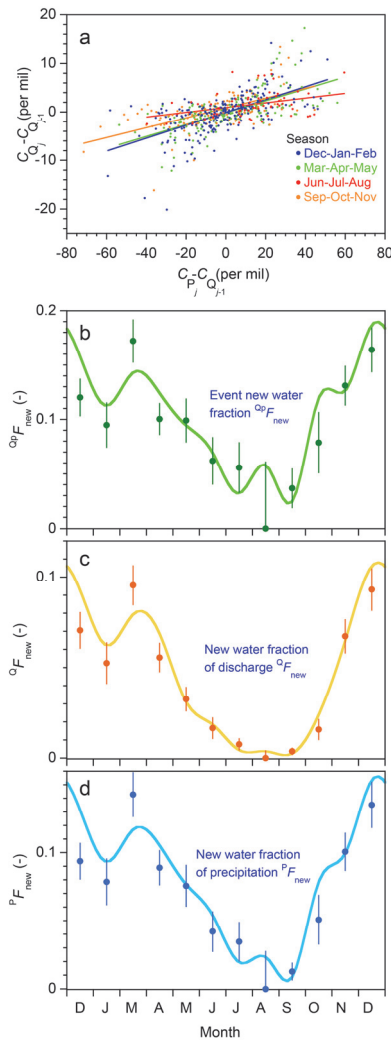
Figure 9. Seasonality in new water fractions under Mediterranean climate precipitation forcing. (a) Relationship between tracer concentrations in precipitation and streamflow in the flashy benchmark model run shown in Fig. 1, stratified by season. Each season's event new water fraction can be estimated from the slope of the regression line fitted to the corresponding set of points.

5   **(b,c,d) Average event new water fractions ($^{Qp}F_{new}$), new water fractions of discharge ($^{Q}F_{new}$), and "forward" new water fractions of precipitation ($^{P}F_{new}$) calculated from ensembles of all points within each month, across the five years of benchmark model simulations. Error bars show standard errors, where these are larger than the plotting symbols. Curves are drawn through true monthly average new water fractions, as determined by age tracking in the benchmark model. Ensemble hydrograph separation reproduces this seasonal pattern in new water fractions reasonably well. The uncertainty estimates also realistically predict the**

10   **average deviation of the ensemble hydrograph separation estimates from the "true" age tracking determinations. Values shown here are generated by the benchmark model with the flashy catchment parameter set and Smith River (Mediterranean climate) precipitation forcing. The new water fractions would exhibit less pronounced seasonality if the rainfall forcing were less strongly seasonal or the catchment response were less flashy.**

15   One implication of the forgoing considerations is that seasonal differences in storm size and frequency should also be reflected in seasonal variations in new water fractions. Figure 9a shows a scatterplot of tracer fluctuations in streamflow and

precipitation, color-coded by season, for the "flashy" catchment simulation shown in Fig. 1. The regression lines (whose slopes define the event new water fractions $^{Qp}F_{new}$ for the corresponding seasons) show that tracer concentrations in streamflow and precipitation are more tightly coupled in winter and spring than in summer and autumn. Figures 9b-d demonstrate large variations in the event new water fraction $^{Qp}F_{new}$, the new water fraction of discharge $^{Q}F_{new}$, and the

5   "forward" new water fraction of precipitation $^{P}F_{new}$ from month to month, with a broad seasonal trend towards larger new water fractions in winter and spring. The month-to-month variations in the age tracking results (the smooth curves) are usually quantified by the ensemble hydrograph separation estimates (the solid dots) within their calculated uncertainties (as shown by the error bars). Thus Fig. 9 suggests that ensemble hydrograph separation can be used to quantify how catchment transport behavior is shaped by seasonal patterns in precipitation forcing.

10   **3.6 Effects of evaporative fractionation**

Any analysis based on water isotopes must deal with the potential effects of isotopic fractionation due to evaporation (e.g., Laudon et al., 2002; Taylor et al., 2002; Sprenger et al., 2017; Benettin et al., 2018). A detailed treatment of evaporative fractionation would necessarily be site-specific and thus beyond the scope of this paper. Nonetheless, it is possible to make a simple first estimate of how much evaporative fractionation could affect new water fractions estimated from ensemble

15   hydrograph separation. The benchmark model does not explicitly simulate evapotranspiration and its effects on the catchment mass balance, but the issue to be addressed here is different: how much could evaporative fractionation alter the isotope values measured in streamflow, and how could this affect the resulting estimates of new water fractions?

To explore this question, I first adjusted the isotope values of infiltration entering the model in Fig. 1 to mimic the effects of

20   seasonally varying evaporative fractionation. I assumed that evaporative fractionation was a sinusoidal function of the time of year, ranging from zero in mid-winter to 20 per mil in mid-summer. Thus I assumed that evaporative fractionation effectively doubled the seasonal isotopic cycle in the water entering the model catchment (but in not the sampled rainfall itself, since any fractionation that occurs before the rainfall is sampled will not distort the ensemble hydrograph separation). I then calculated new water fractions based on the time series of sampled precipitation tracer concentrations and of

25   streamflow tracer concentrations (altered by the lagged and mixed effects of evaporative fractionation), and compared these to the "true" new water fractions calculated by age tracking within the model.

The results are shown in Fig. 10, which compares 1000 Monte Carlo trials with evaporative fractionation (the blue dots) and another 1000 Monte Carlo trials without evaporative fractionation (the gray dots). One can see that in these simulations,

30   evaporative fractionation leads to a slight tendency to underestimate new water fractions. Nonetheless, the blue and gray dots largely overlap, and both generally follow the 1:1 lines. These results are reassuring, because the modeled fractionation effects were designed to be a worst-case scenario, in the following sense. Because ensemble hydrograph separation is based

on patterns of fluctuations in precipitation and streamflow tracers, any fractionation process that created a constant offset between inputs and outputs would introduce no bias. For the same reason, any fractionation process that was uncorrelated to the input isotopic signature would also introduce no bias; thus, for example, the modeled seasonal fractionation cycle would have had no effect if there were no seasonal pattern in the precipitation isotopes themselves. But because the seasonal fractionation cycle is correlated with the seasonal pattern in the precipitation isotopes, it can potentially bias the resulting estimates of new water fractions. The fact that these biases are small, as shown in Fig. 10, suggests that ensemble hydrograph separation should yield realistic estimates of new water fractions, even with substantial confounding by evaporative fractionation.
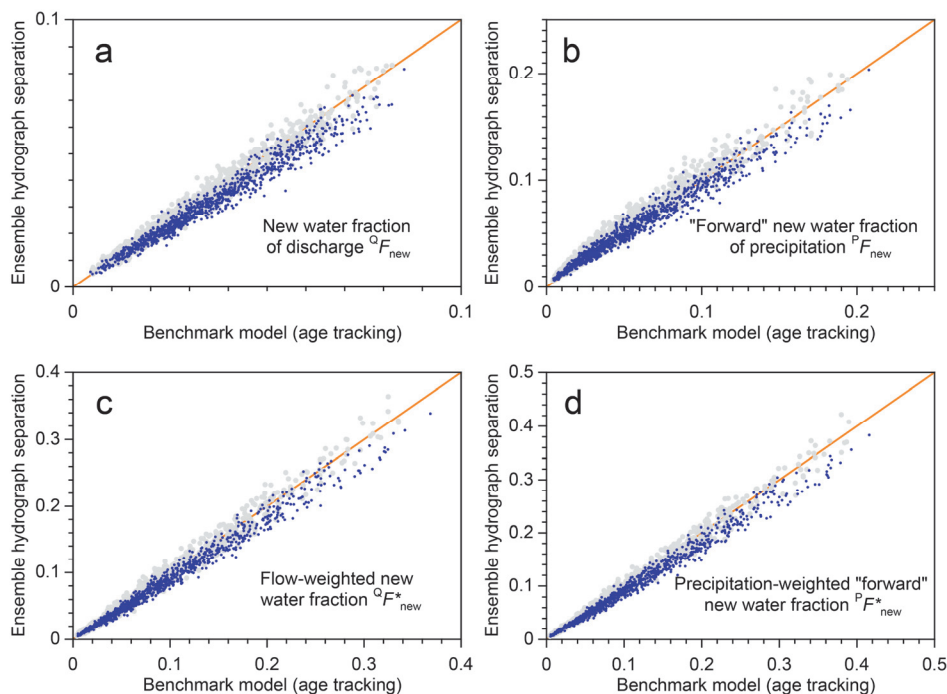
Figure 10. Effects of seasonally varying evaporative fractionation on new water fractions estimated by ensemble hydrograph separation. Points show new water fractions predicted from tracer fluctuations in precipitation and streamflow (on the y-axis), compared to averages of time-varying new water fractions determined by age tracking in the benchmark model (on the x-axis). Blue points show 1000 model runs in which precipitation undergoes seasonally varying evaporative fractionation ranging from zero in winter to 20 per mil in summer. Gray background points show 1000 model runs without evaporative fractionation (analogous to Fig. 2). Each model run has a different random set of model parameters, measurement errors, and missing values, but the precipitation driver (Smith River daily precipitation) is the same in all cases. The blue data clouds closely follow the 1:1 line, indicating that ensemble hydrograph separation can reliably estimate new water fractions even in the presence of substantial evaporative fractionation.

4 Estimating transit time distributions by ensemble hydrograph separation

A natural extension of the approach outlined in Sect. 2 would be to quantify the contributions of precipitation to streamflow over a range of lag times: to quantify, in other words, the catchment transit time distribution. In principle this should be straightforward, although in practice several challenges must be overcome. Below, I describe these issues and outline

5 techniques for addressing them. Readers who are not interested in the methodological details can proceed directly from Sect. 4.1 to Sect. 4.5, skipping over Sects. 4.2-4.4.

4.1 Definitions

I assume that catchment inputs and outputs are sampled at the same fixed time interval Δt, and define the time that a parcel of water enters the catchment (via rainfall, snowmelt, etc.) as t_i and the time that it exits via streamflow as t_j. The lag

10 interval between precipitation and streamflow is indexed as $k = j\text{-}i$. P_i is the rate that precipitation or snowmelt (net of evaporative losses) enters the catchment at time t_i, and Q_j is the rate of discharge that exits the catchment at time t_j. C_{P_i} and C_{Q_j} are the tracer concentrations in precipitation and streamflow, respectively. The water flux that enters as precipitation at time t_i and leaves as streamflow k time steps later (at time $t_j = t_{i+k}$) is represented as q_{jk}. The sum of q_{jk} over all lag times k (corresponding to all previous entry times $i = j\text{-}k$) is the total discharge Q_j. Each of the q_{jk} will be a fraction of the total

15 precipitation falling at time $t_{i=j\text{-}k}$ and a (typically different) fraction of the total discharge at time t_j. The fraction of discharge exiting at time t_j that entered k time steps earlier is q_{jk}/Q_j, and the distribution of q_{jk}/Q_j over lag time k yields the transit time distribution conditioned on the exit time t_j (also called the "backward" transit time distribution). The fraction of precipitation entering at time t_i that subsequently leaves as streamflow k time steps later is $q_{jk}/P_{j-k} = q_{i+k,k}/P_i$, and the distribution of $q_{i+k,k}/P_i$ over lag time k yields the transit time distribution conditioned on the entry time t_i (also called the

20 "forward" transit time distribution).

In practice, precipitation fluxes are typically measured as averages over discrete time intervals, and tracer concentrations in precipitation are likewise volume-averaged over discrete intervals (such as a day or a week) during which the sample accumulates in the precipitation collector. By contrast, discharge fluxes are typically measured instantaneously, and

25 discharge tracer concentrations are typically measured in instantaneous grab samples. In most of what follows, I will assume that P_i and C_{P_i} are averages over the interval $t_{(i-1)} < t \leq t_i$, and Q_j and C_{Q_j} are instantaneous values at $t = t_j$. However, in a few catchment studies, discharge concentrations have instead been measured in time-integrated samples. The analysis presented below is the same, whether the discharge tracer concentrations C_{Q_j} are instantaneous at $t = t_j$ or are integrated over each time interval $t_{(j-1)} < t \leq t_j$. The interpretation is slightly different, however, because the average lag time

30 corresponding to a given lag interval k will depend on how precipitation and streamflow are sampled. Usually, streamwater samples are collected more-or-less instantaneously (grab sampling), and precipitation samples are integrated over the time

interval that the sampler is open. A typical daily sampling scheme, for example, might involve collecting a precipitation sample at noon (which integrates precipitation that fell over the previous 24 hours), and also collecting a grab sample of streamflow at noon. In this case, the average lag time between a raindrop falling as precipitation and being sampled in the same day's streamflow (i.e., $k = 0$) would be 12 hours, assuming that, on average, the probability of rainfall is independent

5   of the time of day. Thus in this conventional sampling scheme, the average lag time will be $(k + 0.5)\Delta t$, where Δt is the sampling interval. If, instead, the stream samples were daily composites, then (for example) the "same day" raindrops appearing the first hour's subsample of streamflow would have an average lag time of 30 minutes, the second hour's would be 60 minutes, and so forth, and therefore the daily average lag time would be 6 hours. Thus if stream samples are time-integrated composites, the average lag time will be $(k + 0.25)\Delta t$.

I now outline the fundamentals of the ensemble hydrograph separation approach to estimating transit time distributions. Conservation of water mass requires that the discharge at time step j equals the contributions from all lag times k (corresponding to all previous entry times $i = j\text{-}k$):

$$Q_j = \sum_{k \geq 0} q_{jk} \quad . \tag{31}$$

15   Because tracing contributions to streamflow from all previous time steps would be impractical, it will be necessary to truncate the summation in (31) at some maximum lag, which I will denote as m, and to combine the unmeasured older contributions in a water flux Q_{older_j}:

$$Q_j = \sum_{k=0}^{m} q_{jk} + Q_{\text{older}_j} \quad , \qquad Q_{\text{older}_j} = \sum_{k=m+1}^{\infty} q_{jk} = Q_j - \sum_{k=0}^{m} q_{jk} \quad . \tag{32}$$

Conservation of tracer mass requires that the tracer fluxes add up similarly, again with a catch-all flux $Q_{\text{older}_j} C_{\text{older}_j}$:

20   $$Q_j C_{Q_j} = \sum_{k=0}^{m} q_{jk} C_{P_{j-k}} + Q_{\text{older}_j} C_{\text{older}_j} = \sum_{k=0}^{m} q_{jk} C_{P_{j-k}} + \left(Q_j - \sum_{k=0}^{m} q_{jk} \right) C_{\text{older}_j} \quad . \tag{33}$$

Dividing (33) by Q_j and rearranging terms directly yields

$$\left(C_{Q_j} - C_{\text{older}_j} \right) = \sum_{k=0}^{m} \frac{q_{jk}}{Q_j} \left(C_{P_{j-k}} - C_{\text{older}_j} \right) \quad , \tag{34}$$

which readers will recognize as the multi-lag counterpart of Eq. (7).

25   Analogous to the approach in Sect. 2, here I account for the concentration of older inputs C_{older_j} using the streamflow concentration at lag $m + 1$, just beyond the longest lag m, with the goal of filtering out long-term patterns that could

otherwise distort the correlations between $C_{P_{j-k}}$ and C_{Q_j}. Thus $C_{Q_{j-m-1}}$ serves as a reference level for measuring fluctuations in precipitation and streamflow tracer concentrations, analogous to $C_{Q_{j-1}}$ in Eq. (8). Adding a bias term α and an error term ε_j yields

$$\left(C_{Q_j} - C_{Q_{j-m-1}}\right) = \sum_{k=0}^{m} \frac{q_{jk}}{Q_j}\left(C_{P_{j-k}} - C_{Q_{j-m-1}}\right) + \alpha + \varepsilon_j \quad , \tag{35}$$

5   which almost looks like a conventional multiple linear regression equation,

$$y_j = \sum_{k=0}^{m} \beta_k \, x_{jk} + \alpha + \varepsilon_j \quad , \tag{36}$$

where

$$y_j = \left(C_{Q_j} - C_{Q_{j-m-1}}\right) \quad \text{and} \quad x_{jk} = \left(C_{P_{j-k}} - C_{Q_{j-m-1}}\right) \quad , \tag{37}$$

with the difference that the coefficients β_k in (36) are constant over all exit times j and differ only as a function of the lag

10   time k, whereas the q_{jk}/Q_j terms in (35) can differ among both lag times k and exit times j. Nonetheless, by analogy with the mathematical arguments in Appendix A and those at the end of Appendix B, one can expect that β_k will closely approximate the average of the time-varying contributions q_{jk}/Q_j to streamflow over the ensemble of exit times j (please note that this is not the same as assuming that the transit time distribution is time-invariant!). Substituting β_k as an ensemble estimate of q_{jk}/Q_j, one obtains the ensemble hydrograph separation equation for estimating transit time distributions,

$$\left(C_{Q_j} - C_{Q_{j-m-1}}\right) = \sum_{k=0}^{m} \beta_k \left(C_{P_{j-k}} - C_{Q_{j-m-1}}\right) + \alpha + \varepsilon_j \quad . \tag{38}$$

When appropriately re-scaled as described in Sects. 4.5-4.7 below, the coefficients β_k in Eq. (38) – or more precisely, their regression estimates $\hat{\beta}_k$ – can be used to estimate the time-averaged (also sometimes called the "marginal") transit time distribution.

4.2 Solution method

20   Using $\mathbf{Y}$ to represent the vector of reference-corrected streamflow tracer concentrations $y_j = C_{Q_j} - C_{Q_{j-m-1}}$ and $\mathbf{X}$ to represent the matrix of reference-corrected input tracer concentrations $x_{jk} = C_{P_{j-k}} - C_{Q_{j-m-1}}$, we can rewrite (38) in the array form of a multiple regression equation:

$$\mathbf{Y} = \sum_{k=0}^{m} \beta_k \, \mathbf{X}_k + \alpha + \boldsymbol{\varepsilon} \quad , \tag{39}$$

where X_k is the kth column vector of $\mathbf{X}$, and $\boldsymbol{\varepsilon}$ is the vector of the errors ε_j. The least-squares solution for multiple regressions like (39) can be expressed in matrix form as

$$
\begin{pmatrix} \hat{\beta}_0 \\ \hat{\beta}_1 \\ \hat{\beta}_2 \\ \vdots \\ \hat{\beta}_m \end{pmatrix} = \begin{pmatrix} \text{cov}(X_0, X_0) & \text{cov}(X_0, X_1) & \text{cov}(X_0, X_2) & \cdots & \text{cov}(X_0, X_m) \\ \text{cov}(X_1, X_0) & \text{cov}(X_1, X_1) & \text{cov}(X_1, X_2) & \cdots & \text{cov}(X_1, X_m) \\ \text{cov}(X_2, X_0) & \text{cov}(X_2, X_1) & \text{cov}(X_2, X_2) & \cdots & \text{cov}(X_2, X_m) \\ \vdots & \vdots & \vdots & \ddots & \vdots \\ \text{cov}(X_m, X_0) & \text{cov}(X_m, X_1) & \text{cov}(X_m, X_2) & \cdots & \text{cov}(X_m, X_m) \end{pmatrix}^{-1} \begin{pmatrix} \text{cov}(X_0, Y) \\ \text{cov}(X_1, Y) \\ \text{cov}(X_2, Y) \\ \vdots \\ \text{cov}(X_m, Y) \end{pmatrix} \quad , \qquad (40)
$$

where the regression coefficients $\hat{\beta}_k$ are the least-squares estimators of the true (but unknowable) coefficients β_k. Equation

5   (40) is the multi-dimensional counterpart to Eq. (10). The first term on the right-hand side of (40) is the inverse of the matrix of the covariances of the X_k at each lag with each other lag, and the second term is a vector of the covariances between $\boldsymbol{Y}$ and the X_k at each lag. Equation (40) is equivalent to the more widely known "normal equation" for solving multiple regressions,

$$
\hat{\boldsymbol{\beta}} = (\mathbf{X}^{\text{T}}\mathbf{X})^{-1}\,\mathbf{X}^{\text{T}}\boldsymbol{Y} \quad , \qquad (41)
$$

10   if one first normalizes $\boldsymbol{Y}$ and each of the X_k by subtracting their respective means; doing so has no effect on the estimates of the regression coefficients $\hat{\beta}_k$. (The elements of the square matrix $\mathbf{X}^{\text{T}}\mathbf{X}$ are the covariances between the X_k's at each pair of lags, multiplied by the number of samples; likewise the elements of the column matrix $\mathbf{X}^{\text{T}}\boldsymbol{Y}$ are the covariances between each of the X_k's and $\boldsymbol{Y}$, multiplied by the number of samples.)

15   Astute readers will immediately notice a fundamental problem with applying Eqs. (40) or (41) in practice, namely that they require precipitation tracer concentrations $C_{P_{j-k}}$ for all time steps $j = 1..n$ and lags $k = 0..m$. In every practical case, many precipitation tracer concentrations will be missing, for two reasons. Some tracer concentrations will be missing due to sampling or measurement failures, and many more will be inherently missing because precipitation tracer concentrations cannot exist for time steps without precipitation. As we will see shortly, missing measurements that arise for these two

20   different reasons must be handled in two different ways. But regardless of its origins, each missing tracer concentration C_{P_i} at time step i will create a diagonal line of missing values in the matrix x_{jk}, causing a missing value in the first column ($k = 0$) at $j = i$, and another in the second column ($k = 1$) at $j = i + 1$, and so on up to the last column ($k = m$) at $j = i + m$.

So-called "missing data problems" arise frequently in the statistical literature, and several approaches have been proposed for

25   handling them (Little, 1992). One approach, termed "listwise deletion" or "complete-case analysis", involves discarding all cases (meaning all rows j in the matrix x_{jk}) in which any variables are missing, and analyzing only the remaining (complete) cases. In our situation, this would mean analyzing only exit times t_j that are preceded by unbroken series of rainy periods, up to the maximum lag m for which we want to estimate the coefficients $\hat{\beta}_k$. Such ensembles of points would be mathematically convenient, but they would also be very strongly biased in a hydrological sense, because they would

represent periods of unusually consistent rainfall (and thus unusually wet catchment conditions). Furthermore, if the maximum lag m is sufficiently long, records with continuous rainfall over all $m + 1$ lags ($k = 0 \ldots m$) will become impossible to find. For these reasons, complete case analysis is not a feasible approach to our problem.

5   A second class of approaches to the missing data problem involves imputing values to the missing data (Little, 1992). In our case, however, many of the missing data are not simply unmeasured, but cannot exist at all (because rainless days have no rainfall concentrations), so it is not obvious how to impute the missing values.

A third approach, termed "pairwise deletion" or "available-case analysis", first proposed by Glasser (1964), entails
10   evaluating each of the covariances in (40) using any cases for which the necessary pairs of observations exist. Thus the covariances in (40) are replaced by

$$\mathrm{cov}(\boldsymbol{X}_k, \boldsymbol{X}_\ell)_{(k\ell)} = \frac{1}{n_{(k\ell)} - 1} \sum_{j \in (k\ell)} \left(x_{jk} - \bar{x}_{k(k\ell)} \right)\left(x_{j\ell} - \bar{x}_{\ell(k\ell)} \right) \tag{42}$$

and

$$\mathrm{cov}(\boldsymbol{X}_k, \boldsymbol{Y})_{(ky)} = \frac{1}{n_{(ky)} - 1} \sum_{j \in (ky)} \left(x_{jk} - \bar{x}_{k(ky)} \right)\left(y_j - \bar{y}_{(ky)} \right) \quad , \tag{43}$$

where the notation $(k\ell)$ indicates terms that are evaluated over all cases j for which both x_{jk} and $x_{j\ell}$ exist (e.g., $\bar{x}_{k(k\ell)}$ is the mean of the column vector $\boldsymbol{X}_k$ for rows j where neither x_{jk} nor $x_{j\ell}$ is missing, and $n_{(k\ell)}$ is the number of such cases), and (ky) indicates terms that are evaluated over all cases j for which x_{jk} and y_j exist.

20   Glasser's approach can potentially handle the problem of tracer measurements that are missing at random due to sampling or analysis failures. However, it will not correctly handle the problem of tracer concentrations that are missing due to a lack of sufficient precipitation, because it assumes that the missing values occur randomly and therefore that Eqs. (42)-(43) are unbiased estimators of the covariances that one would obtain if no samples were missing. But when little or no precipitation falls on the catchment, it delivers little or no tracer to subsequent streamflow, and thus its contribution to the covariance
25   between precipitation and streamflow concentrations will be nearly zero. Therefore different handling is required for precipitation tracer concentrations that are missing because they were not measured, versus those that are missing because they never existed at all (because no rain fell). As shown in Appendix B, periods without precipitation must be taken into account with weighting factors on the off-diagonal elements of the covariance matrix (because the tracer covariances will be less strongly coupled to one another, the less frequently precipitation falls). When the approach outlined in Appendix B is
30   combined with Glasser's method for estimating each of the covariances, the end result is

$$
\begin{pmatrix} \hat{\beta}_0 \\ \hat{\beta}_1 \\ \hat{\beta}_2 \\ \vdots \\ \hat{\beta}_m \end{pmatrix} = \begin{pmatrix} \text{cov}(X_0, X_0)_{(0,0)} & \frac{n_{x_0 x_1}}{n_{x_0}}\text{cov}(X_0, X_1)_{(0,1)} & \frac{n_{x_0 x_2}}{n_{x_0}}\text{cov}(X_0, X_2)_{(0,2)} & \cdots & \frac{n_{x_0 x_m}}{n_{x_0}}\text{cov}(X_0, X_m)_{(0,m)} \\ \frac{n_{x_1 x_0}}{n_{x_1}}\text{cov}(X_1, X_0)_{(1,0)} & \text{cov}(X_1, X_1)_{(1,1)} & \frac{n_{x_1 x_2}}{n_{x_1}}\text{cov}(X_1, X_2)_{(1,2)} & \cdots & \frac{n_{x_1 x_m}}{n_{x_1}}\text{cov}(X_1, X_m)_{(1,m)} \\ \frac{n_{x_2 x_0}}{n_{x_2}}\text{cov}(X_2, X_0)_{(2,0)} & \frac{n_{x_2 x_1}}{n_{x_2}}\text{cov}(X_2, X_1)_{(2,1)} & \text{cov}(X_2, X_2)_{(2,2)} & \cdots & \frac{n_{x_2 x_m}}{n_{x_2}}\text{cov}(X_2, X_m)_{(2,m)} \\ \vdots & \vdots & \vdots & \ddots & \vdots \\ \frac{n_{x_m x_0}}{n_{x_m}}\text{cov}(X_m, X_0)_{(m,0)} & \frac{n_{x_m x_1}}{n_{x_m}}\text{cov}(X_m, X_1)_{(m,1)} & \frac{n_{x_m x_2}}{n_{x_m}}\text{cov}(X_m, X_2)_{(m,2)} & \cdots & \text{cov}(X_m, X_m)_{(m,m)} \end{pmatrix}^{-1} \begin{pmatrix} \text{cov}(X_0, Y)_{(0,y)} \\ \text{cov}(X_1, Y)_{(1,y)} \\ \text{cov}(X_2, Y)_{(2,y)} \\ \vdots \\ \text{cov}(X_m, Y)_{(m,y)} \end{pmatrix},
$$

$$(44)$$

where the covariance terms are defined by Eqs. (42)-(43), n_{x_k} is the number of time steps j for which precipitation fell at time $i = j - k$ (whether or not that precipitation was sampled and analyzed), and $n_{x_k x_\ell}$ is the number of time steps j for which precipitation fell at both $j - k$ and $j - \ell$ (again, whether or not those precipitation events were sampled and analyzed).

5   As explained in Appendix B, the estimated coefficients $\hat{\beta}_k$ will closely approximate the average of the time-varying coefficients $\beta_{j,k} = q_{jk}/Q_j$, averaged over times j for which precipitation fell at times $i = j - k$ (but not over rainless periods, from which no streamflow can originate and thus $\beta_{j,k} = q_{jk}/Q_j$ must be zero). In practice, a single droplet of mist does not make a rainstorm, so there will be some threshold rate of precipitation below which there will be too little water to have any detectable effect on streamflow (and too little water to analyze). Thus n_{x_k} and $n_{x_k x_\ell}$ will be determined by

10   counting the time steps that exceed this precipitation threshold:

$$
n_{x_k} = \sum_{j=1}^{n} \begin{cases} 1 : P_{j-k} \geq P_{\text{threshold}} \\ 0 : P_{j-k} < P_{\text{threshold}} \end{cases}
$$

$$
n_{x_k x_\ell} = \sum_{j=1}^{n} \begin{cases} 1 : P_{j-k} \geq P_{\text{threshold}} \text{ and } P_{j-\ell} \geq P_{\text{threshold}} \\ 0 : P_{j-k} < P_{\text{threshold}} \text{ or } P_{j-\ell} < P_{\text{threshold}} \end{cases} , \quad (45)
$$

In the calculations presented here, I have assumed a precipitation threshold of 1 mm/day, but expert judgment may lead to other values of $P_{\text{threshold}}$ in real-world situations. Note that some measurements will usually also be missing due to sampling or measurement failures in addition to precipitation intermittency. Thus $n_{(ky)}$ and $n_{(k\ell)}$ in Eqs. (42)-(43), which

15   account for both types of missing data, will typically be smaller than n_{x_k} and $n_{x_k x_\ell}$ in Eq. (44).

4.3 Tikhonov-Phillips regularization

Gaps in the underlying data imply that, unlike covariance matrices in conventional multiple regressions, the covariance matrix in (40) is not guaranteed to be positive definite (and thus may not be invertible). Even when the covariance matrix is invertible, it may be ill-conditioned, making its inversion unstable. This issue arises frequently in inversion problems

20   whenever different combinations of lagged inputs will have nearly equivalent effects on the output, making it difficult for the inversion to decide among them (this is the multi-dimensional analogue to nearly dividing by zero in Eq. 10). In minimizing the sum of squared deviations from the observations, inversions like Eq. (40) can potentially yield wildly oscillating solutions, with huge negative values of $\hat{\beta}_k$ at some lags delicately balancing huge positive values at other lags. Such results

are not just unrealistic; they are also unstable, with tiny differences in the underlying data potentially having huge effects on the $\hat{\beta}_k$ estimates.

A standard therapy for this disease is Tikhonov-Phillips regularization (Phillips, 1962; Tikhonov, 1963). This technique

5 (also known by many other names, including Tikhonov regularization, Tikhonov-Miller regularization, and the Phillips-Twomey method) is commonly used to solve ill-conditioned geophysical inversion problems (Zhadanov, 2015) but is less widely known in hydrology. Whereas conventional least-squares inversion finds the set of parameters $\hat{\beta}_k$ that will minimize the misfit between the predicted and observed y_j, no matter how strange those $\hat{\beta}_k$ values may be, Tikhonov-Phillips regularization adds a second criterion that quantifies the strangeness of the $\hat{\beta}_k$ values themselves, and finds the set of

10 parameters $\hat{\beta}_k$ that will minimize the sum of both criteria. Phillips (1962) first showed how this joint minimization could be formulated as a simple extension of the normal matrix approach to solving linear inversion problems. This formulation, applied to our problem, is:

$$
\left(\hat{\beta}_k \right) = \left(\mathbf{C} + \lambda\mathbf{H} \right)^{-1} \left(\text{cov}(X_k, Y)_{(ky)} \right) , \tag{46}
$$

where $\mathbf{C}$ is the matrix of covariance terms in Eq. (44), and the parameter λ controls the relative weight given to the two

15 criteria, namely the mean squared deviations of the predicted and observed y_j values (controlled by the covariance matrix $\mathbf{C}$) and the deviations from ideal behavior of the $\hat{\beta}_k$ values (controlled by the matrix $\mathbf{H}$).

The form of $\mathbf{H}$ is determined by the criterion of reasonableness that is applied to the $\hat{\beta}_k$. One possible criterion (among many that can be found in the literature) can be called *parsimony*: minimize the mean square of the $\hat{\beta}_k$, thus penalizing solutions

20 with large $\hat{\beta}_k$ values. Minimizing the functional $\langle \hat{\beta}_k^2 \rangle$ yields the identity matrix for $\mathbf{H}$ (Tikhonov, 1963):

$$
\mathbf{H} = \begin{pmatrix} 1 & 0 & 0 & \cdots & 0 \\ 0 & 1 & 0 & \cdots & 0 \\ \vdots & & \ddots & & \vdots \\ 0 & \cdots & 0 & 1 & 0 \\ 0 & \cdots & 0 & 0 & 1 \end{pmatrix} . \tag{47}
$$

This approach, also called "ridge regression" because it adds a "ridge" of extra weight along the diagonal of the covariance matrix, was Tikhonov's original regularization criterion and is widely used in geophysical inversions (including unit hydrograph estimation). In our case, however, it would have the undesirable effect of creating a systematic underestimation

25 bias in our estimates of recent contributions to streamflow, by always making the $\hat{\beta}_k$ smaller than they would be otherwise.

A second possible criterion is *consistency*: minimize the variance of the $\hat{\beta}_k$, thus penalizing solutions with individual $\hat{\beta}_k$ values that differ greatly from the mean of all the $\hat{\beta}_k$. Minimizing the functional $\langle(\hat{\beta}_k - \langle\hat{\beta}_k\rangle)^2\rangle$, where angled brackets indicate averages from $k = 0$ to $k = m$, leads to an **H** matrix of the form (Press et al., 1992),

$$\mathbf{H} = \begin{pmatrix} 1 & -1 & 0 & 0 & 0 & \cdots & 0 \\ -1 & 2 & -1 & 0 & 0 & \cdots & 0 \\ 0 & -1 & 2 & -1 & 0 & \cdots & 0 \\ \vdots & & & \ddots & & & \vdots \\ 0 & \cdots & 0 & -1 & 2 & -1 & 0 \\ 0 & \cdots & 0 & 0 & -1 & 2 & -1 \\ 0 & \cdots & 0 & 0 & 0 & -1 & 1 \end{pmatrix}. \tag{48}$$

5 Like (47), this minimum-variance criterion is also widely used, and has the advantage that, unlike (47), it does not lead to systematic biases in the average $\hat{\beta}_k$ values. However, if the transit time distribution is strongly skewed, with large contributions to streamflow at short lags, minimizing the variance of the $\hat{\beta}_k$ will tend to suppress this short-lag peak in the transit time distribution. This distortion of the transit time distribution is undesirable when one seeks to quantify recent contributions to streamflow.

A third possible criterion is *smoothness*: minimize the mean square of the second derivatives of the $\hat{\beta}_k$, thus penalizing $\hat{\beta}_k$ values that deviate greatly from their neighbors. Minimizing the second derivative functional $\langle(\hat{\beta}_{k-1} - 2\hat{\beta}_k + \hat{\beta}_{k+1})^2\rangle$, where the angled brackets indicate an average from $k = 1$ to $k = m\text{-}1$, leads to an **H** matrix of the form (Phillips, 1962; Press et al., 1992),

$$\mathbf{H} = \begin{pmatrix} 1 & -2 & 1 & 0 & 0 & 0 & 0 & \cdots & 0 \\ -2 & 5 & -4 & 1 & 0 & 0 & 0 & \cdots & 0 \\ 1 & -4 & 6 & -4 & 1 & 0 & 0 & \cdots & 0 \\ 0 & 1 & -4 & 6 & -4 & 1 & 0 & \cdots & 0 \\ \vdots & & & & \ddots & & & & \vdots \\ 0 & \cdots & 0 & 1 & -4 & 6 & -4 & 1 & 0 \\ 0 & \cdots & 0 & 0 & 1 & -4 & 6 & -4 & 1 \\ 0 & \cdots & 0 & 0 & 0 & 1 & -4 & 5 & -2 \\ 0 & \cdots & 0 & 0 & 0 & 0 & 1 & -2 & 1 \end{pmatrix}. \tag{49}$$

This criterion, first used by Phillips (1962) has the advantage of strongly suppressing rapid oscillations in the $\hat{\beta}_k$ while barely affecting the larger-scale structure of the inferred transit time distribution. Therefore this will be the regularization criterion employed here.

20 The solution to Eq. (46) will depend on the value of the parameter λ, which determines the relative weight given to the regularization criterion versus the goodness-of-fit criterion. How should the value of λ be chosen? One can first note that for $\lambda\mathbf{H}$ to be dimensionally consistent with the covariance matrix, λ must have the same dimensions as the variance of X_k. The second point to note is that the regularization criterion and the goodness-of-fit criterion will have roughly equal weight in determining the $\hat{\beta}_k$ if the trace of $\lambda\mathbf{H}$ equals the trace of the covariance matrix **C** (Press et al., 1992). Combining these two

considerations, we can define a dimensionless parameter v that ranges between 0 and 1 and expresses the fractional weight given to the regularization criterion, and then calculate the corresponding value of λ as,

$$\lambda = \frac{v}{1-v} \frac{\text{Tr}(\mathbf{C})}{\text{Tr}(\mathbf{H})} \quad . \tag{50}$$

As one can see from Eq. (50), when $v = 0.5$, the trace of $\lambda\mathbf{H}$ will equal the trace of the covariance matrix $\mathbf{C}$, and the two

5   criteria will have roughly equal weight in determining the $\hat{\beta}_k$. As v grows toward 1, the solution will be increasingly dominated by the regularization criterion; conversely, if $v = 0$ the regularization criterion will be ignored, and Eq. (46) will become equivalent to Eq. (40).

The question remains as to what the most appropriate value of v (or λ) would be for any particular situation. An appropriate

10   degree of regularization will prevent the predicted values of y_j from fitting the data more closely than they should (that is, it will prevent "fitting the noise" with unrealistic values of $\hat{\beta}_k$). Thus a theoretically optimal value of v or λ would be one that makes the variance of the prediction errors of the y_j similar to the expected variance of the ε_j (Press et al., 1992). This approach will not work for our problem, for three reasons. First, the variance of the ε_j is not known a priori. Second, directly calculating the predicted y_j, and thus the prediction errors, is impossible if many values of x_{jk} are missing, as will

15   usually be the case. Third, and perhaps most importantly, equation (39) is, strictly speaking, structurally incorrect for our system, because $\hat{\beta}_k$ is only an approximation to the time-varying q_{jk}/Q_j. Therefore in our case a more pragmatic approach (which is also taken in many geophysical applications of regularization methods) is to follow the advice of Phillips (1962) that "in practice several values... should be tried and the best value should be the one that appears to take out the oscillation without appreciably smoothing the [solution]", while keeping in mind that an element of subjectivity is inevitably

20   introduced. In the analyses presented here, $v = 0.5$ and thus the regularization criterion and the least-squares criterion have roughly equal weight in determining the values of the $\hat{\beta}_k$. Regularization usually has little effect on the estimated transit time distributions presented below, but it can serve as a safeguard against obtaining wildly unrealistic results, particularly with large fractions of missing measurements.

4.4 Uncertainties

25   In conventional multiple regression analysis, calculating the uncertainties in the $\hat{\beta}_k$ requires estimating the variance s_ε^2 of the prediction errors ε_j,

$$s_\varepsilon^2 = \frac{n-1}{n-(m+1)-1} \text{var}(\varepsilon_j)$$

$$\varepsilon_j = y_j - \sum_{k=0}^{m} \hat{\beta}_k x_{jk} - \alpha = \left(C_{Q_j} - C_{Q_{j-m-1}} \right) - \sum_{k=0}^{m} \hat{\beta}_k \left(C_{P_{j-k}} - C_{Q_{j-m-1}} \right) - \alpha \quad . \tag{51}$$

It may seem that calculating (51) is impossible in our case, because values of $C_{P_{j-k}}$ are missing for all days $i = j\text{-}k$ without rain. However, as noted in Sect. 4.2 above, for those points the true value of $\beta_{j,k}$ is known to be zero, so the rainless terms can simply be ignored because they will have no effect on the predicted y_j. Thus if sampling and measurement failures account for only a small fraction of the missing tracer concentrations, Eq. (51) may yield adequate estimates of s_ε^2. Where

5 there are many sampling and measurement failures, we can use the error variance formula of Glasser (1964), adapted to our problem as

$$s_\varepsilon^2 = \frac{n-1}{n - (m+1) - 1}\left(s_y^2 - \sum_{k=0}^{m} \hat{\beta}_k \left(\frac{n_{x_k}}{n}\right) \text{cov}(X_k, Y)_{(ky)} \right) \quad, \tag{52}$$

which is the mean square error of the estimated y_j values. The factor n_{x_k}/n accounts for the fact that there are n values of y_j, but only n_{x_k} of them are affected by $\hat{\beta}_k$; for the other $n - n_{x_k}$, x_{jk} is missing and $\hat{\beta}_k$ has no influence on y_j. In both (51)

10 and (52), the factor $\frac{n-1}{n-(m+1)-1}$ corrects for degrees of freedom. If one removes this degree-of-freedom correction, one gets the "population" mean square error (i.e., the error variance of the fit to these particular data). With the degree-of-freedom correction, one gets the "sample" mean square error (i.e., an estimate of the prediction error for data drawn from the same population, but not used to fit the model in the first place). When applied to complete data sets (without missing values, and without regularization), Eq. (52) equals the conventional error variance for multiple regression, and it usually works

15 reasonably well with missing values and with unbiased regularization, e.g., with the consistency criterion of Eq. (48) or the smoothness criterion of Eq. (49). However, unlike in conventional multiple regression, there is no absolute guarantee that the variance of the predicted values (the summation in Eq. 52) will be smaller than the variance of the observed values of y_j. Users should therefore be aware that Eq. 52 could potentially yield nonsensical negative values (or unrealistically small positive values) for the error variance in particular cases.

In conventional multiple regression, the covariance matrix of the coefficients $\hat{\beta}_k$ equals the inverse of the covariance matrix $\mathbf{C}$, scaled by the error variance s_ε^2 divided by the sample size n. This approach must be adapted to account for the effects of regularization, yielding the following expression for the covariances of the $\hat{\beta}_k$:

$$\left(\text{cov}(\hat{\beta}_k, \hat{\beta}_\ell) \right) = \frac{s_\varepsilon^2}{n_{\text{eff}}} \left(\mathbf{C} + \lambda \mathbf{H} \right)^{-1} \left(\mathbf{C} \right) \left(\mathbf{C} + \lambda \mathbf{H} \right)^{-1}, \tag{53}$$

25 where s_ε^2 is the error variance as estimated in Eq. (51) or (52), and n_{eff} is the sample size n, adjusted to account for serial correlation in the residuals using Eq. (13). (Where there are so many measurement or analysis failures that residuals cannot be calculated reliably, it is better to guess a reasonable value for their serial correlation than to assume it is zero, which will typically lead to overestimates of n_{eff} and thus underestimates of the associated uncertainties.) The standard errors of the $\hat{\beta}_k$ will be the square roots of the diagonal elements of the matrix defined by Eq. (53),

$$\text{s.e.}\left(\hat{\beta}_k\right) = \frac{s_\varepsilon}{\sqrt{n_{\text{eff}}}} \sqrt{\left[\left(\mathbf{C} + \lambda\mathbf{H}\right)^{-1}\left(\mathbf{C}\right)\left(\mathbf{C} + \lambda\mathbf{H}\right)^{-1}\right]_{kk}} \,, \qquad (54)$$

Benchmark data sets verify that Eqs. (53) and (54) perform as they should: the root-mean-square averages of the calculated s.e. $\left(\hat{\beta}_k\right)$ are close to the root-mean-square averages, over many replicate data sets, of the deviation of the fitted coefficients $\hat{\beta}_k$ from the true β_k used to generate the synthetic data. This result holds both with and without substantial fractions of missing values, strong correlations among the $\mathbf{X}_k$, and substantial additive noise.

There is one important caveat to this generalization, however: it holds only if the assumptions underlying the regularization criterion *are actually true*. For example, if the true β_k vary smoothly with k, then regularization using Eq. (49) will retrieve a set of smoothly varying coefficients $\hat{\beta}_k$ that deviate from the true β_k by amounts that are well approximated by the calculated standard errors s.e. $\left(\hat{\beta}_k\right)$. But if (say) the true β_k oscillate wildly from one k to the next, regularization using Eq. (49) will generate a smoothly varying set of $\hat{\beta}_k$ which will deviate from the true (wildly oscillating) β_k by much more than the calculated standard errors s.e. $\left(\hat{\beta}_k\right)$ as calculated from Eq. (54). Regularization methods are forced to assume that the β_k obey the regularization criterion (with the strength of this assumption determined by the parameter λ), and thus they cannot be used to test whether this assumption is true. Thus what the calculated standard errors tell us is that *if* the true β_k vary smoothly over k, then the estimation errors of the $\hat{\beta}_k$ should be on the order of s.e. $\left(\hat{\beta}_k\right)$.

4.5 Transit time distribution of discharge

The coefficients $\hat{\beta}_k$ determined by Eqs. (40)-(54) estimate the average contribution to discharge Q_j that originated as precipitation k time steps earlier; that is, they estimate the average of q_{jk}/Q_j for combinations of times j and k for which precipitation occurred at $i = j - k$. They do not account for times i when no precipitation occurred, and thus for which $q_{jk} = 0$ at the corresponding time steps $j = i + k$.

To estimate the average contribution q_{jk}/Q_j of precipitation to discharge across all time steps, both with and without precipitation, we need to include values of $q_{jk} = 0$ for times without precipitation (and thus without any contribution of precipitation to discharge). This is done by re-scaling the coefficients $\hat{\beta}_k$ and their uncertainties s.e. $\left(\hat{\beta}_k\right)$ by n_{x_k}/n, the ratio of "event" time steps (those with precipitation) to all time steps. We also need to divide by the time step length Δt to obtain the transit time distribution in the correct dimensions (fraction per unit time). With these normalizations, the coefficients $\hat{\beta}_k$ yield the transit time distribution of discharge $^Q TTD_k$ (also termed the "backward" transit time distribution, or the transit time distribution conditioned on exit time):

$$^{Q}TTD_k = \frac{\hat{\beta}_k}{\Delta t}\frac{n_{x_k}}{n} \quad , \quad \text{s.e.}\left(^{Q}TTD_k\right) = \frac{\text{s.e.}\left(\hat{\beta}_k\right)}{\Delta t}\frac{n_{x_k}}{n} \quad . \tag{55}$$
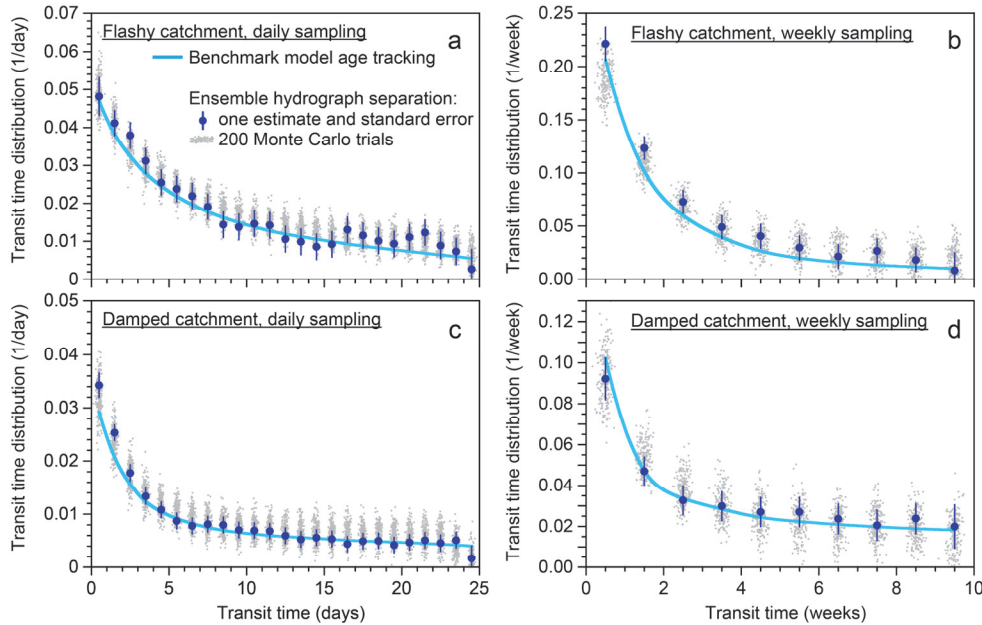
Figure 11. Transit time distributions of discharge estimated by ensemble hydrograph separation based on both daily and weekly tracer sampling, versus true transit time distributions determined by benchmark model age tracking (light blue curves). Upper and lower rows show TTD's for the modeled flashy and damped catchments, both driven by Smith River (Mediterranean climate) precipitation. Dark blue symbols show transit time distributions estimated from one time series. Data clouds show ensemble hydrograph separation results (slightly jittered on the x-axis) from 200 different realizations of random precipitation tracer values, random missing data, and random measurement errors. Ensemble hydrograph separation correctly reveals the shapes of the transit time distributions and also quantifies their values, within the calculated uncertainties, at most lags. It can clearly distinguish the transit time distributions of the two catchments under either daily or weekly tracer sampling.

These transit time distributions can be tested by comparing them to time-averaged streamwater age distributions calculated by age tracking in the benchmark model (Sect. 3.1). Figure 11 shows the results of several such tests, using both daily and weekly tracer data as input (left and right columns, respectively). The light blue curves indicate the true time-averaged transit time distribution (determined from age tracking in the benchmark model), the dark blue symbols show transit time distributions estimated from one tracer time series, and the gray data clouds show 200 more transit time distributions from the same model with different realizations of the random inputs. The weekly TTD's are larger, in absolute terms, than the daily TTD's, because streamflow will always contain at least as much water that originated as precipitation during the previous week as during the previous day (for the simple reason that the previous day is part of the previous week). Figure 11 shows that ensemble hydrograph separation correctly estimates the general shapes of the TTD's, and their quantitative values. Furthermore, the gray data clouds show that no TTD estimates deviate too wildly from the age tracking curves.
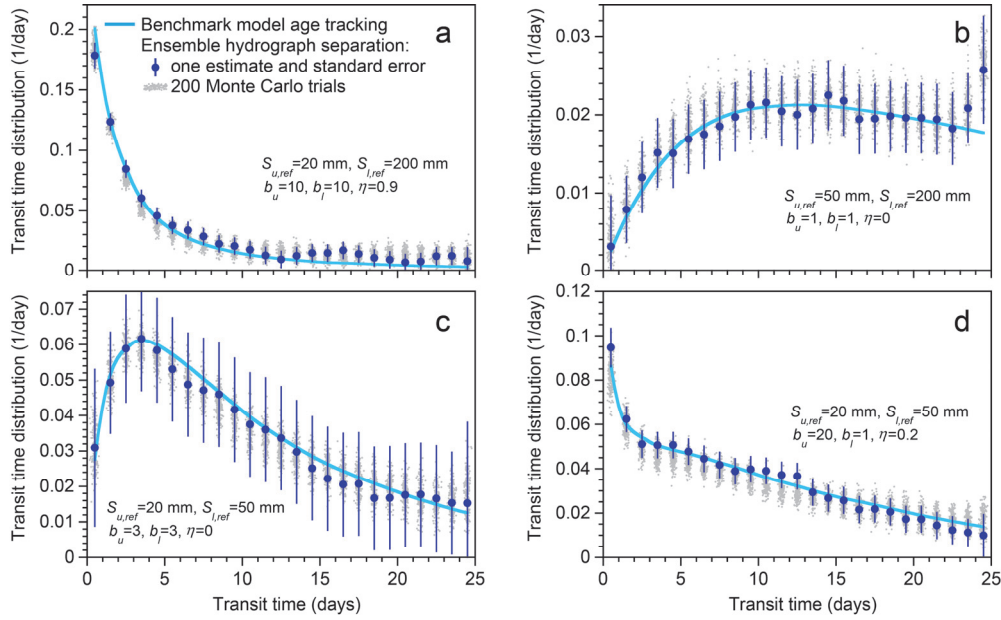
Figure 12. Transit time distributions (TTD's) of discharge estimated by ensemble hydrograph separation based on daily sampling, compared to true TTD's determined by benchmark model age tracking (light blue curves), for four model parameter sets yielding diverse patterns of transport behaviour. Dark blue symbols show transit time distributions estimated from one time series. Data clouds show ensemble hydrograph separation results (slightly jittered on the x-axis) from 200 different realizations of random precipitation tracer values, random missing data, and random measurement errors. Vertical axis scales differ greatly. Ensemble hydrograph separation correctly reveals the shapes of the TTD's and also quantifies their values at most lags. However, panels b and c show that standard errors are overestimated for TTD's that result in strong serial correlation in the modelled time series (see text).

Real-world transit time distributions could potentially have different shapes from those shown in Fig. 11. To test whether ensemble hydrograph separation can correctly estimate transit time distributions with more widely varying shapes, I explored the benchmark model's parameter space, in some cases venturing beyond the nominal parameter ranges outlined in Sect. 3.1. As Fig. 12 illustrates, widely differing time-averaged (or "marginal") transit time distributions generated by the benchmark model (solid lines) are well approximated by the ensemble hydrograph separation estimates (blue dots) calculated from the tracer time series. The standard errors are overestimated for humped TTD's, which generate strongly autocorrelated time series. The reason appears to be that when the benchmark model's parameters generate a strongly autocorrelated tracer time series, the residuals will also be strongly autocorrelated; thus the effective sample size n_{eff} will be small (Eq. 13) and the resulting uncertainties s. e. $\left({}^{Q}TTD_k \right)$ will be correspondingly large (Eqs. 54-55). One can also see that in some TTD's, the last few lags can exhibit substantial deviations from the age tracking results (e.g., Figs. 11c and 12b). This may be an aliasing effect that arises when $C_{Q_{j-m-1}}$ does not adequately capture the effects of the unmeasured older fluxes (see Eqs. 32-35), in which case one would expect it to be strongest when the TTD does not approach zero at the longest measured lags

(such as in Fig. 12b). It may also arise for other unknown reasons. In any case, a pragmatic solution is to estimate the TTD over a few more lags than desired, and then to simply ignore the last few lags of the estimated TTD. These caveats notwithstanding, Figs. 11 and 12 demonstrate that ensemble hydrograph separation can reliably quantify transit time distributions with widely varying shapes.

5 **4.6 Volume-weighted transit time distribution**

The transit time distributions defined in Eq. (55) are ensemble averages in which each day counts equally; that is, for a given lag k, $^Q TTD_k$ estimates the average of the ratio q_{jk}/Q_j across all time steps, including zeroes at time steps for which there was no precipitation at the corresponding time step $i = j - k$. Thus Eq. (55) estimates *time-weighted* average TTD's, which quantify the distribution of temporal origins of an average *day* of discharge.

For many purposes, it would be useful to estimate the temporal origins of an average *liter* of discharge instead, that is, the *volume-weighted* TTD, which we can denote $^Q TTD_k^*$ (where, following the convention in Sect. 2, the asterisk indicates volume-weighting). Instead of estimating the average of the ratio q_{jk}/Q_j (the time-weighted average), a volume-weighted TTD approximates the ratio of the average q_{jk} to the average Q_j across all time steps (the ratio of the averages rather than

15 the average of the ratios). This is the multi-dimensional analogue to the volume-weighted new water fraction presented in Sect. 2.4, and is handled similarly. The multiple regression in Eq. (36) can be volume-weighted by replacing the covariances in Eqs. (42-43) with volume-weighted covariances (Galassi et al., 2016) instead:

$$\text{cov}^*(\boldsymbol{X}_k, \boldsymbol{X}_\ell)_{(k\ell)} = \frac{\sum_{j\in(k\ell)} Q_j}{\left(\sum_{j\in(k\ell)} Q_j\right)^2 - \sum_{j\in(k\ell)} Q_j^2} \sum_{j\in(k\ell)} \left(x_{jk} - \bar{x}_{k(k\ell)}^*\right)\left(x_{j\ell} - \bar{x}_{\ell(k\ell)}^*\right) \tag{56}$$

and

20 $$\text{cov}^*(\boldsymbol{X}_k, \boldsymbol{Y})_{(ky)} = \frac{\sum_{j\in(ky)} Q_j}{\left(\sum_{j\in(ky)} Q_j\right)^2 - \sum_{j\in(ky)} Q_j^2} \sum_{j\in(ky)} \left(x_{jk} - \bar{x}_{k(ky)}^*\right)\left(y_j - \bar{y}_{(ky)}^*\right) \quad, \tag{57}$$

where

$$\bar{x}_{k(k\ell)}^* = \frac{\sum_{j\in(k\ell)} Q_j x_{jk}}{\sum_{j\in(k\ell)} Q_j}, \quad \bar{x}_{\ell(k\ell)}^* = \frac{\sum_{j\in(k\ell)} Q_j x_{j\ell}}{\sum_{j\in(k\ell)} Q_j}, \quad \bar{x}_{k(ky)}^* = \frac{\sum_{j\in(ky)} Q_j x_{jk}}{\sum_{j\in(ky)} Q_j}, \quad \text{and} \quad \bar{y}_{(ky)}^* = \frac{\sum_{j\in(ky)} Q_j y_j}{\sum_{j\in(ky)} Q_j} \tag{58}$$

are the volume-weighted means of the $\boldsymbol{X}_k$'s, $\boldsymbol{X}_\ell$'s, and $\boldsymbol{Y}$'s, and x's and y's, and where the notations $j \in (k\ell)$ and $j \in (ky)$ indicate sums taken over all j for which x_{jk} and $x_{j\ell}$ (or, respectively, x_{jk} and y_j) are not missing. With these volume-

25 weighted covariances in place of the unweighted covariances from Eqs. (42-43), the volume-weighted regression can be solved by the same procedures described in Sects. 4.2-4.4, yielding volume-weighted estimates of the coefficients $\hat{\beta}_k^*$ (where, as above, the asterisk indicates volume-weighting). Following the approach of Sect. 2.5, one should account for the unevenness of the weighting when calculating the effective sample size n_{eff} to be used in Eq. (54) to estimate the uncertainties in the $\hat{\beta}_k^*$,

$$n_{\text{eff}_k} = \frac{\left(\sum Q_{j(ky)}\right)^2}{\sum\left(Q_{j(ky)}^2\right)} \qquad , \tag{59}$$

where n_{eff_k} is the effective sample size at lag k, and $Q_{j(ky)}$ denotes discharge during time steps j for which pairs of y_j and x_{jk} exist (for a given lag k).

5   To estimate the volume-weighted TTD, we must average over all discharge (including discharge after time steps with no precipitation). Thus the coefficients $\hat{\beta}_k^*$ and their uncertainties should be re-scaled, following the approach in Sect. 2.5, as follows:

$$^{Q}TTD_k^* = \frac{\bar{Q}_{x_k}}{\bar{Q}} \frac{n_{x_k}}{n} \frac{\hat{\beta}_k^*}{\Delta t} \qquad , \qquad \text{s.e.}\left(^{Q}TTD_k^*\right) = \frac{\bar{Q}_{x_k}}{\bar{Q}} \frac{n_{x_k}}{n} \frac{\text{s.e.}\left(\hat{\beta}_k^*\right)}{\Delta t} \tag{60}$$

where $\bar{Q}_{x_k}$ is the average discharge during the n_{x_k} time steps j for which precipitation fell at $i = j - k$, $\bar{Q}$ is the average

10   discharge over all time steps (including rainless periods), n_{x_k}/n is the fraction of time steps with precipitation, and $\hat{\beta}_k^*$ and s.e. $\left(\hat{\beta}_k^*\right)$ are estimated from the multiple regression in Eq. (54), with the effective sample size n_{eff_k} defined in Eq. (59). The ratio $\bar{Q}_{x_k}/\bar{Q}$ corrects for any differences in average discharge during sampled and un-sampled time steps, and the ratio n_{x_k}/n corrects for rain-free periods, which contribute no "new" water to streamflow.
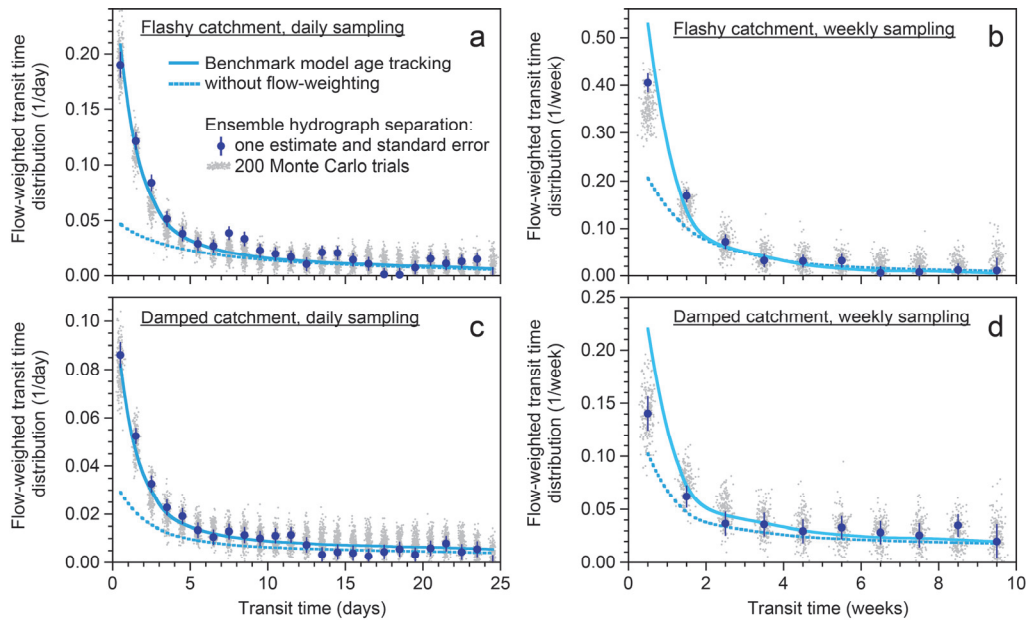
Figure 13. Volume-weighted transit time distributions (TTD's) of discharge estimated by ensemble hydrograph separation (Eq. 60) compared to benchmark model age tracking. Upper and lower panels show TTD's for rapid and damped response parameters, respectively; model is driven by Smith River precipitation in both cases. Ensemble hydrograph separation estimates from tracer fluctuations (dark blue symbols) are broadly consistent with true TTD from age tracking in benchmark model (solid curve). Data clouds show ensemble hydrograph separation results (slightly jittered on the x-axis) from 200 different realizations of random precipitation tracer values, random missing data, and random measurement errors. Dashed curve is unweighted benchmark model TTD from Fig. 11 for comparison.

4.7 Forward transit time distribution

In addition to the "backward" transit time distributions q_{jk}/Q_j, which estimate the fraction of streamflow that originated as precipitation k time steps earlier, it may also be useful to estimate "forward" transit time distributions $q_{jk}/P_{j-k} = q_{i+k,k}/P_i$, which estimate the fraction of precipitation that becomes streamflow k time steps later. Instantaneous, time-varying forward and backward transit time distributions can differ markedly at any point in time. For example, today's backward transit time distribution strongly depends on the timing and magnitude of previous precipitation supplying today's streamflow, whereas the forward transit time distribution strongly depends on how future precipitation mobilizes water stored from today's rainfall. These individual differences become less prominent when averaged over a large ensemble of events. Systematic differences nonetheless persist, because forward transit time distributions are defined only during periods with precipitation (otherwise both q_{jk} and P_{j-k} are both zero and their ratio is undefined), and during these periods precipitation must be higher, on average, than discharge (otherwise there can be no recharge of the storages that supply discharge during rainless periods.

Forward transit time distributions are less straightforward to estimate from tracers than backward distributions are, for the simple reason that although streamflow is a mixture of contributions from previous precipitation events, the converse does not hold: that is, precipitation cannot be expressed as a mixture of subsequent streamflows. Although it is algebraically straightforward to rewrite Eq. (35) as either

$$\left(C_{Q_j} - C_{Q_{j-m-1}} \right) = \sum_{k=0}^{m} \frac{q_{jk}}{P_{j-k}} \left(\frac{P_{j-k}}{Q_j} \left(C_{P_{j-k}} - C_{Q_{j-m-1}} \right) \right) + \alpha + \varepsilon_j \tag{61}$$

or

$$Q_j \left(C_{Q_j} - C_{Q_{j-m-1}} \right) = \sum_{k=0}^{m} \frac{q_{jk}}{P_{j-k}} \left(P_{j-k} \left(C_{P_{j-k}} - C_{Q_{j-m-1}} \right) \right) + \alpha + \varepsilon_j \quad , \tag{62}$$

regressions based on these equations do not reliably predict the average of q_{jk}/P_{j-k} when applied to synthetic data from the benchmark model. (Note that these are the multi-dimensional counterparts to Eqs. (25) and (26), which likewise fail benchmark tests. Although Eqs. (35), (61), and (62) are algebraically equivalent, they behave differently as TTD estimators because the variance introduced by Q_j will affect the results differently when it appears on right-hand side versus the left-hand side).

Instead, by analogy Eq. (21), we can estimate the forward transit time distribution from the regression coefficients $\hat{\beta}_k$ of Eq. (44), rescaled as

$$^P TTD_k = \frac{\hat{\beta}_k}{\Delta t} \frac{\bar{Q}_{x_k}}{\bar{P}_{x_k}} \quad , \quad \text{s.e.} \left(^P TTD_k \right) = \frac{\text{s.e.} \left(\hat{\beta}_k \right)}{\Delta t} \frac{\bar{Q}_{x_k}}{\bar{P}_{x_k}} \quad , \tag{63}$$

where

$$\bar{P}_{x_k} = \frac{1}{n_{x_k}} \sum_{j=1}^{n} \begin{cases} P_{j-k} & : P_{j-k} \geq P_{\text{threshold}} \\ 0 & : P_{j-k} < P_{\text{threshold}} \end{cases} \tag{64}$$

is the average precipitation rate during time steps with precipitation, and

$$\bar{Q}_{x_k} = \frac{1}{n_{x_k}} \sum_{j=1}^{n} \begin{cases} Q_j & : P_{j-k} \geq P_{\text{threshold}} \\ 0 & : P_{j-k} < P_{\text{threshold}} \end{cases} \tag{65}$$

is the average of the discharges that occur k time steps after each of these precipitation intervals. Figure 14 shows that forward transit time distributions estimated with Eq. (63) are broadly consistent with true forward TTD's calculated by age tracking in the benchmark model.

It should be emphasized that $^\mathrm{P}TTD_k$ represents the forward transit time distribution of water that enters the catchment as precipitation and subsequently exits as streamflow, because these are the entry and exit fluxes in which the tracers are measured. The forward transit time distribution of water that exits by other pathways (such as evapotranspiration) may be different. That distribution will be unmeasurable without catchment-scale tracer data from those other pathways, which are

5   not available at present. Thus, echoing the principle outlined in Sects. 2.3 and 2.6, one should not interpret $^\mathrm{P}TTD_k$ as the forward transit time distribution of all precipitation entering the catchment, but only of the precipitation that exits as streamflow.
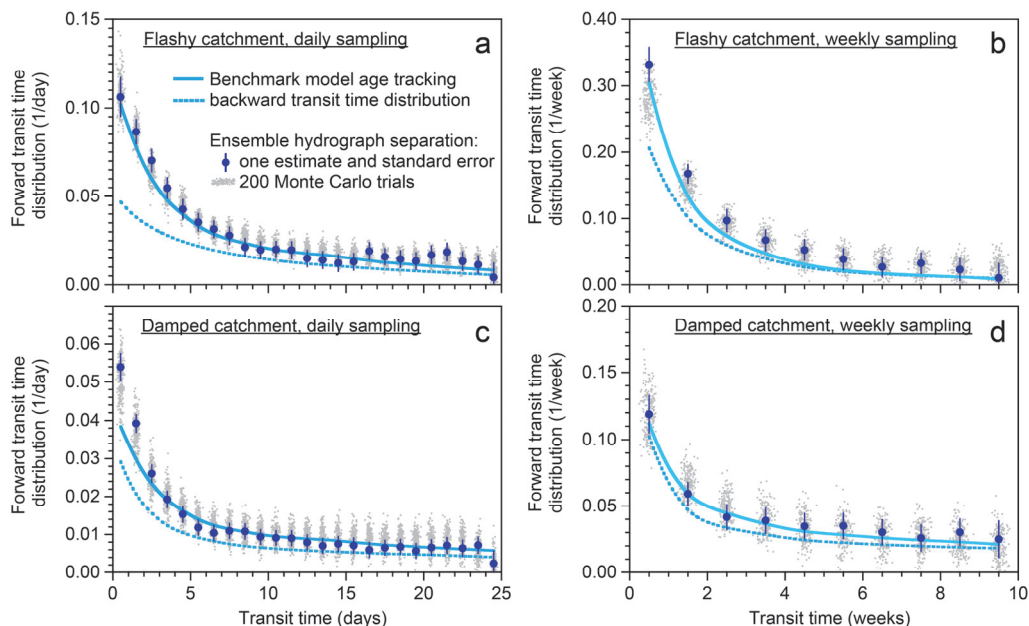
10   **Figure 14. Forward transit time distributions (the fraction of precipitation that leaves the catchment within one time step, two time steps, and so on) estimated by ensemble hydrograph separation (Eq. 63) compared to benchmark model age tracking. Upper and lower panels show TTD's for flashy and damped catchments, respectively; the model is driven by Smith River (Mediterranean climate) precipitation in both cases. Ensemble hydrograph separation estimates from tracer fluctuations (dark blue symbols) are broadly consistent with true TTD's from age tracking in the benchmark model (solid curve). Data clouds show ensemble**
15   **hydrograph separation results (slightly jittered on x-axis) from 200 different realizations of random precipitation tracer values, random missing data, and random measurement errors. Dashed curve is the benchmark model backward TTD from Fig. 11 for comparison.**

The volume-weighted forward transit time distribution $^\mathrm{P}TTD_k^*$ can also be calculated by rescaling arguments, analogous to
20   the approach in Sect. 2.7. The key is to recognize that we are seeking the ratio between the total volume of precipitation that will leave the catchment k days after falling as precipitation (the sum of q_{jk} over all j), and the total volume of precipitation that fell on the catchment during the corresponding rainy days. The numerator of this ratio is identical to the numerator of

the volume-weighted "backward" transit time distribution $^Q TTD_k^*$, but the denominator is total precipitation rather than total discharge. Thus the precipitation-weighted forward transit time distribution can be estimated as

$$^P TTD_k^* = \frac{\bar{Q}}{\bar{P}} \, ^Q TTD_k^* = \frac{\bar{Q}_{x_k}}{\bar{P}} \frac{n_{x_k}}{n} \frac{\hat{\beta}_k^*}{\Delta t} \quad , \quad \text{s.e.}\left(^P TTD_k^*\right) = \frac{\bar{Q}}{\bar{P}} \, \text{s.e.}\left(^P TTD_k^*\right) = \frac{\bar{Q}_{x_k}}{\bar{P}} \frac{n_{x_k}}{n} \frac{\text{s.e.}\left(\hat{\beta}_k^*\right)}{\Delta t} \quad . \tag{66}$$

Because the benchmark model in Fig. 1 has no evaporative losses and thus $\bar{Q} = \bar{P}$, benchmark tests of the precipitation-weighted forward TTD ($^P TTD_k^*$) and the discharge-weighted backward TTD ($^Q TTD_k^*$) will yield identical results; thus the benchmark test of $^Q TTD_k^*$ (Fig. 13) will not be repeated here as a test of $^P TTD_k^*$.

4.8 Variations in transit time distributions with discharge, precipitation, antecedent moisture, and seasonality

Like the new water fraction F_{new}, estimating the transit time distribution $^Q TTD_k$ does not require unbroken time series. Thus, using approaches similar to those outlined in Sect. 3.5, one can estimate transit time distributions for subsets (including discontinuous subsets) of the precipitation and streamflow time series that reflect conditions of particular interest. In the case of new water fractions, subdividing the source data is relatively simple, because new water fractions are estimated from precipitation and streamflow tracers at the same time steps; thus when one subdivides the streamflow time series one also subdivides the precipitation time series, and vice versa. Transit time distributions are not so simple, because each discharge time j is potentially affected by $k = 0 \ldots m$ precipitation time steps $i = j - k$; thus the precipitation and streamflow time series can be subdivided differently, according to different criteria.

For example, we can choose to subdivide the data set according to the discharge time j, thus evaluating Eq. (36) only for time steps j that meet particular criteria (for example, to analyze time steps with high or low flows separately). Doing so has the effect of creating blank rows in the vector $\boldsymbol{Y}$ and matrix $\boldsymbol{X}$ in Eq. (39) for each excluded value of j. Figure 15 shows the results of estimating transit time distributions $^Q TTD_k$ using only the highest 20% of discharges (the corresponding $^Q TTD_k$'s calculated from the entire time series are also shown for comparison). Because large inputs of recent precipitation are likely to result in high flows, one would intuitively expect that high flows should contain larger contributions from recent precipitation. But how much larger? As Fig. 15 shows, this question can be answered, at least on average, by examining the transit time distributions of high-flow discharges. Figure 15 shows that ensemble hydrograph separation can accurately estimate the transit time distributions of both high flows and normal flows, and thus can accurately quantify how transport behavior is different under high-flow conditions.
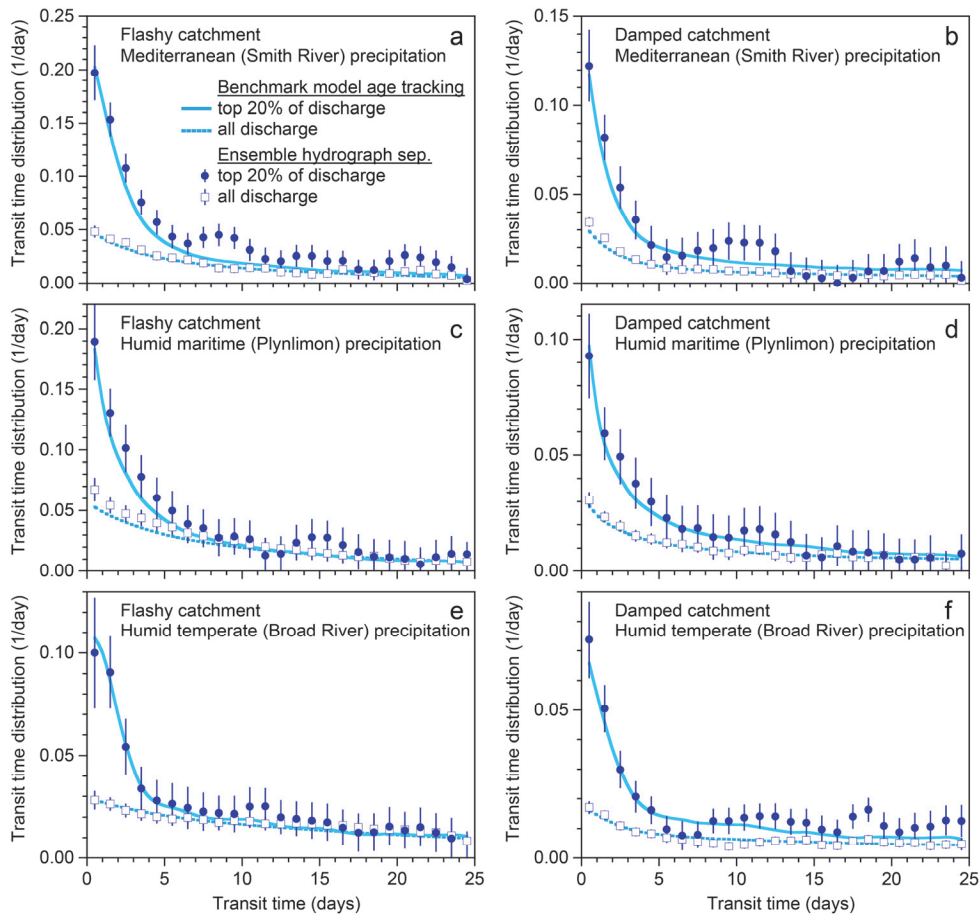
Figure 15. Transit time distributions $^{Q}TTD_{k}$ for high flows (the highest 20% of daily discharges; solid curve and solid circles), compared to transit time distributions for all flows (dashed curve and open squares). Solid circles and open squares show $^{Q}TTD_{k}$ estimates from ensemble hydrograph separation (Eq. 55); solid and dashed curves show true $^{Q}TTD_{k}$ determined by age tracking
5 **in the benchmark model. Left and right panels show TTD's for flashy and damped catchments, respectively; the three rows of panels represent three different precipitation drivers. Note that vertical axis scales differ substantially. High flows have much larger contributions of recent precipitation than average flows do. Ensemble hydrograph separation quantitatively captures this behavior across flashy and damped model catchments with all three precipitation drivers.**

10   In a Mediterranean climate (as depicted by, for example, the Smith River precipitation record shown in Fig. 1), one would

intuitively expect rainy-season streamflow to have larger contributions from recent precipitation. Conversely, one would

expect that dry-season streamflow will have much smaller contributions from recent rainfall (because there is so little of it,

among other reasons). But how big are the differences between rainy-season and dry-season transit time distributions? As

an illustration of what may be possible with real-world data, I took the five-year daily and weekly time series for the

15   benchmark model driven by the Mediterranean climate (Smith River) precipitation record, and separated them into summer

(dry) and winter (wet) seasons, and analyzed the two seasons separately. Figure 16 shows that, as expected, the

contributions of recent precipitation to streamflow are much larger during the wet season than the dry season. But more importantly, Figure 16 also shows that these differences can be accurately quantified, directly from data.
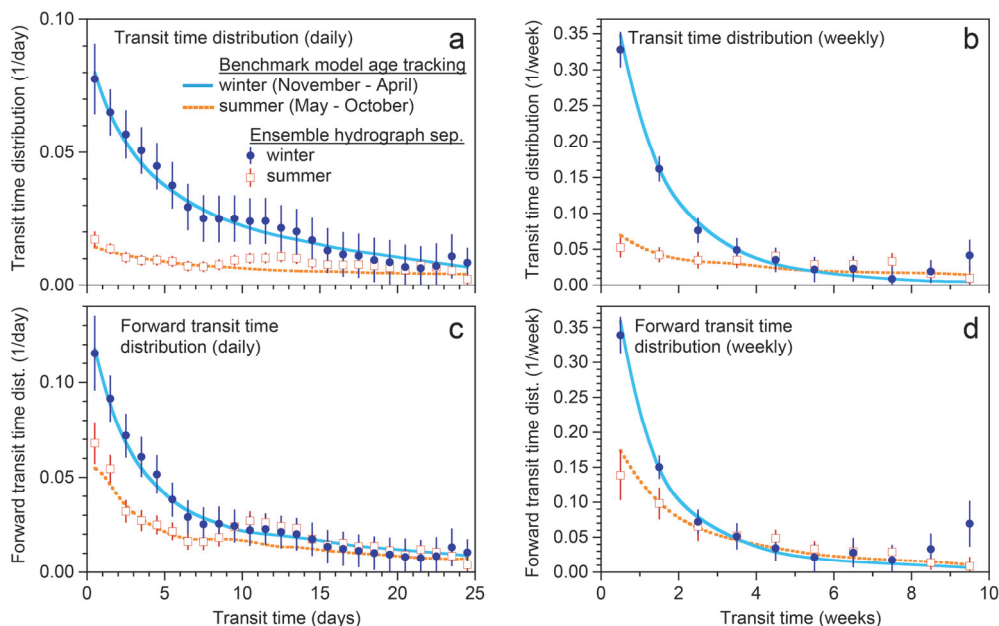
Figure 16. **Backward and forward transit time distributions (upper and lower panels, respectively) compared for summer (May-October) and winter (November-April) months, from benchmark model with Mediterranean (Smith River) precipitation climatology and flashy catchment parameters. Solid circles and open squares show estimates from ensemble hydrograph separation (Eqs. 55 and 63); solid and dashed curves show the true TTD's determined by age tracking in the benchmark model. Left and right panels show TTD's estimated from daily and weekly sampling, respectively. Owing to larger and more frequent rainfalls during winter (see Fig. 1), transit time distributions calculated for the winter months show a much larger contribution of recent rainfall to current streamflow (upper panels), and a much larger fraction of current precipitation becoming streamflow in the near future (lower panels). Ensemble hydrograph separation quantitatively captures the seasonal differences in the benchmark model's transit time distributions.**

The examples above are based on subdividing the data set according to the discharge time j. It is also possible to subdivide the data according to precipitation times $i = j - k$ that meet particular criteria (for example, to analyze time steps with large and small rainstorms separately). Doing so has the effect of creating diagonal stripes of blanks in the matrix $\mathbf{X}$ in Eq. (39) at $j = i + k$ for each excluded value of i. These are in addition to the diagonal stripes of missing values that arise because of sampling and measurement failures, or more commonly because no rain fell. Thus they pose no new mathematical challenges, and can be handled by the methods outlined in Sect. 4.2.

One question that can be explored by subdividing the time series according to precipitation is whether larger rainfall events propagate faster through catchments. Intuition suggests that intense rainfall should lead to larger contributions to streamflow from faster flowpaths. But how much larger? Figure 17 illustrates how this kind of question could potentially be explored.

In Fig. 17, the forward transit time distributions of the highest 20% of precipitation are compared to the average transit time distributions of all precipitation events, for the damped and flashy parameter sets and all three precipitation climatologies. One can see that large rain events are associated with much larger amounts of water reaching the stream quickly, but this effect largely disappears after about 2-3 days. Moreover, the magnitude and timing of this effect are nearly the same in the estimates derived from ensemble hydrograph separation and benchmark model age tracking, suggesting that they could also be reliably estimated from real-world data.
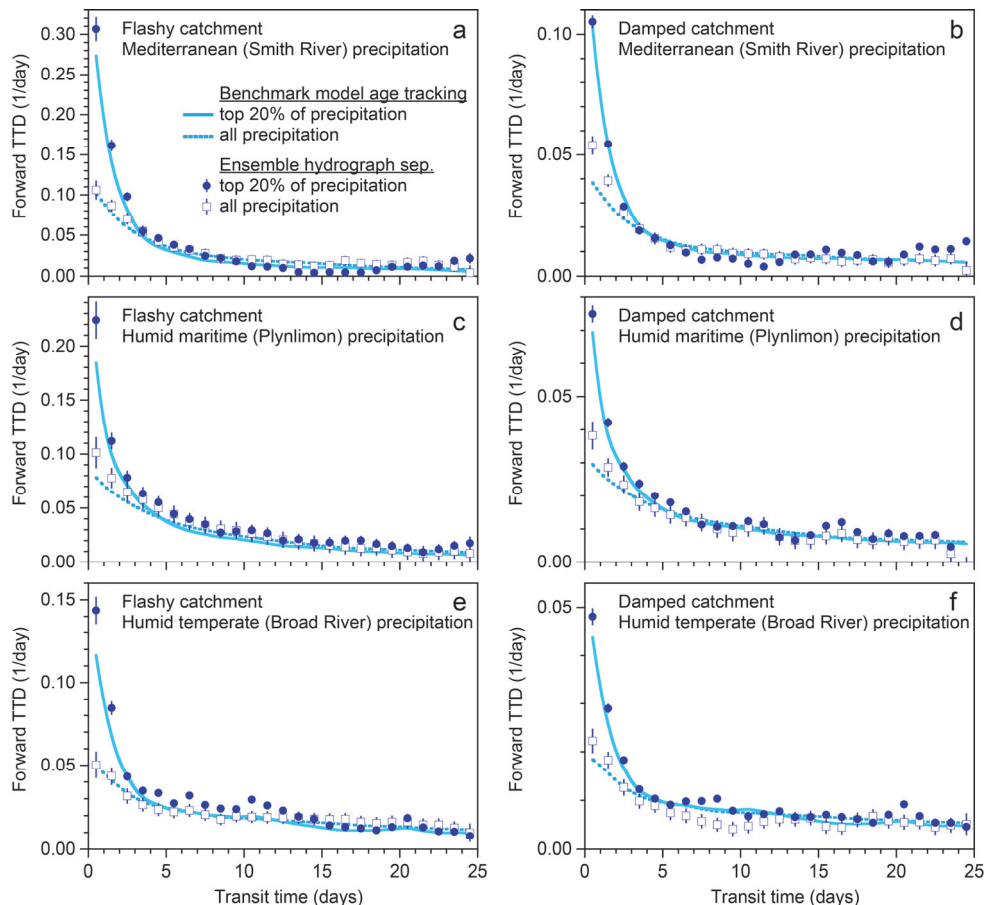
Figure 17. Forward transit time distributions $^\mathrm{P}TTD_k$ for intense precipitation (the highest 20% of daily precipitation totals; solid curve and solid circles), compared to forward transit time distributions for all precipitation (dashed curve and open squares). Solid circles and open squares show $^\mathrm{P}TTD_k$ estimates from ensemble hydrograph separation (Eq. 63); solid and dashed curves show the true $^\mathrm{P}TTD_k$ determined by age tracking in the benchmark model. Left and right panels show TTD's for flashy and damped catchments, respectively; the three rows of panels represent three different precipitation drivers. Note that vertical axis scales differ greatly. Despite a tendency for ensemble hydrograph separation to over-predict $^\mathrm{P}TTD_k$ for short lag times, the differences between the ensemble hydrograph separation estimates for intense precipitation and normal precipitation (open squares and solid circles) closely mirror the differences between the solid and dashed curves. Thus ensemble hydrograph separation can estimate the relative effect of intense precipitation on forward transit times, across widely differing precipitation drivers and catchment characteristics.

Antecedent wetness has been recognized as a controlling factor in catchment storm response (e.g., Detty and McGuire, 2010; Merz et al., 2006; Penna et al., 2011), but its effects on solute transport at the catchment scale have rarely been quantified, outside of the context of calibrated simulation models(e.g., van der Velde et al., 2012; Heidbüchel et al., 2012; Harman,

5   2015; Rodriguez et al., 2018). To assess whether the antecedent moisture dependence of solute transport might be measurable directly from field data, I binned the benchmark model time series into ranges of antecedent moisture (as measured by the upper box storage values S_u at the end of the previous day), and estimated the new water fractions $^Q F_{new}$ and $^P F_{new}$ using ensemble hydrograph separation. I used the upper box storage as a proxy for measurements of soil moisture or shallow groundwater levels, which are commonly used as indicators of antecedent wetness in catchment studies

10   (one could use antecedent discharge as a proxy instead; this would yield nearly equivalent results). As Figs. 18a and c show, ensemble hydrograph separation accurately predicts how both "backward" and "forward" new water fractions increase as functions of antecedent moisture.

To visualize how high antecedent moisture affects transit time distributions, I isolated the discharge times t_j associated with

15   the highest 10% of antecedent moisture values, and calculated the corresponding backward transit time distribution $^Q TTD_k$ (Fig. 18b). This TTD shows that high antecedent moisture is associated with large contributions of recent rainfall to streamflow, up to lags of about 3-4 days. The peak of the transit time distribution does not come at the shortest possible lag (same-day precipitation), but instead at a lag of 1.5 days (i.e., previous-day precipitation). This is the inevitable result of selecting points with high previous-day moisture, which are likely to be associated with high previous-day precipitation (and

20   thus high contributions of that previous-day precipitation to current streamflow). Storms typically last about 2-3 days in the Smith River precipitation record underlying the simulations in Fig. 18, so much of the backward TTD could potentially just reflect the pattern of precipitation, combined with the fact that points with high antecedent moisture have been selected.

One can even question why one would expect a *backward* TTD to help in understanding the effects of antecedent moisture at

25   all, given that the backward TTD will mostly reflect precipitation inputs that came *before* (and, in some cases, created) the antecedent moisture conditions themselves. A *forward* TTD, on the other hand, might help in quantifying how antecedent moisture affects the transmission of *future* precipitation to streamflow. I therefore isolated the precipitation times $t_i = t_{j-k}$ associated with the highest 10% of antecedent moisture values (thus, as explained above, filtering the matrix **X** in Eq. (39) along diagonal lines), and calculated the corresponding forward transit time distribution $^P TTD_k$ (Fig. 18d). As Fig. 18d

30   shows, in this model system, high antecedent moisture roughly doubles the proportion of precipitation that reaches the stream, but only out to lags of approximately two days, beyond which there is no clearly detectable effect. Naturally, these inferences pertain only to the model system, and do not tell us how real-world catchments might behave. However, because Fig. 18 shows that new water fractions and transit time distributions could be accurately quantified across a range of

antecedent moisture conditions directly from field data, it illustrates how ensemble hydrograph separation could be used to explore the effects of antecedent moisture in real-world catchments.
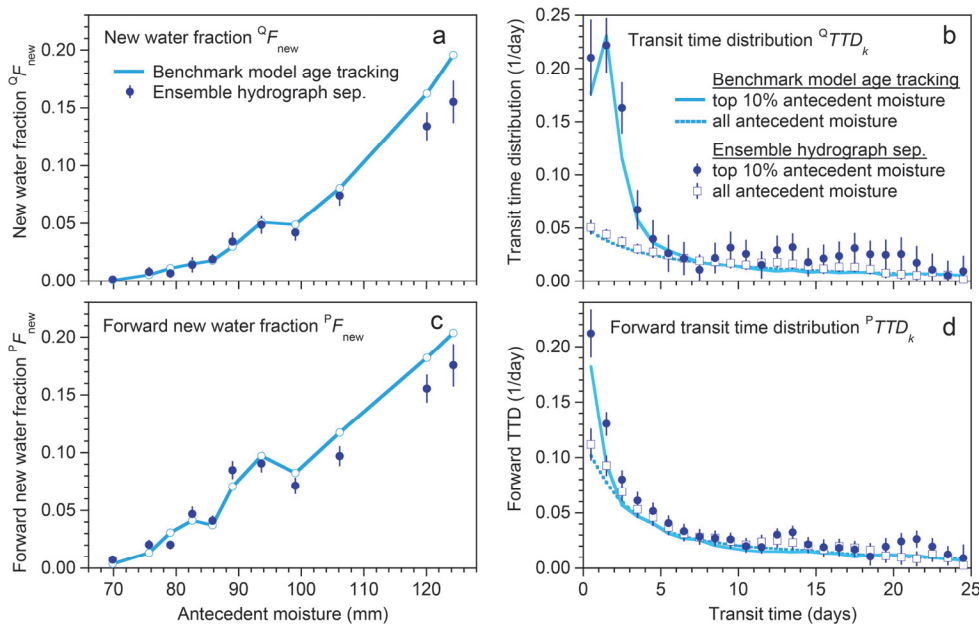
Figure 18. Effects of antecedent moisture on new water fractions and transit time distributions (upper panels) and their "forward" counterparts (lower panels). Left-hand panels show new water fractions from benchmark model age tracking (solid curves) and ensemble hydrograph separation (solid circles) stratified by percentiles of antecedent moisture (previous-day storage S_u in the benchmark model's upper box). Right-hand plots show transit time distributions for high antecedent moisture conditions (the highest 10% of previous-day storage levels in the upper box of the benchmark model; solid curve and solid circles), compared to transit time distributions for all antecedent moisture levels (dashed curve and open squares). All panels are derived from simulations with flashy catchment parameter set driven by Smith River (Mediterranean climate) precipitation time series. Error bars are one standard error.

5 Discussion

Over 20 years ago, Rodhe et al. (1996) wrote that transit times, despite their importance to modeling discharge, were "impractical to determine experimentally except in rare manipulative experiments where catchment inputs can be adequately controlled." Despite over two decades of effort, including increasingly elaborate theoretical discussions of transit time distributions, the problem identified by Rodhe et al. remains: how can we measure transit times, and transit time distributions, of real-world catchments under real-world conditions? And how can we verify whether the estimates we get are realistic ones? The theory and benchmark tests presented in Sects. 2-4 aim to provide a partial answer.

5.1 Comparisons with other approaches

Particularly because their names are similar, it is important to recognize how *ensemble* hydrograph separation contrasts with conventional hydrograph separation. Although one could view Eq. (9) as an algebraic re-arrangement of the conventional hydrograph separation equation (Eq. 3), with both sides multiplied by $(C_{new}-C_{old})$ and $C_{Q_{j-1}}$ substituted in place of C_{old}, there are important differences between the two approaches:

1. Conventional hydrograph separation estimates the *time-varying* new water fraction F_{new_j} at each individual point in time. By contrast, ensemble hydrograph separation estimates the *average* new water fraction F_{new} over an *ensemble* of points (hence the name).

2. Conventional hydrograph separation assumes that the end-member tracer signatures are *constant*, but ensemble hydrograph separation assumes them to be *time-varying*; indeed, it exploits their variability through time as its main source of information.

3. Conventional hydrograph separation requires that all end-members that contribute to streamflow must be identified, sampled, and measured. Ensemble hydrograph separation, by contrast, requires tracer measurements only from streamflow and any end-members whose contributions to streamflow are to be estimated. There is no need to assume that all end-members have been identified and measured, just that tracer fluctuations in any unmeasured end-members are not strongly correlated with those in measured end-members and in streamflow.

4. Conventional hydrograph separation requires that the end-members' tracer concentrations are distinct from one another; otherwise the solution to Eq. (3) becomes unstable because the denominator is nearly zero. By contrast, ensemble hydrograph separation estimates the new water fraction by regression, and points where the new water and old water concentrations overlap will have almost no leverage on the regression slope (they correspond to points near zero on the x-axes of Figs. 6a-b, 7a-b, 9a, or A1d, for example).

5. Conventional hydrograph separation is vulnerable to biases in tracer measurements, such as could arise from isotopic evaporative fractionation. By contrast, these same biases should have relatively little effect on ensemble hydrograph separation (e.g., Sect. 3.6), because it is based on regressions between tracer fluctuations, and regression slopes are unaffected by constant offsets on either the x or y axes.

It is also useful to contrast ensemble hydrograph separation with other methods for estimating transit time distributions from conservative tracers. As reviewed by McGuire and McDonnell (2006), these approaches typically convolve the precipitation tracer time series with an assumed transit time distribution, and then adjust the parameters of that distribution to achieve a best fit with the streamflow tracer time series. This convolution approach differs from ensemble hydrograph separation in several important respects:

1. In the convolution approach, the functional form of the transit time distribution must be assumed (although shape parameters often allow the shape of the TTD to be fitted, within a given family of distributions). By contrast, the

ensemble hydrograph separation approach makes no assumption about the shape of the distribution; instead, the TTD values at each lag k are estimated directly from data.

2. Ensemble hydrograph separation quantifies the transit time distribution out to a maximum lag m, beyond which it makes no assumptions (and draws no inferences) about the behavior of the TTD. By contrast, because convolution approaches assume a shape for the entire TTD, their results include the long tails that are missing from TTD's estimated from ensemble hydrograph separation. However, these long tails will typically be poorly constrained by data in any case, because the long-timescale signal of conservative tracers is typically so weak that it cannot be reliably separated from the noise (DeWalle et al., 1997; Stewart et al., 2010; Seeger and Weiler, 2014; Kirchner, 2016b). This is not an algorithmic problem and it does not have an algorithmic solution; instead it arises from the limited information content of conservative tracer time series on these long time scales. Although convolution approaches seek to get around this problem by assuming a (potentially parameterized) shape for the TTD, the long tails will largely reflect the underlying assumptions that are made, rather than any substantial influence of the tracer data themselves.

3. Convolution approaches are based on convolution *integrals*, and thus errors in the input terms accumulate over time. By contrast, the ensemble hydrograph separation approach is based on local *derivatives* of the stream tracer concentrations, and their covariances with fluctuations in the input tracer concentrations at various lags; as a result, errors in the input terms do not accumulate.

4. Missing input data pose a fundamental problem for convolution integrals, whereas they can be readily accommodated in the ensemble hydrograph separation approach (Sect. 4.2).

These considerations also generally apply to approaches that use tracer concentrations in rainfall and streamflow to calibrate storage selection (SAS) functions, instead of time-invariant transit time distributions (e.g., van der Velde et al., 2012; Harman, 2015). SAS function estimation also faces the additional difficulty that the SAS functions for streamflow and evapotranspiration are interrelated, because they both depend on, and jointly determine, the age distribution of catchment storage (e.g., Eqs. 2-8 of Botter, 2012; Rigon et al., 2016). Because we currently have no practical way to determine the age distributions of catchment storage or evapotranspiration, estimating SAS functions for streamflow requires making unverifiable assumptions concerning evampotranspiration ages, and the effects of these assumptions have not been quantified. By contrast, ensemble hydrograph separation directly quantifies the forward and backward transit time distributions of precipitation that subsequently leaves the catchment as streamflow, without needing to estimate, or to make any assumption about, the ages of waters that leave the catchment by other pathways.

Another approach that is coming into more frequent use is to calibrate a conceptual or physically based model to reproduce, as closely as possible, the observed hydrograph and streamflow tracer time series, and then infer the catchment transit time distribution or SAS function from particle tracking within the model (e.g., Benettin et al., 2013; Benettin et al., 2015; Remondi et al., 2018). For these inferences to be valid, the model must not only be a good predictor of the calibration data;

its underlying processes must also be the correct ones. In other words, the model must get the right answers for the right reasons, and it will generally be difficult to verify whether this is the case. Thus it will be difficult to know how much the inferred transit times are determined by the tracer data or by the structural assumptions of the underlying model. Nor does a good fit to the observational data verify the correctness of the model and the inferences drawn from it, because a good fit can

5   imply either that the model is doing everything correctly, or that it is doing multiple things wrong, in offsetting ways.

One can argue that every data analysis approach also implies some underlying model, and one might argue that ensemble hydrograph separation is based on the (implausible) assumption that the transit time distribution is time-invariant. Such an argument would be mistaken. As I have shown, ensemble hydrograph separation neither assumes nor requires that the transit

10 time distribution is stationary (see Appendices A and B). Instead, ensemble hydrograph separation quantifies the ensemble average of a catchment's *time-varying* transit time distribution, even when that distribution is highly dynamic.

5.2 Benchmark testing

Considerable effort has been devoted to benchmark tests of the methods proposed in Sects. 2 and 4. One may naturally ask: why bother? Why not just describe how ensemble hydrograph separation works, and apply it to several field data sets, and

15 see whether it gives reasonable results? One answer is that whether the results seem reasonable only reflects whether they agree with our preconceptions, not whether they (or our preconceptions) are correct. A second answer is that only through properly designed benchmark tests can we assess how accurate the method is, and what factors might affect its accuracy. Yet another answer is that the benchmark model gives the analysis method a precise target to hit, thus better revealing its strengths and weaknesses.

Benchmark tests also have a role to play in the day-to-day application of data analysis methods like those proposed here. Users may wonder: will this approach work with data from my catchment? Given the data I have, how accurately can I estimate the ensemble average transit time distribution? What kinds of tracer data will be needed to distinguish between two different conceptualizations of catchment-scale storage and transport? Carefully designed benchmark tests with synthetic

25 data can be helpful in addressing questions such as these.

It should be emphasized that in the tests presented here, the benchmark model knows nothing about how the analysis method works; in fact, its nonlinearity and nonstationarity rather badly violate the assumptions underlying the analysis. Conversely, the analysis method knows nothing about the inner workings of the benchmark model. It knows the model inputs and

30 outputs (the water fluxes and tracer concentrations in rainfall and streamflow), but it does not know – and, importantly, it does not need to know – how those outputs were generated. This is important because, for ensemble hydrograph separation to be useful in real-world catchments, its validity must not depend on the particular mechanisms that regulate flow and transport at the catchment scale.

Likewise, its validity must not depend on having unrealistically accurate or complete data. For this reason, the benchmark tests include substantial measurement errors, and substantial numbers of missing values (Sect. 3.1).

5   Thus these benchmark tests are much stricter than many in the literature. For example, some benchmark tests generate the benchmark data set using the same assumptions that underlie the analysis method itself (e.g., Klaus et al., 2015). Such tests usually generate very nice-looking results, but they are guaranteed to succeed because they are performing the same calculations twice (first forwards, then backwards). At the same time, such tests are not realistic, because they would only be relevant to real-world cases where all of the assumptions underlying the analysis method were exactly true. Such cases

10   are unlikely to exist.

One could argue that the benchmark model presented here would be more realistic if it were (for example) a spatially-distributed three-dimensional model based on Richards' equation, calibrated to a particular research watershed. However, the benchmark model's purpose is to generate a wide variety of targets for the analysis method to hit, with each target

15   precisely defined, rather than to realistically mimic any particular catchment. All that is essential is that it must generate realistically complex patterns of behavior, and exactly compute the "true" new water fractions and transit time distributions by age tracking. The relatively simple two-box conceptual model that has been used here was chosen because it fulfills both criteria, not because it embodied a particular mechanistic view of flow and transport. Likewise, consistency with the assumptions underlying ensemble hydrograph separation was not one of the criteria, nor should it be.

For the same reason, it should be clear that real-world catchments may not necessarily exhibit similar patterns of behavior to those of the benchmark model, as shown in Figs. 6-9 and 15-18. Thus the analyses presented here do not necessarily mean, for example, that we should expect new water fractions in real-world catchments to be roughly linear functions of discharge (Fig. 6), precipitation (Fig. 7), or antecedent moisture (Fig. 18). These patterns of behavior reflect the properties of the

25   benchmark model and its precipitation forcing. Whether real-world catchments behave similarly or differently is an open question. The benchmark tests demonstrate that these analyses are reliable (which cannot be demonstrated with real-world data because we cannot know independently what the right answer is), but they should not be taken as examples of what the real-world results would necessarily look like.

5.3 Errors, biases and uncertainties

30   The analysis methods outlined in Sects. 2 and 4 include explicit procedures for estimating the uncertainties (as quantified by standard errors) in both new water fractions (Eqs. 11, 15, and 20) and transit time distributions (Eqs. 54, 55, 60, 69, and 66). These uncertainties are generally realistic predictors of how much the ensemble hydrograph separation estimates deviate from the "true" benchmark values determined from age tracking: the scatter in Figs. 2 and 5, for example, is consistent with

the estimated standard errors, and the error bars in Figs. 6, 7, 9, and 11-18 (one standard error in all cases) are usually reasonable estimates of the deviations from the benchmark values (exceptions include the "humped" transit time distributions in Fig. 12, where the uncertainties are overestimated).

5   Unsurprisingly, the standard errors scale with the scatter (error variance) in the data, and inversely with the square root of the effective number of degrees of freedom. Thus the uncertainties will be larger when the data set is sparse and noisy, and when the new water fraction and/or transit time distribution explains only a small fraction of its variance. It should also be noted that the *relative* standard error can be large, for example when the TTD is small at long lags.

10   Because ensemble hydrograph separation does not require continuous input data, it can facilitate comparisons among various subsets of a catchment time series, as demonstrated in Sects. 3.5 and 4.7. However, it should be kept in mind that as one cuts the data set into more (and thus smaller) pieces, the statistical sampling variability among the data points remaining in each piece will become more and more influential, and the inferences drawn on each piece will become correspondingly more uncertain. Thus there will be practical limits to the granularity of the subsampling that can be applied in real-world cases.

One should also keep these considerations in mind when choosing m, the largest TTD lag to be estimated. Although m can be any value that the user chooses, as m increases, the uncertainties in TTD_k at each lag also increase, in essence because the user is choosing to distribute the (limited) information contained in the tracer time series among a larger number of TTD_k values. Conversely, if one sets m to zero and thus estimates only the amount of same-day or same-week water in streamflow

20   (whereupon the approaches outlined in Sects. 2 and 4 become equivalent), one brings all the available information to bear on estimating that one quantity. The tradeoff between TTD length and precision will depend on the length of the time series and the gaps that it contains, as well as the characteristic storage times of the catchment and the noise characteristics of the data (which will often be unknown). Thus it is difficult to give general guidance on appropriate values of m, but benchmark tests with synthetic data could be used to illustrate the tradeoffs involved.

In some TTD's, the last few lags exhibit unusually large deviations from the "true" TTD curves derived from age tracking (e.g. Figs. 12b, 13a and c, 14c, 16b and d, and 17b and d; in several of these cases the last point is below zero and thus does not appear on the plot). As noted in Sect. 4.5, I suspect (but cannot prove) that this is an aliasing effect that arises when the effects of fluxes beyond the longest measured lag are not adequately accounted for by the reference concentration $C_{\mathrm{older}_j} =$

30   $C_{Q_{j-m-1}}$. In practice this means that TTD values for the last few lags should not be taken too literally, particularly if they deviate from the trend in the previous lags.

Because ensemble hydrograph separation is based on correlations among tracer fluctuations, it is relatively insensitive to systematic biases that produce persistent offsets in the underlying data. For example, isotope ratios in precipitation often vary with altitude, leading to potential biases in precipitation tracer samples (depending on the sampling location). To the extent that these biases are constant, however, they should not alter regression slopes between tracer fluctuations in precipitation and streamflow (e.g., Figs. A1d, 6a-b, and 7a-b), or their multidimensional counterparts that determine the TTD. The same applies to randomly fluctuating precipitation tracer biases, unless they are large compared to the standard deviation of the tracer concentrations themselves – i.e., unless the fluctuating biases account for most of the variability in the precipitation tracer measurements. Likewise, confounding by any unmeasured end-members should be small, unless the unmeasured end-members are correlated with the measured ones, and have a strong influence on stream tracer concentrations.

The uncertainties calculated here, like all error propagation results, depend on the assumptions underlying the analysis (in this case, ensemble hydrograph separation). Under different assumptions, the errors in estimating the average F_{new} by regression could be larger. For example, if the means of C_{old_j} and C_{new_j} differed by much more than their pooled standard deviations, then variations in C_{Q_j} would mostly be driven by variations in F_{new} rather than variations in C_{new_j}. This highlights the important contrast between conventional and ensemble methods of hydrograph separation. Conventional hydrograph separation is based on comparing stream tracer values to constant end-members, and therefore works best when the end-members have widely separated means and small variability. By contrast, ensemble hydrograph separation works best when the variations in the end-members are large compared to the differences among their means, because it relies on correlating tracer fluctuations in streamflow with fluctuations in measured end-members.

5.4 Potential applications and extensions

The techniques proposed here quantify the timescales over which catchments store and transport water, and quantify how those timescales change with precipitation, discharge, and antecedent moisture. Such descriptive methods are often grouped under the heading of "catchment characterization". One should keep in mind, however, that a catchment's storage and transport behavior also depends on its external forcing. If its precipitation climatology were wetter (or drier), for example, its timescales of storage and transport would decrease (or increase) accordingly. Thus transport and storage timescales are not characteristics of the catchment alone, but rather of the catchment and its particular precipitation climatology. By mapping out how a catchment's storage and transport behavior changes with hydrologic forcing (e.g., Figs. 6, 7, 15, 17, and 18), however, ensemble hydrograph separation can contribute to a more complete picture of catchment response. Alternatively, these patterns of response to hydrologic forcing can be considered as catchment characteristics in their own right.

Because new water fractions and transit time distributions from ensemble hydrograph separation closely match benchmark model age tracking, one might consider using them as a model for catchment transport processes. This will usually be a bad idea. One must remember that ensemble hydrograph separation quantifies ensemble *averages*, which will not be good models of catchment processes unless the real-world transit time distribution is approximately time-invariant. That is unlikely to be the case.

This observation raises an important point. Ensemble hydrograph separation yields inferences that are phenomenological, not mechanistic. It quantifies *how catchments behave*, but does not, by itself, explain *how they work*. It can nonetheless contribute to mechanistic understanding by precisely quantifying catchment transport behavior, and thus facilitating more incisive comparisons with models. Examples of possible comparisons include:
- Do the model and the real-world catchment have similar new water fractions, and "forward" new water fractions (Figs. 2 and 5)?
- Do these new water fractions change similarly as functions of precipitation and discharge (Figs. 6 and 7)?
- Do they exhibit similar seasonal patterns (Fig. 9)?
- Do the model and the real-world catchment have similar transit time distributions, including "forward" transit time distributions (Figs. 11-14)?
- Do these transit time distributions change similarly as functions of precipitation, discharge, antecedent moisture, and seasonality (Figs. 15-18)?

In this approach to hypothesis testing, key signatures of behavior are extracted from both the model and the data before they are compared (Kirchner et al., 1996; Kirchner, 2006). This approach stands in contrast to the conventional model-testing paradigm in which model predictions are compared with observational time series through standard goodness-of-fit statistics. The conventional approach ignores the important question of *in what ways* the model predictions deviate from the data. Exploring this question requires diagnostic signatures of catchment behavior like those presented here, and is essential to improving models of catchment processes.

The analysis methods developed here can potentially be extended in several ways. For example, these methods could potentially be applied to infer transit times in other catchment fluxes, such as groundwater seepage or evapotranspiration. They could also be applied to other systems where transit times could be inferred from the propagation of fluctuating tracer inputs; potential examples include not only lakes, oceans, and aquifers, but also the atmosphere and perhaps even organisms.

The multiple regression analysis presented in Sect. 4 demonstrates that one can quantify the contributions of multiple end-members using a single conservative tracer. This is not possible in conventional end-member mixing analysis, which assumes that the end-members are constant and consequently requires that the number of end-members cannot exceed the number of tracers plus one. But because ensemble hydrograph separation is based on correlations of tracer fluctuations, one

tracer can potentially identify many end-members as long as their fluctuations are not too tightly correlated. This is potentially useful, because hydrologists typically have very few truly conservative tracers to work with (arguably only one, in the case of stable isotopes, because ^{18}O and ^{2}H are strongly correlated with one another). In the analysis in Sect. 4, the TTD's can be considered to represent 25 different end-members (which are all precipitation, at different lags). However the same approach could be used to analyze (for example) precipitation and snowmelt as sources of streamflow, if tracer time series are available in both candidate end-members and they are not too strongly correlated with one another. Similarly, in large river basins one could potentially quantify the contributions (and transit time distributions) of waters sourced from precipitation in different parts of the catchment – if, again, tracer time series are available for these multiple precipitation sources, and are not too strongly correlated with one another.

Last but not least, the approach presented here can also, with some modifications, be applied to rainfall and streamflow rates in order to quantify the time lags in catchments' hydraulic response to precipitation (reflecting the celerity of hydraulic potentials, as distinct from the velocity of water transport). A follow-up paper describing this "ensemble unit hydrograph" analysis is currently in preparation.

Competing interests. The author declares that he has no conflict of interest.

Acknowledgments. This work was motivated by discussions with Chris Soulsby and Doerthe Tetzlaff during long walks in the Scottish countryside. I also thank Jana von Freyberg, Andrea Rücker, Julia Knapp, Wouter Berghuijs, Paolo Benettin, and Greg Quenell for helpful discussions, Riccardo Rigon, Nicolas Rodriguez, and an anonymous reviewer for their comments, and Melissa Heyer for proofreading assistance.

Table 1. Definition of symbols (with defining equation, or equation of first use, in parentheses)

Symbol	Definition

Indices / subscripts

Symbol	Definition
i	index for precipitation time steps
j	index for discharge time steps
$k = j - i$	index for lags between precipitation and discharge
ℓ	second index for lags between precipitation and discharge
(xy)	parentheses indicate that analysis applies to cases j where neither x_j nor y_j is missing
(ky)	parentheses indicate that analysis applies to cases j where neither x_{jk} nor y_j is missing
$(k\ell)$	parentheses indicate that analysis applies to cases j where neither x_{jk} nor $x_{j\ell}$ is missing

Benchmark model variables and parameters

Symbol	Definition
b_u , b_l	upper- and lower-box drainage exponents in benchmark model (Fig. 1)
η	partitioning coefficient for upper-box drainage in benchmark model (Fig. 1)
L	drainage rate from upper box in benchmark model (Fig. 1)
Q_l	drainage rate from lower box in benchmark model (Fig. 1)
S_u , S_l	upper- and lower-box storage in benchmark model (Fig. 1)
$S_\mathrm{u,ref}$, $S_{l,\mathrm{ref}}$	reference storage levels in upper and lower boxes of benchmark model (Fig. 1)

Other symbols

Symbol	Definition
α	regression intercept (9)
β , $\hat{\beta}$	true regression slope (9), and its regression estimate (10)
β^* , $\hat{\beta}^*$	true discharge-weighted regression slope (16), and its regression estimate (18)
β_k , $\hat{\beta}_k$	true multiple regression slope as function of lag time k (36), and its regression estimate (40)
$\boldsymbol{\hat{\beta}}$	vector of regression estimates $\hat{\beta}_k$ (41)
Δt	sampling interval (55)
ε_j	regression error term (9)
$\boldsymbol{\varepsilon}$	vector of regression errors ε_j (39)
λ	regularization parameter (46)
ν	dimensionless regularization parameter (50)
$C_{\mathrm{Q}j}$	tracer concentration in stream discharge at time step j (1)
C_new , C_old	tracer concentration in new and old water (2)
$C_{\mathrm{new}j}$, $C_{\mathrm{old}j}$	time-varying tracer concentration in new and old water (5)
$C_{\mathrm{P}j-k}$	tracer concentration in precipitation at time step $i = j - k$ (33)
$C_{\mathrm{older}j}$	concentration effects of older tracer inputs, beyond maximum lag m (33)
$\mathbf{C}$	covariance matrix (46)
$F_{\mathrm{new}j}$	fraction of new water in streamflow at time step j (3)
F_new	ensemble average of $F_{\mathrm{new}j}$ (10)
$^\mathrm{Qp}F_\mathrm{new} = \hat{\beta}$	ensemble average of new water fraction in discharge during time steps with rain (Sect. 2.3)
$^\mathrm{Q}F_\mathrm{new}$	ensemble average of new water fraction in discharge, including rainless time steps (14)
$^\mathrm{Qp}F^*_\mathrm{new} = \hat{\beta}^*$	volume-weighted new water fraction in discharge during time steps with rain (18)
$^\mathrm{Q}F^*_\mathrm{new}$	volume-weighted new water fraction in discharge, including rainless time steps (18)

	$^{\mathrm{P}}F_{\mathrm{new}}$	new water fraction of precipitation (21, 27)
	$^{\mathrm{P}}F_{\mathrm{new}}^*$	volume-weighted new water fraction in precipitation (28)
	$\mathbf{H}$	Tikhonov-Philips regularization matrix (46)
	m	maximum lag in transit time distribution
5	n	number of discharge time steps
	n_{eff}	effective sample size, adjusted for serial correlation and/or uneven weighting (12, 19, 20)
	n_{p}	number of time steps with precipitation (14)
	n_{xy}	number of pairs of x_j and y_j (12)
	n_{x_k}	number time steps j with above-threshold precipitation at time step $i = j - k$ (45)
10	$n_{x_k x_\ell}$	number time steps j with above-threshold precipitation at both $i = j - k$ and $i = j - \ell$ (45)
	P_j	precipitation rate during time step j (22)
	$\bar{P}_{\mathrm{p}}$	average precipitation rate excluding rainless periods (22)
	$P_{\mathrm{threshold}}$	threshold precipitation rate below which tracer inputs are ignored (Sect. 3.1; Eq. 45)
	$\bar{P}_{x_k}$	average precipitation rate during time steps $i = j - k$ with above-threshold precipitation (64)
15	Q_j	stream discharge at time step j (1)
	$Q_{\mathrm{new}_j}, Q_{\mathrm{old}_j}$	new-water and old-water components of stream discharge (1)
	$\bar{Q}$	average stream discharge (18)
	$\bar{Q}_{\mathrm{p}}$	average stream discharge during time steps with precipitation (18)
	$\bar{Q}_{x_k}$	average stream discharge during time steps j with above-threshold precipitation at step $i = j - k$ (65)
20	$Q_{j(xy)}$	stream discharge during time steps j for which neither x_j nor y_j is missing (13)
	Q_{older_j}	unmeasured fluxes from older precipitation inputs, beyond maximum lag m (32)
	q_{jk}	volume of water entering as precipitation in time step $i = j - k$ and exiting in time step j (31)
	r_{xy}	correlation between x_j and y_j (11)
	r_{sc}	lag-1 serial correlation in regression residuals (12)
25	$s.e.()$	standard error (11)
	s_ε^2	variance of regression prediction errors (51, 52)
	$^{\mathrm{Q}}TTD_k$	"backward" transit time distribution of discharge, conditioned on exit time (55)
	$^{\mathrm{Q}}TTD_k^*$	discharge-weighted "backward" transit time distribution (60)
	$^{\mathrm{P}}TTD_k$	"forward" transit time distribution of precipitation, conditioned on entry time (63)
30	$^{\mathrm{P}}TTD_k^*$	volume-weighted "forward" transit time distribution (66)
	x_j	explanatory variable in linear regression (9)
	x_{jk}	explanatory variable in multiple linear regression (36)
	$\mathbf{X}$	matrix of reference-corrected input tracer concentrations x_{jk} (39)
	y_j	response variable in linear regression (9, 36)
35	$\mathbf{Y}$	vector of reference-corrected streamflow tracer concentrations y_j (39)

Appendix A: Estimating non-constant "constants" via regression

A conventional linear regression equation has the form

$$y_j = \beta\, x_j + \alpha + \varepsilon_j \quad , \tag{A1}$$

where y_j and x_j are response and explanatory variables, respectively, measured for individual cases j, where α and β are

5   (unknown) constants, and where ε_j is a random (and unknown) additive error term with mean of zero (alternatively, one can

consider $\alpha + \varepsilon_j$ to represent all of the unmeasured factors that influence y_j). Under the assumption that these unmeasured

factors are uncorrelated with x_j, linear regression obtains unbiased estimates of β from any of several functionally equivalent

formulas, including

$$\hat{\beta} \;=\; \frac{\mathrm{cov}(y,x)}{\mathrm{var}(x)} \;=\; \frac{\frac{1}{n-1}\sum_{j=1}^{n}(y_j-\bar{y})(x_j-\bar{x})}{\frac{1}{n-1}\sum_{j=1}^{n}(x_j-\bar{x})^2} \;=\; \frac{\langle y_j\, x_j\rangle - \langle y_j\rangle\langle x_j\rangle}{\langle x_j^2\rangle - \langle x_j\rangle^2} \;=\; \frac{\langle y_j'\, x_j'\rangle}{\langle x_j'^{\,2}\rangle} \quad , \tag{A2}$$

10   where $\hat{\beta}$ denotes the conventional least-squares estimator of β, primes denote deviations from means, and means over all j

may be denoted by either angled brackets or overbars, depending on context.

In many practical situations, the unknown constant β may not in fact be constant, but instead may differ among the cases j.

In such situations, the true relationship among the variables is not Eq. (A1), but instead

15   $$y_j = \beta_j\, x_j + \alpha + \varepsilon_j \quad , \tag{A3}$$

where the small but important difference between (A1) and (A3) is the subscript j on β. It may be unclear *a priori* whether

β is a constant or not, and therefore whether (A1) or (A3) applies. In other words, (A1) represents a special case of the more

general relationship represented by (A3), and it may be unclear whether we are dealing with the special case or the general

one.

Thus, in environmental work, regression equations are often used to estimate "constants" that are not known to be constant,

or, even more pointedly, "constants" that we know are not constant. Regression equations are nonetheless used, under the

assumption that the result will provide a useful estimate of some central tendency of the non-constant "constant". The basis

for this assumption and its range of validity are unclear.

The problem at hand can be stated like this: if the unknown coefficient β_j differs among the cases j, as in (A3), but one

nonetheless calculates a conventional least squares estimator $\hat{\beta}$ using (A2), how will the calculated value of $\hat{\beta}$ depend on the

properties of the (unknown) β_j, including their possible relationships with the values x_j of the explanatory variable? The

answer can be obtained straightforwardly by substituting y_j from (A3) into (A2) and solving for $\hat{\beta}$. The math is streamlined

somewhat if one separates x, y, β, and ε into their (sample) means and deviations (replacing x_j with $\bar{x} + x_j'$, and similarly for y, β, and ε), where primed quantities indicate deviations from means. One can begin by expressing (A3) in terms of deviations from means,

$$y_j' = y_j - \bar{y} = \beta_j\, x_j - \langle \beta_j\, x_j \rangle + (\varepsilon_j - \bar{\varepsilon}) = (\bar{\beta} + \beta_j')(\bar{x} + x_j') - \langle (\bar{\beta} + \beta_j')(\bar{x} + x_j') \rangle + \varepsilon_j' \quad , \tag{A4}$$

and then by multiplying the terms in parentheses, yielding

$$y_j' = \underline{\bar{\beta}\,\bar{x}} + \bar{\beta}\, x_j' + \bar{x}\, \beta_j' + \beta_j'\, x_j' - \underline{\langle \bar{\beta}\,\bar{x} \rangle} - \underline{\underline{\langle \bar{\beta}\, x_j' \rangle}} - \underline{\underline{\langle \bar{x}\, \beta_j' \rangle}} - \langle \beta_j'\, x_j' \rangle + \varepsilon_j' \quad , \tag{A5}$$

The single-underlined terms in (A5) cancel each other, and the double-underlined terms are zero because primed quantities will always average to zero (although products of two or more primed quantities usually will not). Removing all underlined terms, multiplying by $x_j' = x_j - \bar{x}$, averaging over all j, and dividing by the variance of x yields directly:

$$\hat{\beta} = \frac{\text{cov}(y,x)}{\text{var}(x)} = \frac{\langle y_j'\, x_j' \rangle}{\langle x_j'\, x_j' \rangle} = \frac{\bar{\beta}\, \langle x_j'\, x_j' \rangle + \bar{x}\, \langle \beta_j'\, x_j' \rangle + \langle \beta_j'\, x_j'\, x_j' \rangle + \underline{\underline{\langle \langle \beta_j'\, x_j' \rangle\, x_j' \rangle}} + \langle \varepsilon_j'\, x_j' \rangle}{\langle x_j'\, x_j' \rangle} \quad . \tag{A6}$$

The double-underlined term in the numerator of (A6) is zero, because the inner average is a constant and therefore just re-scales x_j', which in turn averages to zero. Simplifying the remaining terms, one obtains

$$\hat{\beta} = \bar{\beta} + \bar{x}\, \frac{\text{cov}(\beta,x)}{\text{var}(x)} + \frac{\langle \beta_j'\, x_j'^{2} \rangle}{\text{var}(x)} + \frac{\text{cov}(\varepsilon,x)}{\text{var}(x)} \quad . \tag{A7}$$

Equation (A7) cannot be evaluated in practice, because the true coefficients β_j and the errors ε_j will not be known. Nonetheless it can be useful to understand how their properties influence $\hat{\beta}$, so that regression results can be properly interpreted. In this regard, each of the four terms of (A7) has a story to tell. The first term of (A7) says that the linear regression coefficient $\hat{\beta}$ will be a good approximation to the (sample) mean of the β_j, if the other terms are negligible.

The second term says that the linear regression coefficient $\hat{\beta}$ can also be affected by correlations between β_j and x_j. The magnitude of this effect will be the average value of x, multiplied by the regression slope of the relationship between x and β. This second term will vanish if $\bar{x}$ is zero or if there is no correlation between x_j and β_j.

The third term can be viewed as a weighted average of the deviations of the β_j from their mean, where the weighting factors are the squared deviations of the x_j from their mean (in statistical terms, these weighting factors are called leverages). Thus the third term of (A7) expresses the effect of a cup-shaped relationship between β_j and x_j; for example, if x_j values with greater leverage on $\hat{\beta}$ (because they lie farther from $\bar{x}$) are also associated with higher values of β_j (and thus a steeper relationship between x_j and y_j), the estimate of $\hat{\beta}$ will be biased upward. Note in particular that the third term could be non-zero even if the correlation between β_j and x_j is zero (that is, the relationship between β_j and x_j could be cup-shaped even if

it has a slope of zero overall). Conversely, the third term is insensitive to linear correlations (even strong ones) between β_j and x_j.

The fourth term says that $\hat{\beta}$ could also be biased by correlations between the error term and the explanatory variable; the
5   magnitude of this possible bias equals the regression slope of ε_j as a function of x_j. This is the well-known problem of artifactual correlation (also called the "third variable problem" or "hidden variable problem"): if hidden (unmeasured) variables are correlated with the measured explanatory (x) variable, their effects on the response (y) variable will be falsely attributed to the x variable instead, distorting its regression coefficient.

10   It should be noted that the means, variances, and covariances in (A2)-(A7) are sample statistics calculated over the sample cases j, which may differ from the true means, variances, and covariances of the underlying distributions. Thus there will be additional uncertainty resulting from sampling variability (in addition to the biases quantified by the second, third, and fourth terms in Eq. A7), if one interprets the regression slope as an estimate of the true mean of β rather than the sample mean of the β_j for the particular cases j that have been sampled.

To illustrate the analysis outlined above, I conducted a simple numerical experiment based on ensemble hydrograph separation. I created a synthetic data set based on the mixing equation

$$C_{Q_j} = F_{new_j} C_{new_j} + \left(1 - F_{new_j}\right) - C_{Q_{j-1}} \quad , \tag{A8}$$

where C_{Q_j}, the concentration in the stream, is a volume-weighted average of the (measured) new-water concentration C_{new_j}
20   and the old-water concentration $C_{Q_{j-1}}$ from the previous time step, weighted by the new water fraction F_{new_j} and its complement $1 - F_{new_j}$. Values of F_{new_j} for each time step j are randomly chosen from a beta distribution,

$$\text{Beta}(\alpha, \beta) = \frac{x^{\alpha-1} (1-x)^{\beta-1}}{\text{B}(\alpha, \beta)} \quad , \tag{A9}$$

where x is a random variable that, appropriately for a fraction, ranges from 0 to 1, the beta function $\text{B}(\alpha, \beta) = \Gamma(\alpha)\Gamma(\beta)/\Gamma(\alpha + \beta)$ is a normalization constant that ensures that the cumulative probability is 1, and α and β are shape
25   parameters that are related to the mean (μ) by $\mu = 1/(1 + \beta/\alpha)$, or equivalently $\beta = \alpha[(1-\mu)/\mu]$. In the simulations shown here (Fig. A1a-e), the α parameter is fixed at 1.

Values of C_{new_j} for each point in time j are randomly chosen from a normal distribution with a standard deviation of 10 (Fig. A1b). Values of C_{Q_j} are calculated for the whole time series using Eq. (A8), and measurement errors (normally distributed,
30   with a standard deviation of 1) are added to both C_{new} and C_Q. Then an ensemble estimate of the average F_{new} is obtained

by linear regression of $y_j = C_{Q_j} - C_{Q_{j-1}}$ on $x_j = C_{\text{new}_j} - C_{Q_{j-1}}$, following Eq. (9) in the main text. A plot of such a regression is shown in Fig. A1d. In this particular ensemble, the individual F_{new_j} values for each time step varied between 0.0001 and 0.71, with a mean of 0.20 and a standard deviation of 0.16. The ensemble hydrograph separation estimate of the average F_{new} was 0.205±0.009 (mean ± standard error), deviating from the true mean value by roughly its standard error, as

5   one would expect. This analysis was repeated 1000 times for mean F_{new} values randomly chosen between 0.025 and 0.975. The results are summarized in Fig. A1e, which compares the regression estimates of the average F_{new} against the true means of the F_{new} values in each sample. Although the individual F_{new_j} values that make up each mean vary widely (as indicated by the horizontal width of the shading in Fig. A1e), the regression estimates of the average F_{new} cluster tightly around the 1:1 line, with a root-mean-square deviation of less than 0.02 across the full range of average F_{new} (this root-mean-square

10   deviation scales, as one would expect, inversely with the square root of the number of data points in the simulated time series).

In the simulations shown in Fig. A1, F_{new_j} is independent of C_{new_j}, $C_{Q_{j-1}}$, and the measurement errors; therefore the biases quantified in Eq. A7 are expected to be small. Nonetheless, one should be aware that in the specific case of Eq. A8 there

15   could be two additional sources of bias that Eq. A7 does not account for. Large measurement errors in C_{new} (meaning measurement errors that are not small compared to the standard deviation of C_{new} itself) could potentially create negative biases in estimates of the average F_{new}, because they would add spurious variation to the x axis of regressions like Fig. A1d. Conversely, large measurement errors in C_Q – which again means errors that are not small compared to the standard deviation of C_{new} (not C_Q) – could potentially create positive biases in estimates of the average F_{new}, because $C_{Q_{j-1}}$ appears

20   on both axes of the regression in Fig. A1d, so large errors in $C_{Q_{j-1}}$ would spuriously increase the correlation between the x and y axes of regressions like Fig. A1d. Both of these biases should be negligible in real-world cases, however, because the measurement uncertainties in C_{new} and C_Q are typically much smaller than the variability in C_{new}.
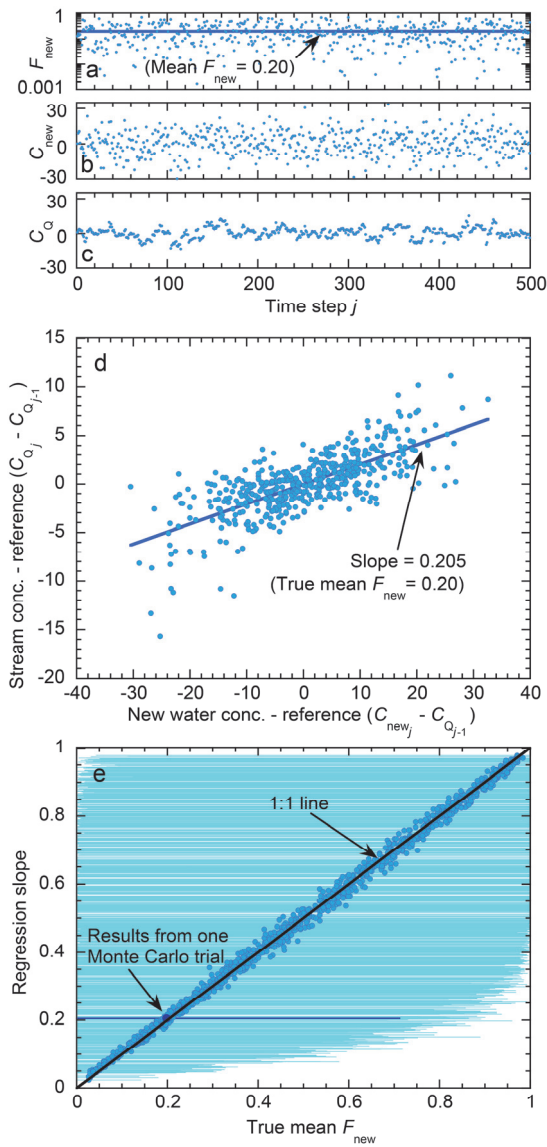
Figure A1. Benchmark test of regression estimates of mean new water fractions, using data from a simple two-component mixing model. In that mixing model (Eq. A8), a randomly varying new water fraction F_{new} (a) determines the relative proportions of new and old water (C_{new_j} and $C_{Q_{j-1}}$, respectively) which are combined to yield a mixture with concentration C_{Q_j} (c). Among the 500-point time series shown in panels (a)-(c), the new water fraction F_{new} varies between 0.0001 and 0.71, with a mean of 0.20 and a standard deviation of 0.15. Plotting the concentration of the mixture in the stream as a function of the concentration in the new-water end-member (e) yields a regression slope of 0.205±0.009, which agrees within error with the true average of F_{new} of $\mu=0.20$. Repeating this analysis 1000 times, with mean values of F_{new} ranging from nearly zero to nearly one, yields regression slopes that agree with the means of the F_{new} for each Monte Carlo trial with an RMS error of only 0.02 (panel e). In panel (e), the circles show the regression slopes and mean F_{new}, and the horizontal light blue lines show the range of F_{new}, for each Monte Carlo trial. The dark circle and dark line show the results for the individual Monte Carlo trial shown in panels (a)-(d).

Appendix B: Accounting for rain-free periods, and estimating non-constant "constants" by multiple regression

Assume a multiple linear regression equation with non-constant unknown coefficients,

$$y_j = \sum_{k=0}^{m} \beta_{j,k}\, x_{j,k} + \alpha + \varepsilon_j \quad , \tag{B1}$$

which can be more explicitly represented, for a series of sampling times $j = 1 \dots n$ as

$$
\begin{aligned}
y_1 &= \beta_{1,0}\, x_{1,0} + \beta_{1,1}\, x_{1,1} + \beta_{1,2}\, x_{1,2} + \beta_{1,3}\, x_{1,3} \dots + \beta_{1,m}\, x_{1,m} + \alpha + \varepsilon_1 \\
y_2 &= \beta_{2,0}\, x_{2,0} + \beta_{2,1}\, x_{2,1} + \beta_{2,2}\, x_{2,2} + \beta_{2,3}\, x_{2,3} \dots + \beta_{2,m}\, x_{2,m} + \alpha + \varepsilon_2 \\
y_3 &= \beta_{3,0}\, x_{3,0} + \beta_{3,1}\, x_{3,1} + \beta_{3,2}\, x_{3,2} + \beta_{3,3}\, x_{3,3} \dots + \beta_{3,m}\, x_{3,m} + \alpha + \varepsilon_3 \\
y_4 &= \beta_{4,0}\, x_{4,0} + \beta_{4,1}\, x_{4,1} + \beta_{4,2}\, x_{4,2} + \beta_{4,3}\, x_{4,3} \dots + \beta_{4,m}\, x_{4,m} + \alpha + \varepsilon_4 \\
&\qquad\qquad\qquad\qquad\qquad \ddots \\
y_n &= \beta_{n,0}\, x_{n,0} + \beta_{n,1}\, x_{n,1} + \beta_{n,2}\, x_{n,2} + \beta_{n,3}\, x_{n,3} \dots + \beta_{n,m}\, x_{n,m} + \alpha + \varepsilon_n \quad .
\end{aligned}
\tag{B2}
$$

For simplicity, and without loss of generality, assume that the y_j's and $x_{j,k}$'s have means of zero. Assume further that for each k, the coefficients $\beta_{j,k}$ either have a constant value of β_k (when precipitation is present at time step $i = j - k$), or have a value of 0 (when precipitation in missing at time step $i = j - k$). In the latter case the value of $x_{j,k}$ will be undefined, but it will also be irrelevant because it is multiplied by zero. The resulting system of equations will then have the following form, with missing values along diagonal stripes (this illustration shows just one possible set of missing values):

$$
\begin{aligned}
y_1 &= \beta_0\, x_{1,0} + \qquad\quad\; + \beta_2\, x_{1,2} + \beta_3\, x_{1,3} \dots + \beta_m\, x_{1,m} + \alpha + \varepsilon_1 \\
y_2 &= \qquad\quad\; + \beta_1\, x_{2,1} + \qquad\quad\; + \beta_3\, x_{2,3} \dots + \beta_m\, x_{2,m} + \alpha + \varepsilon_2 \\
y_3 &= \beta_0\, x_{3,0} + \qquad\quad\; + \beta_2\, x_{3,2} + \qquad\quad\; \dots + \beta_m\, x_{3,m} + \alpha + \varepsilon_3 \\
y_4 &= \beta_0\, x_{4,0} + \beta_1\, x_{4,1} + \qquad\quad\; + \beta_3\, x_{4,3} \dots + \qquad\quad\; + \alpha + \varepsilon_4 \\
&\qquad\qquad\qquad\qquad \ddots \\
y_n &= \beta_0\, x_{n,0} + \beta_1\, x_{n,1} + \beta_2\, x_{n,2} + \qquad\quad\; \dots + \beta_m\, x_{n,m} + \alpha + \varepsilon_n \quad .
\end{aligned}
\tag{B3}
$$

Multiplying the left and right sides of Eq. (B3) by the transpose of $\boldsymbol{X}_0$ (to take one example) yields

$$
\sum_{j=1}^{n} (y_j\, x_{j,0})_{P_{j-k}>0} = \beta_0 \sum_{j=1}^{n} (x_{j,0}\, x_{j,0})_{P_{j-0}>0} + \beta_1 \sum_{j=1}^{n} (x_{j,1}\, x_{j,0})_{P_{j-1}>0,\, P_{j-0}>0}
$$

$$
+ \beta_2 \sum_{j=1}^{n} (x_{j,2}\, x_{j,0})_{P_{j-2}>0,\, P_{j-0}>0} + \dots + \beta_m \sum_{j=1}^{n} (x_{j,m}\, x_{j,0})_{P_{j-m}>0,\, P_{j-0}>0} \quad , \tag{B4}
$$

where the constant α and the error term ε_j drop out because their sums of cross-products with the $x_{j,0}$ are zero. One can see that each of the summations of cross-products equals the covariance of the respective vectors, multiplied by the number of points in the summation. In contrast to a typical multiple regression, these numbers of points are not the same. For the left-hand side of Eq. (B4), the summation is taken over the non-missing members of $\boldsymbol{X}_0$; if we use n_{x_0} to express the number of such members, this summation equals $n_{x_0} \mathrm{cov}(\boldsymbol{X}_0, \boldsymbol{Y})$. The first term on the right hand side can also be evaluated for all n_{x_0} non-missing members of $\boldsymbol{X}_0$; there are n_{x_0} of these, so this term becomes $\beta_0\, n_{x_0} \mathrm{cov}(\boldsymbol{X}_0, \boldsymbol{X}_0) = \beta_0\, n_{x_0} \mathrm{var}(\boldsymbol{X}_0)$. The

second term on the left-hand side, on the other hand, can only be evaluated when both X_0 and X_1 are non-missing. If we

denote the number of such cases as $n_{x_0 x_1}$, the second term equals $\beta_1 \, n_{x_0 x_1} \operatorname{cov}(X_0, X_1)$, the third term equals

$\beta_2 \, n_{x_0 x_2} \operatorname{cov}(X_0, X_2)$, and so forth. Thus when re-expressed as covariances, Eq. (B3) becomes

$$n_{x_0} \operatorname{cov}(X_0, Y) = \beta_0 \; n_{x_0} \operatorname{cov}(X_0, X_0) + \beta_1 \, n_{x_0 x_1} \operatorname{cov}(X_0, X_1) + \beta_2 \, n_{x_0 x_2} \operatorname{cov}(X_0, X_2) + \; \dots \; \beta_m \, n_{x_0 x_m} \operatorname{cov}(X_0, X_m)$$
$$n_{x_1} \operatorname{cov}(X_1, Y) = \beta_0 \, n_{x_1 x_0} \operatorname{cov}(X_1, X_0) + \beta_1 \; n_{x_1} \operatorname{cov}(X_1, X_1) + \beta_2 \, n_{x_1 x_2} \operatorname{cov}(X_1, X_2) + \; \dots \; \beta_m \, n_{x_1 x_m} \operatorname{cov}(X_1, X_m)$$
$$n_{x_2} \operatorname{cov}(X_2, Y) = \beta_0 \, n_{x_2 x_0} \operatorname{cov}(X_2, X_0) + \beta_1 \, n_{x_2 x_1} \operatorname{cov}(X_2, X_1) + \beta_2 \; n_{x_2} \operatorname{cov}(X_2, X_2) + \; \dots \; \beta_m \, n_{x_2 x_m} \operatorname{cov}(X_2, X_m)$$
$$\ddots$$
$$n_{x_m} \operatorname{cov}(X_m, Y) = \beta_0 \, n_{x_m x_0} \operatorname{cov}(X_m, X_0) + \beta_1 \, n_{x_m x_1} \operatorname{cov}(X_m, X_1) + \beta_2 \, n_{x_m x_2} \operatorname{cov}(X_m, X_2) + \; \dots \; \beta_m \, n_{x_m} \operatorname{cov}(X_m, X_m) \quad . \tag{B5}$$

5   Dividing through by the n_{x_k} terms on the left-hand side, one directly obtains the following system of m equations in m

unknowns,

$$\operatorname{cov}(X_0, Y) = \beta_0 \operatorname{cov}(X_0, X_0) + \beta_1 \frac{n_{x_0 x_1}}{n_{x_0}} \operatorname{cov}(X_0, X_1) + \beta_2 \frac{n_{x_0 x_2}}{n_{x_0}} \operatorname{cov}(X_0, X_2) + \; \dots \; \beta_m \frac{n_{x_0 x_m}}{n_{x_0}} \operatorname{cov}(X_0, X_m)$$

$$\operatorname{cov}(X_1, Y) = \beta_0 \frac{n_{x_1 x_0}}{n_{x_1}} \operatorname{cov}(X_1, X_0) + \beta_1 \operatorname{cov}(X_1, X_1) + \beta_2 \frac{n_{x_1 x_2}}{n_{x_1}} \operatorname{cov}(X_1, X_2) + \; \dots \; \beta_m \frac{n_{x_1 x_m}}{n_{x_1}} \operatorname{cov}(X_1, X_m)$$

$$\operatorname{cov}(X_2, Y) = \beta_0 \frac{n_{x_2 x_0}}{n_{x_2}} \operatorname{cov}(X_2, X_0) + \beta_1 \frac{n_{x_2 x_1}}{n_{x_2}} \operatorname{cov}(X_2, X_1) + \beta_2 \operatorname{cov}(X_2, X_2) + \; \dots \; \beta_m \frac{n_{x_2 x_m}}{n_{x_2}} \operatorname{cov}(X_2, X_m)$$

$$\ddots$$

$$\operatorname{cov}(X_m, Y) = \beta_0 \frac{n_{x_m x_0}}{n_{x_m}} \operatorname{cov}(X_m, X_0) + \beta_1 \frac{n_{x_m x_1}}{n_{x_m}} \operatorname{cov}(X_m, X_1) + \beta_2 \frac{n_{x_m x_2}}{n_{x_m}} \operatorname{cov}(X_m, X_2) + \; \dots \; \beta_m \operatorname{cov}(X_m, X_m) \quad , \tag{B6}$$

which can be solved by the usual matrix inversion approach, yielding:

$$
\begin{pmatrix} \hat{\beta}_0 \\ \hat{\beta}_1 \\ \hat{\beta}_2 \\ \vdots \\ \hat{\beta}_m \end{pmatrix} =
\begin{pmatrix}
\operatorname{cov}(X_0, X_0) & \frac{n_{x_0 x_1}}{n_{x_0}} \operatorname{cov}(X_0, X_1) & \frac{n_{x_0 x_2}}{n_{x_0}} \operatorname{cov}(X_0, X_2) & \cdots & \frac{n_{x_0 x_m}}{n_{x_0}} \operatorname{cov}(X_0, X_m) \\
\frac{n_{x_1 x_0}}{n_{x_1}} \operatorname{cov}(X_1, X_0) & \operatorname{cov}(X_1, X_1) & \frac{n_{x_1 x_2}}{n_{x_1}} \operatorname{cov}(X_1, X_2) & \cdots & \frac{n_{x_1 x_m}}{n_{x_1}} \operatorname{cov}(X_1, X_m) \\
\frac{n_{x_2 x_0}}{n_{x_2}} \operatorname{cov}(X_2, X_0) & \frac{n_{x_2 x_1}}{n_{x_2}} \operatorname{cov}(X_2, X_1) & \operatorname{cov}(X_2, X_2) & \cdots & \frac{n_{x_2 x_m}}{n_{x_2}} \operatorname{cov}(X_2, X_m) \\
\vdots & \vdots & \vdots & \ddots & \vdots \\
\frac{n_{x_m x_0}}{n_{x_m}} \operatorname{cov}(X_m, X_0) & \frac{n_{x_m x_1}}{n_{x_m}} \operatorname{cov}(X_m, X_1) & \frac{n_{x_m x_2}}{n_{x_m}} \operatorname{cov}(X_m, X_2) & \cdots & \operatorname{cov}(X_m, X_m)
\end{pmatrix}^{-1}
\begin{pmatrix} \operatorname{cov}(X_0, Y) \\ \operatorname{cov}(X_1, Y) \\ \operatorname{cov}(X_2, Y) \\ \vdots \\ \operatorname{cov}(X_m, Y) \end{pmatrix} .
$$
$$\tag{B7}$$

10   One can see that Eq. (B7) is identical in form to Eq. (40), with the addition of weighting factors on the off-diagonal elements

of the covariance matrix. One consequence of these leading terms is that the weighted covariance matrix will usually not be

completely symmetrical, because (for example) $n_{x_2 x_0}/n_{x_2}$ will often differ from $n_{x_2 x_0}/n_{x_0}$.

It bears emphasis that Eq. (B7) accounts for gaps in precipitation, but not for precipitation or streamflow samples that are

15   missing due to sampling and measurement failures. A gap in precipitation means that the corresponding tracer values never

existed at all, and had no effect on streamflow, whereas tracer values that are missing due to sampling and measurement

failures actually did affect streamflow, but are unknown. Equation (B7) accounts for the fact that the tracer covariances will

necessarily be less strongly coupled to one another, the less frequently precipitation falls. Glasser's method, by contrast,

estimates the covariances themselves from all available pairs of observations, but says nothing about how they are related to

one another. Therefore we can account for both kinds of missing data using Eq. (B7), with the covariances between pairs of variables estimated using Glasser's method (Eqs. 42-43). That approach results in Eq. (44).

Astute readers may notice that Eq. (B3) is equivalent to the normal equations of conventional multiple regression, with the
5   cases of missing precipitation replaced by $x_{j,k} = 0$ (instead of $\beta_{j,k} = 0$). This provides a simple procedure for estimating the β_k if tracer values are only missing due to lack of precipitation, with no sampling or measurement failures. This method proceeds as follows:

1. Normalize $\mathbf{Y}$ and each of the $\mathbf{X}_k$ to zero by subtracting the mean from each vector (excluding any missing values from these means).

10   2. Replace any values that are missing due to lack of precipitation with zeroes.

3. Solve for the β_k using conventional multiple regression.

4. Multiply the standard errors of the β_k (not the β_k themselves!) by $\sqrt{n/n_{(k)}}$ to account for the fact that the zeroes that have been used to in-fill the missing values are not measured values, and thus do not contribute information to constrain the β_k.

15   This method is unlikely to be useful in most practical cases, in which occasional sampling and measurement failures are virtually guaranteed. However, it can provide a useful consistency check for implementations of the more complex approach developed here (Eqs. B7 and 44).

There remains one last important detail. In transitioning from Eq. (B2) to Eq. (B3), I made the simplifying assumption that
20   all of the coefficients $\beta_{j,k}$ for a given k were either equal to zero or had a constant value of β_k instead. The same assumption is made in the derivation presented in Sect. 4. One could naturally ask what happens if the $\beta_{j,k}$ vary individually across the time steps j. Is there is a (nearly) equivalent constant β_k, and if so, how does it relate to the values of the $\beta_{j,k}$?

If we have a variable $\beta_{j,k}$ rather than a constant β_k, each of the terms of Eq. (B4) will be of the form $\sum \beta_{j,k}\, x_{j,k}\, x_{j,\ell}$ instead of
25   $\beta_k \sum x_{j,k}\, x_{j,\ell}$, and each of the terms of Eq. (B5) will be of the form $n_{x_k x_\ell} \mathrm{cov}\left(\beta_{j,k} x_{j,k}, x_{j,\ell}\right)$ instead of $\beta_k\, n_{x_k x_\ell} \mathrm{cov}\left(x_{j,k}, x_{j,\ell}\right)$. Thus the effect of a variable vs. constant β depends on how $\mathrm{cov}\left(\beta_{j,k} x_{j,k}, x_{j,\ell}\right)$ differs from $\beta_k\, \mathrm{cov}\left(x_{j,k}, x_{j,\ell}\right)$. Following the approach in Appendix A, I begin by expanding the three variables into their means and deviations, replacing $\beta_{j,k}$ with $\bar{\beta}_k + \beta'_{j,k}$, $x_{j,k}$ with $\bar{x}_k + x'_{j,k}$, and $x_{j,\ell}$ with $\bar{x}_k + x'_{j,\ell}$. Each covariance on the right-hand side of Eq. (B5) would thus become instead

$$\mathrm{cov}\big(\beta_{j,k}x_{j,k}, x_{j,\ell}\big) = \Big\langle \Big((\bar{\beta}_k + \beta'_{j,k})(\bar{x}_k + x'_{j,k}) - \overline{(\bar{\beta}_k + \beta'_{j,k})(\bar{x}_k + x'_{j,k})} \Big)\Big((\bar{x}_k + x'_{j,\ell}) - \overline{(\bar{x}_k + x'_{j,\ell})} \Big) \Big\rangle$$

$$= \Big\langle \Big((\bar{\beta}_k + \beta'_{j,k})(\bar{x}_k + x'_{j,k}) - \bar{\beta}_k\,\bar{x}_k - \overline{\beta'_{j,k}\,x'_{j,k}} \Big)\Big((\bar{x}_k + x'_{j,\ell}) - \bar{x}_k \Big) \Big\rangle$$

$$= \Big\langle \Big(\bar{\beta}_k\, x'_{j,k} + \bar{x}_k\, \beta'_{j,k} + \beta'_{j,k}\, x'_{j,k} - \overline{\beta'_{j,k}\,x'_{j,k}} \Big)\big(x'_{j,\ell} \big) \Big\rangle$$

$$= \Big\langle \bar{\beta}_k\, x'_{j,k}\, x'_{j,\ell} + \bar{x}_k\, \beta'_{j,k}\, x'_{j,\ell} + \beta'_{j,k}\, x'_{j,k}\, x'_{j,\ell} - \overline{\beta'_{j,k}\,x'_{j,k}}\, x'_{j,\ell} \Big\rangle$$

$$= \bar{\beta}_k \langle x'_{j,k}\, x'_{j,\ell} \rangle + \bar{x}_k \langle \beta'_{j,k}\, x'_{j,\ell} \rangle + \langle \beta'_{j,k}\, x'_{j,k}\, x'_{j,\ell} \rangle \quad , \tag{B8}$$

where angled brackets and overbars indicate averages over j. The final result can thus be written as

$$\mathrm{cov}\big(\beta_{j,k}x_{j,k}, x_{j,\ell}\big) = \bar{\beta}_k\, \mathrm{cov}\big(x_{j,k}, x_{j,\ell}\big) + \bar{x}_k\, \mathrm{cov}\big(\beta_{j,k}, x_{j,\ell}\big) + \langle \beta'_{j,k}\, x'_{j,k}\, x'_{j,\ell} \rangle \quad , \tag{B9}$$

where the first term on the right-hand side expresses the approximation on which the covariance matrices in (B7) and (44)

5 are based; if the second and third terms vanish, then this approximation is exact. The second term on the right-hand side

should be small, unless there is a strong correlation between $\beta_{j,k}$ and $x_{j,\ell}$ (which is unlikely unless storm size is correlated

with tracer concentrations, as explained in Sect. 2.1), _and_ $\bar{x}_k$ is large (which is unlikely because $\bar{x}_k = \langle C_{P_{j-k}} \rangle - \langle C_{Q_{j-m-1}} \rangle$

(see Eq. 37), and mass conservation implies that the averages of C_P and C_Q should be similar). The third term on the right-

hand side is a three-way cross-product, technically termed a co-skewness, that bears the same relation to skewness that

10 covariance does to variance. It has the interesting property that its expected value is zero if the three variables have

symmetrical distributions, even if they are strongly correlated (either positively or negatively, in any combination) with one

another. This behavior arises because the odd number of terms means that, for symmetrical distributions, the product

$\beta'_{j,k}\, x'_{j,k}\, x'_{j,\ell}$ is equally likely to be positive or negative for any j, and thus the positive and negative values of $\beta'_{j,k}\, x'_{j,k}\, x'_{j,\ell}$ will

tend to average out when one averages over all j. If the last two terms of Eq. (B9) are small compared to the first one, Eq.

15 (B9) says that the covariance matrices in (B5)-(B6) will be nearly the same whether β is constant or variable, whenever the

constant β_k is the average of the variable $\beta_{j,k}$. This in turn implies that the analysis presented in Sect. 4 should result in

estimated coefficients $\hat{\beta}_k$ that closely approximate the average of the time-varying $\beta_{j,k}$, as is confirmed by the benchmark

tests of Sects. 4.6-4.8.

References

Bansah, S., and Ali, G.: Evaluating the effects of tracer choice and end-member definitions on hydrograph separation results across nested, seasonally cold watersheds, Water Resour. Res., 53, 8851-8871, https://doi.org/10.1002/2016WR020252, 2017.

5 Bayley, G. V., and Hammersley, J. M.: The effective number of independent observations in an autocorrelated time series, Journal of the Royal Statistical Society, 8, 184-197, https://doi.org/10.2307/2983560, 1946.

Benettin, P., van der Velde, Y., van der Zee, S., Rinaldo, A., and Botter, G.: Chloride circulation in a lowland catchment and the formulation of transport by travel time distributions, Water Resour. Res., 49, 4619-4632, https://doi.org/10.1002/wrcr.20309, 2013.

10 Benettin, P., Kirchner, J., Rinaldo, A., and Botter, G.: Modeling chloride transport using travel-time distributions at Plynlimon, Wales, Water Resour. Res., 51, 3259-3276, https://doi.org/10.1002/2014WR016600, 2015.

Benettin, P., Volkmann, T. H. M., von Freyberg, J., Frentress, J., Penna, D., Dawson, T. E., and Kirchner, J.: Effects of climatic seasonality on the isotopic composition of evaporating soil waters, Hydrol. Earth Syst. Sci., 22, 2881-2890, https://doi.org/10.5194/hess-22-2881-2018, 2018.

15 Bishop, K. H.: Episodic increases in stream acidity, catchment flow pathways and hydrograph separation, PhD dissertation, Department of Geography, University of Cambridge, Cambridge, 1991.

Botter, G.: Catchment mixing processes and travel time distributions, Water Resour. Res., 48, W05545, https://doi.org/10.1029/2011wr011160, 2012.

Brooks, C. E. P., and Carruthers, N. B.: Handbook of Statistical Methods in Meteorology, Meteorological Office, London,
20 412 pp., 1953.

Buttle, J. M.: Isotope hydrograph separations and rapid delivery of pre-event water from drainage basins, Progress in Physical Geography, 18, 16-41, https://doi.org/10.1177/030913339401800102, 1994.

Detty, J. M., and McGuire, K. J.: Topographic controls on shallow groundwater dynamics: implications of hydrologic connectivity between hillslopes and riparian zones in a till mantled catchment, Hydrological Processes, 24, 2222-2236,
25 https://doi.org/10.1002/hyp.7656, 2010.

DeWalle, D. R., Edwards, P. J., Swistock, B. R., Aravena, R., and Drimmie, R. J.: Seasonal isotope hydrology of three Appalachian forest catchments, Hydrological Processes, 11, 1895-1906, https://doi.org/10.1002/(SICI)1099-1085(199712)11:15<1895::AID-HYP538>3.0.CO;2-#, 1997.

Fischer, B. M. C., van Meerveld, H. J., and Seibert, J.: Spatial variability in the isotopic composition of rainfall in a small headwater catchment and its effect on hydrograph separation, J. Hydrol., 547, 755-769, https://doi.org/10.1016/j.jhydrol.2017.01.045, 2017.

Galassi, M., Davies, J., Theiler, J., Gough, B., Jungman, G., Alken, P., Booth, M., Rossi, F., and Ulerich, R.: GNU Scientific
5   Library Reference Manual v. 2.3, https://www.gnu.org/software/gsl/manual/gsl-ref.pdf, 2016.

Genereux, D.: Quantifying uncertainty in tracer-based hydrograph separations, Water Resour. Res., 34, 915-919, doi: 10.1029/98WR00010 1998.

Glasser, M.: Linear regression analysis with missing observations among the independent variables, Journal of the American Statistical Association, 59, 834-844, https://doi.org/10.1080/01621459.1964.10480730, 1964.

10   Harman, C. J.: Time-variable transit time distributions and transport: Theory and application to storage-dependent transport of chloride in a watershed, Water Resour. Res., 51, 1-30, https://doi.org/10.1002/2014WR015707, 2015.

Heidbüchel, I., Troch, P. A., Lyon, S. W., and Weiler, M.: The master transit time distribution of variable flow systems, Water Resour. Res., 48, W06520, https://doi.org/10.1029/2011WR011293, 2012.

Hooper, R. P., and Shoemaker, C. A.: A comparison of chemical and isotopic hydrograph separation, Water Resour. Res.,
15   22, 1444-1454, https://doi.org/10.1029/WR022i010p01444, 1986.

Hubert, P., Marin, E., Meybeck, M., Olive, P., and Siwertz, E.: Aspects hydrologique, gèochimique et sèdimentologique de la crue exceptionnelle de la Dranse du Chablais du 22 septembre 1968, Archives des Sciences (Genève), 22, 581-604, 1969.

Kirchner, J. W., Hooper, R. P., Kendall, C., Neal, C., and Leavesley, G.: Testing and validating environmental models, Sci. Total Environ., 183, 33-47, https://doi.org/10.1016/0048-9697(95)04971-1, 1996.

20   Kirchner, J. W.: A double paradox in catchment hydrology and geochemistry, Hydrological Processes, 17, 871-874, https://doi.org/10.1002/hyp.5108, 2003.

Kirchner, J. W.: Getting the right answers for the right reasons: Linking measurements, analyses, and models to advance the science of hydrology, Water Resour. Res., 42, W03S04, https://doi.org/10.1029/2005WR004362, 2006.

Kirchner, J. W.: Aggregation in environmental systems -- Part 2: Catchment mean transit times and young water fractions
25   under hydrologic nonstationarity, Hydrol. Earth Syst. Sci., 20, 299-328, https://doi.org/10.5194/hess-20-279-2016, 2016a.

Kirchner, J. W.: Aggregation in environmental systems -- Part 1: Seasonal tracer cycles quantify young water fractions, but not mean transit times, in spatially heterogeneous catchments, Hydrol. Earth Syst. Sci., 20, 279-297, https://doi.org/10.5194/hess-20-299-2016, 2016b.

Kish, L.: Survey Sampling, Wiley Classics Library, Wiley, New York, 643 pp., 1995.

Klaus, J., and McDonnell, J. J.: Hydrograph separation using stable isotopes: Review and evaluation, J. Hydrol., 505, 47-64, https://doi.org/10.1016/j.jhydrol.2013.09.006, 2013.

Klaus, J., Chun, K. P., McGuire, K. J., and McDonnell, J. J.: Temporal dynamics of catchment transit times from stable isotope data, Water Resour. Res., 51, 4208-4223, https://doi.org/10.1002/2014wr016247, 2015.

5   Laudon, H., Hemond, H. F., Krouse, R., and Bishop, K. H.: Oxygen 18 fractionation during snowmelt: Implications for spring flood hydrograph separation, Water Resour. Res., 38, https://doi.org/10.1029/2002wr001510, 2002.

Little, R. J. A.: Regression with missing X's: A review, Journal of the American Statistical Association, 87, 1227-1237, https://doi.org/10.2307/2290664, 1992.

Matalas, N. C., and Langbein, W. B.: Information content of the mean, Journal of Geophysical Research, 67, 3441-1448,
10   doi: 10.1029/JZ067i009p03441, 1962.

McDonnell, J. J., Bonell, M., Stewart, M. K., and Pearce, A. J.: Deuterium variations in storm rainfall - Implications for stream hydrograph separation, Water Resour. Res., 26, 455-458, https://doi.org/10.1029/WR026i003p00455, 1990.

McDonnell, J. J., Stewart, M. K., and Owens, I. F.: Effect of catchment-scale subsurface mixing on stream isotopic response, Water Resour. Res., 27, 3065-3073, https://doi.org/10.1029/91WR02025, 1991.

15   McGuire, K. J., McDonnell, J. J., Weiler, M., Kendall, C., McGlynn, B. L., Welker, J. M., and Seibert, J.: The role of topography on catchment-scale water residence time, Water Resour. Res., 41, W05002, https://doi.org/10.1029/2004WR003657, 2005.

McGuire, K. J., and McDonnell, J. J.: A review and evaluation of catchment transit time modeling, J. Hydrol., 330, 543-563, https://doi.org/10.1016/j.jhydrol.2006.04.020, 2006.

20   Merz, R., Bloschl, G., and Parajka, J.: Spatio-temporal variability of event runoff coefficients, J. Hydrol., 331, 591-604, https://doi.org/10.1016/j.jhydrol.2006.06.008, 2006.

Mitchell, J. M., Dzerdzeevskii, B., Flohn, H., Hofmeyr, W. L., Lamb, H. H., Rao, K. N., and Waleen, C. C.: Climatic change: report of a working group of the Commission for Climatology. WMO Technical note No. 79, World Meteorological Organization, Geneva, 79 pp., 1966.

25   Neal, C., and Rosier, P. T. W.: Chemical studies of chloride and stable oxygen isotopes in 2 conifer afforested and moorland sites in the British uplands, J. Hydrol., 115, 269-283, https://doi.org/10.1016/0022-1694(90)90209-G, 1990.

Penna, D., Tromp-van Meerveld, H. J., Gobbi, A., Borga, M., and Dalla Fontana, G.: The influence of soil moisture on threshold runoff generation processes in an alpine headwater catchment, Hydrol. Earth Syst. Sci., 15, 689-702, https://doi.org/10.5194/hess-15-689-2011, 2011.

Phillips, D. L.: A technique for the numerical solution of certain integral equations of the first kind, Journal of the ACM, 9, 84-97, https://doi.org/10.1145/321105.321114, 1962.

Pinder, G. F., and Jones, J. F.: Determination of the groundwater component of peak discharge form the chemistry of total runoff, Water Resour. Res., 5, https://doi.org/10.1029/WR005i002p00438, 1969.

5 Press, W. H., Flannery, B. P., Teukolsky, S. A., and Vetterling, W. T.: Numerical Recipes in C: the Art of Scientific Computing, 2nd ed., Cambridge University Press, New York, 994 pp., 1992.

Remondi, F., Kirchner, J. W., Burlando, P., and Fatichi, S.: Water flux tracking with a distributed hydrological model to quantify controls on the spatiotemporal variability of transit time distributions, Water Resour. Res., 54, 3081-3099, https://doi.org/10.1002/2017WR021689, 2018.

10 Rigon, R., Bancheri, M., and Green, T. R.: Age-ranked hydrological budgets and a travel time description of catchment hydrology, Hydrol. Earth Syst. Sci., 20, 4929-4947, https://doi.org/10.5194/hess-20-4929-2016, 2016.

Rodhe, A.: The origin of streamwater traced by oxygen-18, Ph.D. dissertation, Department of Physical Geography, Uppsala University, Uppsala, 1987.

Rodhe, A., Nyberg, L., and Bishop, K.: Transit times for water in a small till catchment from a step shift in the oxygen-18
15 content of the water input, Water Resour. Res., 32, 3497-3511, https://doi.org/10.1029/95WR01806, 1996.

Rodriguez, N. B., Mcguire, K. J., and Klaus, J.: Time-varying storage-water age relationships in a catchment with a Mediterranean climate, Water Resour. Res., 54, 3988-4008, https://doi.org/10.1029/2017WR021964, 2018.

Seeger, S., and Weiler, M.: Reevaluation of transit time distributions, mean transit times and their relation to catchment topography, Hydrol. Earth Syst. Sci., 18, 4751-4771, https://doi.org/10.5194/hess-18-4751-2014, 2014.

20 Sklash, M. G., Farvolden, R. N., and Fritz, P.: A conceptual model of watershed response to rainfall, developed though the use of oxygen-18 as a natural tracer, Canadian Journal of Earth Sciences, 13, 271-283, https://doi.org/10.1139/e76-029, 1976.

Sklash, M. G.: Environmental isotope studies of storm and snowmelt runoff generation, in: Process Studies in Hillslope Hydrology, edited by: Anderson, M. G., and Burt, T. P., Wiley, Chichester, 401-435, 1990.

25 Sprenger, M., Tetzlaff, D., Tunaley, C., Dick, J., and Soulsby, C.: Evaporation fractionation in a peatland drainage network affects stream water isotope composition, Water Resour. Res., 53, 851-866, https://doi.org/10.1002/2016wr019258, 2017.

Stewart, M. K., Morgenstern, U., and McDonnell, J. J.: Truncation of stream residence time: how the use of stable isotopes has skewed our concept of streamwater age and origin, Hydrological Processes, 24, 1646-1659, https://doi.org/10.1002/hyp.7576, 2010.

Taylor, S., Feng, X. H., Williams, M., and McNamara, J.: How isotopic fractionation of snowmelt affects hydrograph separation, Hydrological Processes, 16, 3683-3690, https://doi.org/10.1002/hyp.1232, 2002.

Tikhonov, A. N.: Solution of incorrectly formulated problems and the regularization method, Soviet Mathematics, 4, 1035-1038, 1963.

van der Velde, Y., Torfs, P. J. J. F., van der Zee, S. E. A. T. M., and Uijlenhoet, R.: Quantifying catchment-scale mixing and its effect on time-varying travel time distributions, Water Resour. Res., 48, W06536, https://doi.org/10.1029/2011WR011310, 2012.

von Freyberg, J., Studer, B., and Kirchner, J. W.: A lab in the field: high-frequency analysis of water quality and stable isotopes in streamwater and precipitation, Hydrol. Earth Syst. Sci., 21, 1721-1739, https://doi.org/10.5194/hess-21-1721-2017, 2017.

von Freyberg, J., Studer, B., Rinderer, M., and Kirchner, J. W.: Studying catchment storm response using event and pre-event water volumes as fractions of precipitation rather than discharge, Hydrol. Earth Syst. Sci., 22, 5847-5865, doi: https://doi.org/10.5194/hess-22-5847-2018, 2018.

Zhadanov, M. S.: Inverse Theory and Applications in Geophysics, Elsevier, Amsterdam, 704 pp., 2015.